NORTHWESTERN UNIVERSITY

An Analysis of the Contribution of the Herpesvirus Major Capsid Protein Apical Region Toward Infection

A DISSERTATION

SUBMITTED TO THE GRADUATE SCHOOL

IN PARTIAL FULFILLMENT OF THE REQUIREMENTS

for the degree

DOCTOR OF PHILOSOPHY

Field of Life Sciences

By

Laura Lee Ruhge

EVANSTON, ILLINOIS

September 2018

© Copyright by Laura Ruhge 2018

All Rights Reserved

Abstract

Herpesvirus virions consist of three layers: nucleocapsid, tegument, and envelope. The innermost layer, the nucleocapsid, initially assembles as an immature procapsid precursor built around viral scaffold proteins. The event that initiates procapsid maturation is unknown but it is dependent upon activation of the internal protease. Scaffold cleavage triggers angularization, or transformation into a polyhedral form, of the shell and its decoration with the accessory capsid-surface proteins – the capsid vertex specific component and the small capsid protein. In both the procapsid and mature angularized capsid, the apical region of the major capsid protein is surface exposed. I investigated whether the major capsid protein apical region contributes to intracellular transport dynamics following entry into primary sensory neurons and also tested the hypothesis that conserved negatively-charged amino acids in the apical region contribute to acquisition of the small capsid protein. To my surprise neither hypothesis proved true. Instead, mutation of glutamic acid residues in the apical region delayed viral propagation and induced focal capsid accumulations in nuclei.

This dissertation reports on the fortuitous discovery that a region of the major capsid protein that is exposed on the outer surface of the capsid also contributes to capsid maturation. Examination of capsid morphogenesis based on epitope unmasking, capsid composition, and ultrastructural analysis indicated that the glutamic acid mutant focal accumulations consisted of procapsids. The results demonstrate that, in addition to established events that occur inside the capsid, the exterior capsid shell promotes capsid morphogenesis and maturation of the megastructure.

In addition, this dissertation presents a modified fluorescent fusion protein design that produced the first described procapsid-specific tag. In this design, a fluorescent protein open reading frame is fused to the amino-terminus of the protease and includes the protease cleavage site immediately following the fluorescent protein's sequence. Consequently, the fluorescent protein is cleaved from the protease upon its activation during capsid maturation and the fluorescent signal is lost from the megastructure. This procapsid-specific tag not only allows for the identification of procapsids in living cells by a single fluorescent marker but also might serve as a fluorescent readout of protease activity.

Acknowledgement

I would like to thank my advisor, Greg Smith, for seeing potential in me. I chose you specifically as a mentor because I knew you would expect the most of me and that I needed that push. I'm inspired by your genuine love for science and hope you always find the time to have conversations with your students that are largely theoretical science, or as I like to call it to venture into science la-la-land.

I thank the members of my dissertation committee – Hank Seifert, Katya Heldwein, Sarah Rice, and Lou Laimins – for your thoughtful and fair evaluation of my science. Your investment in my development has been a privilege.

I thank my lab mates both present and past. Gina, thank you for journeying through graduate school before me and for your vulnerability about your hard lessons. Lexi, thank you for always being invested in my research moving forward, for understanding my Midwestern nature, and for being a great source of joy. Caitlin, thank you for trips to 7-Eleven and McDonald's for sodas, for getting heated on my behalf, for teaching me IFA, for refreshing my Western blotting skills, and for being my lab bestie. Sarah, thank you for being a much-needed listening ear and for seeing me to the finish line. Oana, thank you for being my experimental design sounding board, for always being down to get coffee, and for sharing with me the greatest conversations about life, science, and what it all truly means. I have learned so much from you.

I thank my husband, Tyson, for loving me sacrificially these past six years, for cooking me dinner every night, for listening to my complaints, for dealing with my rampant anxiety and fear, for encouraging me, for escorting me to and from the lab to tend to late time points (especially that time we went in at midnight during a snowstorm), and for always believing in me.

I thank all my family – including my grandparents, 17 aunts and uncles, and 21 first cousins – for constantly telling me how proud you are of me and encouraging me to continue working hard. I additionally thank my parents for providing for me and raising me to be the person I am. I would never have made it here without you, in so many ways. Thank you for supporting me during the refining experiences of higher education and for enabling me to have that privilege. I also thank my brother, Nick, for going before me in all things of life, for frequent phone calls, and for sharing your great sense of humor. Lastly, I thank my cousin, Andrea, for speaking enormous purpose into the graduate school experience, for adjusting my perspective, and for praying me through this.

I thank my friends Noel, Audrey, Cassidy, Mollie, and Jaclyn for being tremendous sources of joy, encouragement, and support during this time. I am blessed by our beautiful friendships. I also thank the Paventi and Navarrette families for their support and sharing their sweet and silly children – being their Aunt is my most favorite role I've played. Spending time with your sweet babies is a source of refreshment and always reminds me of the most important parts of life.

Finally, I thank the following artists for using their creative gifts to make music that was instrumental in keeping me mentally motivated while studying for exams, working long hours in the lab, journeying down reading rabbit holes in the primary literature, and writing this dissertation: Kendrick Lamar, Eminem (The Marshall Mathers LP 2), Yelawolf, NF, Cardi B, Post Malone (beerbongs & bentleys), Breaking Benjamin, Chevelle, 10 Years, Slipknot, Five Finger Death Punch, Index Case, Of Mice and Men, Korn, Bullet for My Valentine, King 810, Fit for a King, For Today, Flyleaf, My Epic, SOJA, Rebelution, Nahko and Medicine for the People, Jennifer Knapp, and KLOVE radio for always playing positive and encouraging music when it's most needed.

Preface

It is estimated that every person carries at least one to two herpesviruses. Because herpesviruses infect and affect us all, and because we all love a good story, I'd like to share a tale about the herpesvirus' journey to deliver its high-profile package – the nucleocapsid.

It starts with a kiss. Not necessarily a romantic kiss. Something more like a mother to a child. Or a greeting from that Great Aunt who needs to kiss your lips and, "get a good look at you!" Whether through viral shedding or an active cold sore, herpesvirus virions are now on your lips, maybe even now in your mouth because you licked your lip.

When most people think about a herpesvirus, they typically envision a malicious, minuscule invader. Perhaps it has a toothy grin or maybe a set of horns. If you've taken a college-level biology course, you might see a small hexagon with legs. In reality, these nanoscopic pathogens are much more like a highly organized, triple-threat infiltration team. The goal of any herpesvirus is to engage a host cell, produce more of itself, and move on to infect neighboring cells.

The first sighting of this herpesvirus came in the 1950s, thanks to electron microscopes. Electron microscopy gathers information about a specimen's appearance by blasting it with a beam of electrons and recording the various signals produced, ultimately creating an image. From experiments like these, scientists determined the herpesvirus is spherical with a diameter of 200 nanometers; to put this in perspective, a single strand of hair on your head is 100,000 nanometers in diameter. More importantly, these first images revealed the herpesvirus consists of three distinguishable layers.

Each one of these layers carries within it a specific directive to complete the mission of infection. The outermost layer of the herpesvirus, called the envelope, is tasked with penetrating a host cell. The envelope is a protective, flexible membrane layer studded with glycoproteins. Glycoproteins pick the host cell's locked door, allowing the virus inside. The envelope is on a kamikaze mission: once successful, it's left behind at the cell's surface.

Loss of the envelope leaves the second layer of the virus, the tegument, exposed to the hostile environment within the host cell. A portion of the tegument layer are hitmen, responsible for silencing any and all obstacles, such as the cell's immune response. Other soldiers from this layer hijack the cell's control center – the nucleus – to prepare the cell for viral takeover. A few members of the tegument are on security detail, personally escorting the third layer, the DNA-containing capsid, to the host cell's nucleus. Successful delivery of the virus' genetic information turns the host cell into a herpesvirus factory.

Arguably, the delivery of this high-profile package is the most important objective for establishing infection. The capsid is like a ticking time bomb stuffed with highly pressurized DNA. Tightly packed DNA exerts extreme pressure on the capsid from the inside, and the capsid must contain this pressure so the bomb doesn't detonate before reaching the nucleus. Failure to deposit the viral DNA into the nucleus terminates the operation and infection cannot spread beyond the initial host cell. Successful deployment of the viral DNA into the nucleus kickstarts the assembly of a fresh fleet of virus tasked with the invasion of neighboring cells.

The herpes simplex virus is cunning, efficiently infiltrating the human population. The mission of many research laboratories around the world is to figure out how we can reprogram this virus, dreaming of the day the herpes simplex virus' ability to proficiently invade human cells is exploited for medical benefit. If we understand the individual pieces involved in building

the virus, how they fit together, as well as which weapons are required for infiltration, perhaps we can build a virus of our own. Imagine the world where the herpesvirus' directive has been altered to specifically engage and destroy a cancer cell or deliver a life-saving gene into a host whose innate genetics left them wanting.

Sixty years have passed since scientists first captured a portrait of the herpesvirus. While that time has afforded the field a clearer picture, we are still fervently trying to figure out this virus' numerous tricks to outsmart our body's defenses. We continue to search for understanding, to pull apart the mechanisms of how the herpesvirus completes its mission so successfully. So, the next time you think about the herpesvirus you may still picture a cold sore – or a tiny blob with horns – but I urge you to also imagine a highly sophisticated, microscopic invader full of possibility.

List of Abbreviations

angstroms (Å)
adenosine triphosphate (ATP)
bacterial artificial chromosome (BAC)
bovine growth serum (BGS)
bovine serum albumin (BSA)
carbon dioxide (CO_2)
capsid vertex specific component (CVSC)
centimeter (cm)
cryo-electron microscopy (cryo-EM)
differential interference contrast (DIC)
Dulbecco's Modified Eagle Medium (DMEM)
dorsal root ganglion (DRG)
electron-multiplying (EM)
Epstein-Barr virus (EBV)
final sample buffer (FSB)
green fluorescent protein (GFP)
Hawkin 97 (HK97) fold
herpes simplex virus type 1 (HSV-1)
herpes simplex virus type 2 (HSV-2)
human cytomegalovirus (HCMV)
human herpesvirus 6a (HHV6a)
human herpesvirus 6b (HHV6b)
human herpesvirus 7 (HHV7)
Kaposi's sarcoma herpesvirus (KSHV)
kilodalton (kDa)
major capsid protein (MCP)
megahertz (MHz)
microliter (μL)
micrometer (μm)
milligram (mg)
milliliter (mL)
millimeter (mm)
millimolar (mM)
millisecond (ms)
multiplicity of infection (MOI)
nanometer (nm)
numerical aperture (NA)
Penicillin-Streptomycin (Pen-Strep)
phosphate buffered saline (PBS)
plaque forming units (PFU)
pseudorabiesvirus (PRV)
red fluorescent protein (RFP)
room temperature (RT)
small capsid protein (SCP)
varicella-zoster virus (VZV)
wild-type (WT)

Table of Contents

List of Figures

List of Tables

CHAPTER 1: Introduction

The *Herpesviridae*

The *Herpesviridae* family of large double-stranded DNA viruses has more than 300 members that infect a diversity of hosts ranging from mollusk to man (1). These viruses emerged from a common ancestor more than 400 million years ago, allowing for a long history of coevolution with their respective hosts. From this common ancestor, herpesviruses share more than 40 genes involved in viral replication (2). Although long evolution resulted in diversified primary sequences of the core genes across the *Herpesviridae*, the protein structures produced share striking similarity (3-8).

In addition to sharing genes, herpesviruses conform to a common virion structure consisting of three layers: nucleocapsid, tegument, and envelope (Fig. 1.1). The nucleocapsid, or DNA-filled capsid, is a proteinaceous shell that holds the tightly packed viral genome, which for the human herpesviruses ranges from 140-240 kilobase pairs in length. These massive genomes are stuffed into capsids approximately 125 nanometers (nm) in diameter and exert tens of atmospheres of pressure against the capsid shell (9). To place these metrics into perspective, the herpesvirus capsid, more than 2,000 times smaller than the period at the end of this sentence, contains 9 times the pressure held in a bottle of champagne. The remarkably stable nucleocapsid is surrounded by a matrix of viral and cellular proteins termed the tegument (10-12). The tegument-decorated nucleocapsid is enclosed in a host-derived, lipid-bilayer envelope studded with viral glycoproteins.

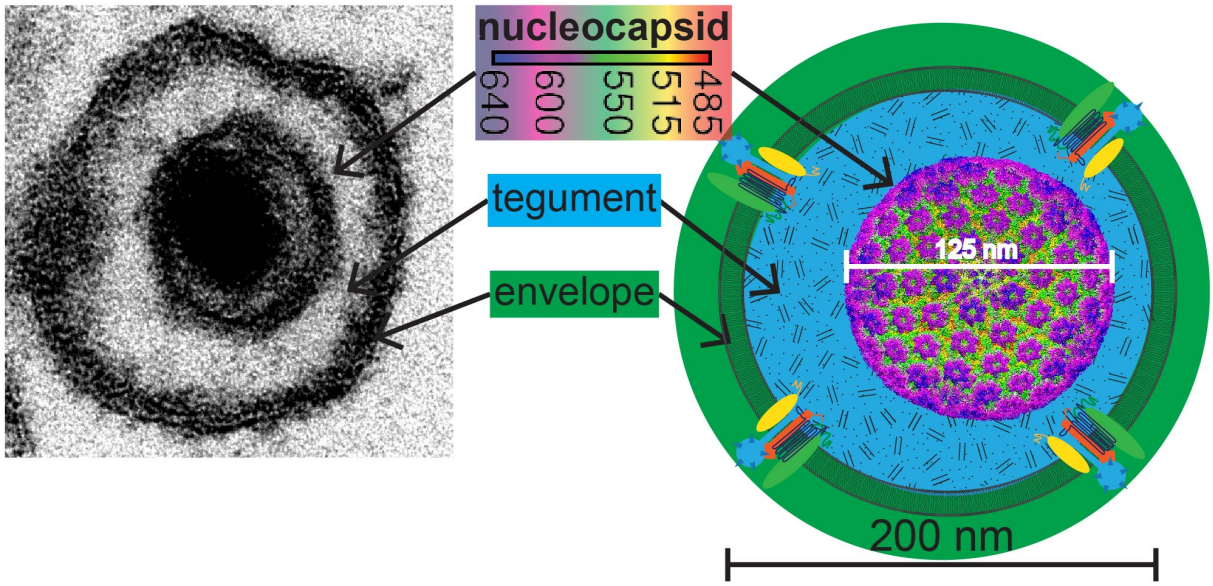

Figure 1.1 The herpesvirus virion structure. The three layers of the herpesvirus virion are labeled on the electron micrograph (left) and cartoon (right). The nucleocapsid is radially colored, as indicated, in angstroms (Å) from the center of the density map. Diameters of the capsid and virion refer to HSV-1.

The *Herpesviridae* is divided into three subfamilies: the *Alpha-*, *Beta-*, and *Gamma-herpesvirinae*. Within each subfamily are human pathogens commonly found in the population (Fig. 1.2), causing varied disease. The *Alphaherpesvirinae* consists of the notorious herpesviruses: the causative agent of chicken pox and shingles, varicella-zoster virus (VZV), and the viruses behind cold sores and genital herpes, herpes simplex virus type 1 (HSV-1) and type 2 (HSV-2). It is estimated that approximately 85% of adolescents have had a history of VZV infection or received two doses of the varicella vaccine and the seroprevalence of HSV-1 and

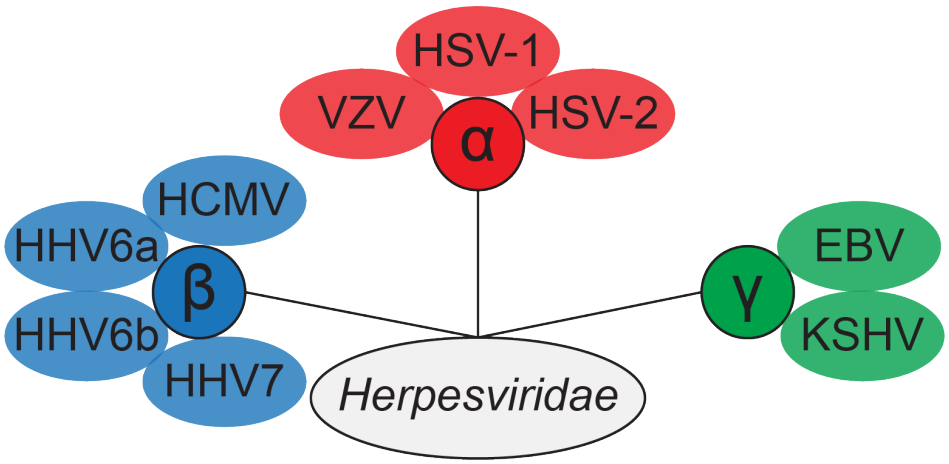

Figure 1.2 Human pathogens of the *Herpesviridae*. Herpesviruses are subdivided into three families: alpha (α), beta (β), and gamma (γ). The abbreviated names of human pathogens within each subfamily are shown.

HSV-2 are approaching 60% and 20%, respectively (13). The *Betaherpesvirinae* consists of four inconspicuous human viruses: human cytomegalovirus (HCMV), human herpesvirus 6a (HHV6a), human herpesvirus 6b (HHV6b), and human herpesvirus 7 (HHV7). HCMV is the most frequent cause of congenital infection but most typically produces asymptomatic or minor symptoms upon infecting an immunocompetent individual (14). HHV6a is more commonly contracted later in life while HHV6b frequently causes Roseola in children, and both are linked to T-cell lymphoproliferative disorders (15). HHV7 has no clear link to any disease at this time. It is estimated that more than 60%, 90%, and 85% of the population is infected with HCMV, HHV6a and b collectively, and HHV7, respectively (16-18). The *Gammaherpesvirinae* consists of two human herpesviruses connected to lymphoproliferative disorders: the common cause of infectious mononucleosis, Epstein-Barr virus (EBV), and Kaposi's sarcoma herpesvirus

(KSHV). EBV is one of the most common human viruses with greater than 90% of the population infected by early adulthood. In contrast, KSHV is less prevalent in the overall population but poses a threat to HIV-positive individuals as the causative agent of Kaposi's sarcoma (19).

In addition to sharing common genes and virion morphology, all herpesviruses exhibit latency or a quiescent infection in which little to no viral progeny is produced. However, during periods of stress the virus exits this dormant state, or reactivates, producing a fresh fleet of virions that travel back to the periphery and cause recurrent disease. Through this latency program, herpesviruses are able to evade immune detection and establish lifelong infection. Alphaherpesviruses establish latency in neuronal cells of the peripheral nervous system while beta- and gammaherpesviruses establish latency in immune cells.

Of particular interest within the *Herpesviridae* is the variation observed in disease outcome during primary infections and reactivation. For example, a primary HSV-1 infection creates cold sores in one individual and in another causes lethal encephalitis. In a similar manner, reactivation of HSV-1 produces a fresh round of cold sores in most people but in some individuals may result in encephalitis (20, 21) or ocular lesions that can lead to blindness (22, 23). Additionally, herpesviruses can confer a new disease burden when an infected individual becomes immunocompromised. For example, EBV primary infection in a child results in cold-like symptoms, however, if in adulthood that individual undergoes an organ transplant, EBV reactivation could cause a life-threatening condition, post-transplant lymphoproliferative disorder (24).

Currently, herpesvirus infections are treated with nucleoside analogs, such as acyclovir, which inhibit viral replication. These drugs effectively combat active replication but fail to

eradicate latent reservoirs of herpesvirus. However, scientists are exploring the potential of the genome editing technology, such as the clustered regularly interspaced short palindromic repeats (CRISPR)/Cas9 system, for the elimination of latent herpesvirus genomes (25). Due to the ubiquitous nature of herpesviruses, the vast disease disparity, and the lifelong nature of herpesvirus infections, it is imperative that new therapies and antivirals are developed.

The *Alphaherpesvirinae*

The *Alphaherpesvirinae* consists of three ubiquitous human viruses – VZV, HSV-1, and HSV-2 – that exhibit robust neuroinvasive ability (26). These viruses initially infect mucosal-epithelial surfaces but quickly spread to innervating nerve termini of the peripheral nervous system. In the nuclei of neuronal cells, typically within the sensory or cranial nerve ganglia, latency is established. During latency, the viral genome is maintained and viral protein expression is suppressed (27). Upon local trauma or systemic stress, the virus exits latency and produces nascent virions which travel back to the periphery producing skin lesions or in rare cases enter the central nervous system with serious if not lethal consequence (28, 29). Although active replication of herpesvirus is cleared from mucosal-epithelial cells, latently infected neurons serve as reservoirs of silent genomes (30, 31). Thus, alphaherpesviruses persist for the lifetime of the host causing recurrent disease.

When infection starts in the mucosal epithelium, the herpesvirus virion attaches to receptors on the cell surface and the viral glycoproteins facilitate fusion of the virion's lipid envelope with the cell's plasma membrane (Fig. 1.3). The glycoproteins gB, gC, gD, gH, and gL comprise the fusogenic machinery (32). Alternatively, the virion can enter the cell via

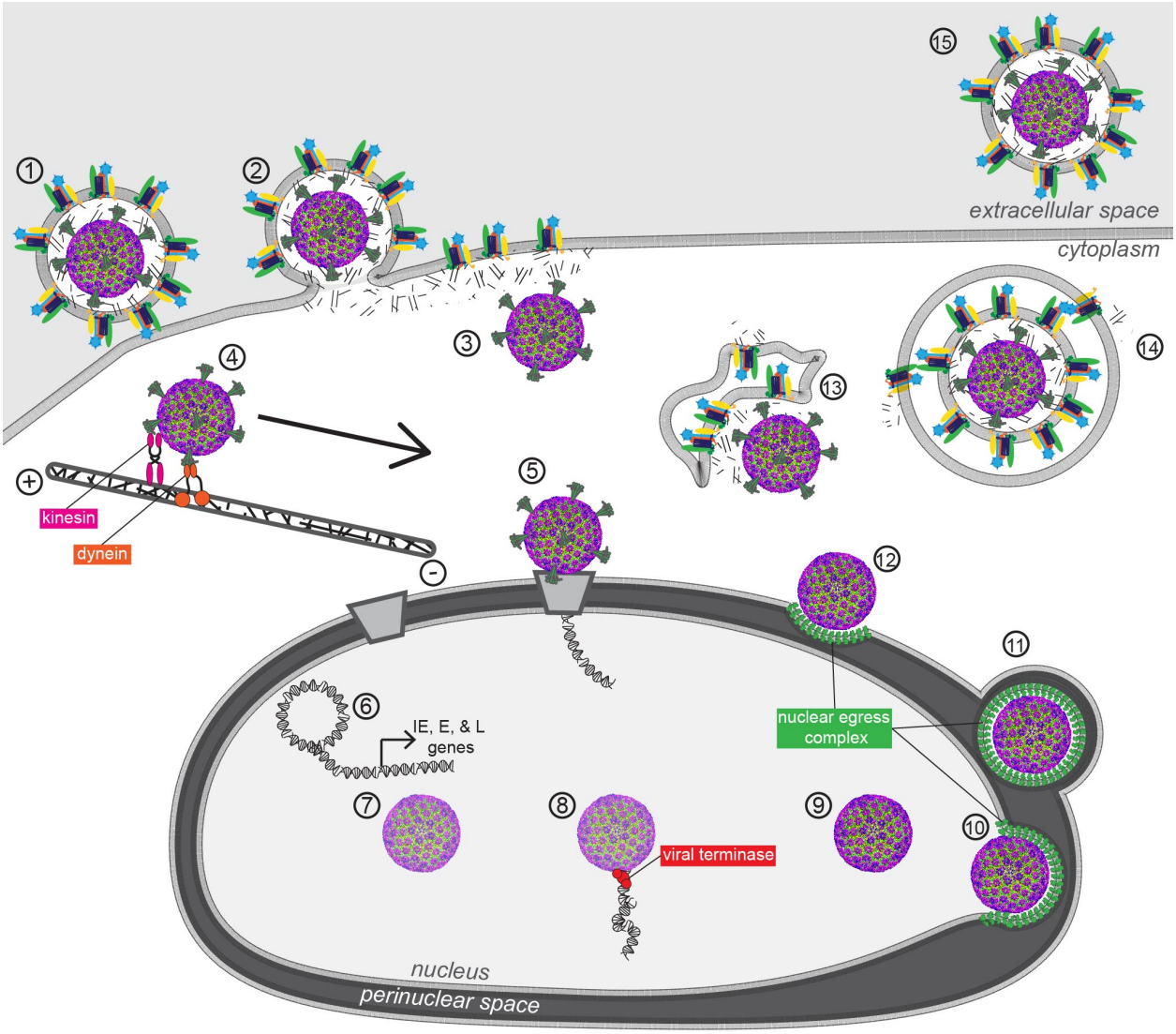

Figure 1.3 The alphaherpesvirus infectious cycle. The herpesvirus virion binds to the surface of a cell with the envelope glycoproteins (1) and fuses the envelope with the cell's plasma membrane (2). The nucleocapsid is deposited into the cytosol and the bulk of the tegument dissociates (3). The nucleocapsid is transported by microtubule-based motors that directly interact with the small subset of tegument proteins associated with the capsid surface (4) ultimately docking at a nuclear pore (5). Release of the viral genome into the nucleus initiates a cascade of viral gene expression (6). Nascent capsids are formed (7) and packaged with the viral genome through an interaction of the terminase with the capsid surface (8). Nucleocapsids migrate to the nuclear periphery (9)

where the capsid surface interacts with the nuclear egress complex to facilitate translocation into the cytoplasm by budding at the inner nuclear membrane (10), primary envelopment in the perinuclear space (11), and de-envelopment at the outer nuclear membrane, depositing the nucleocapsid into the cytosol (12). The nucleocapsid encounters tegument proteins and glycoproteins on cellular membranes (13) and is enveloped for a second time, resulting in the virion wrapped in an additional membrane (14). Finally, the virion exits the cell via the secretory pathway (15).

---

endocytosis and fusion takes place between the viral envelope and endosomal membrane (33). The bulk of the tegument proteins dissociate from the nucleocapsid and perform various functions to prepare the cell for viral replication, such as silencing the innate immune response or regulating host cell and viral transcription (34-36). A small subset of the tegument, referred to as the inner tegument, remains bound to the nucleocapsid. This subset includes the viral kinase, pUS3, the large tegument protein, pUL36, and its binding partner, pUL37 (35, 37, 38). Both pUL36 and pUL37 are effectors of transport, trafficking the nucleocapsid along microtubules, ultimately docking at a nuclear pore (39-46).

After docking at a nuclear pore complex, the nucleocapsid releases the viral genome into the nucleus. A vertex capsid protein, pUL25, is the capsid binding site of pUL36 and both proteins are implicated in the genome release mechanism which may involve proteolysis of pUL36 (47). Temperature-sensitive mutations in pUL36 and pUL25, as well as a carboxyl-terminus truncation mutant of pUL25, result in nucleocapsids that dock at nuclear pores but fail to release the genome (48-51). Deposition of the viral genome within the nucleus initiates a cascade of viral gene expression divided into three classes: immediate early, early, and late. Immediately early gene expression does not require *de novo* viral protein synthesis but is

promoted by the abundant tegument protein VP16. Early gene expression follows next, producing proteins involved in viral DNA replication. The viral DNA is replicated by a rolling circle mechanism creating branched, head-to-tail concatemers of genomes that are cut to unit length for packaging (52). The viral genome is divided into short and long unique segments that are flanked by inverted terminal repeat regions which carry the cleavage and packaging signal recognized by the viral terminase (53). Late gene transcription starts after the onset of viral DNA replication and produces structural proteins involved in assembly and egress which must be translocated into the nucleus for the formation of nascent capsids (54-57).

The infected cell nucleus undergoes dramatic remodeling to accommodate viral DNA replication and capsid morphogenesis. Early in infection, the immediate early protein ICP0 strongly activates viral gene expression and relieves cellular repression of viral transcription through the disruption of promyelocytic leukemia nuclear bodies (58). Additionally, the host cell chromatin is marginalized and viral replication compartments form in the interchromatin space which enlarges as infection persists (59-61). Replication compartments are marked by viral DNA replication proteins such as the DNA binding protein ICP8.

Nucleocapsids are formed within infected cell nuclei when new capsid shells assemble and the viral genome is packaged. This process closely parallels the assembly and encapsidation of bacteriophage. Currently, there are no clear sites of capsid assembly for HSV-1 or pseudorabies virus (PRV), a swine alphaherpesvirus, although VZV has been reported to form sites of capsid assembly (62, 63). As infection persists, capsids localize to replication compartments, presumably, to be filled with DNA (64). However, this event and the proteins involved are poorly understood. To facilitate the efficient exit of nucleocapsids from the nucleus, the nuclear lamina is disrupted via phosphorylation by the viral kinase pUS3 as well as cellular

kinases. Nucleocapsids then escape the nucleus through an elaborate two-step egress mechanism involving virally encoded membrane budding machinery (65-69). Although some tegument proteins assemble on the nucleocapsid prior to egress from the nucleus, the majority of the tegument layer is added in the cytosol (70, 71). Tegument proteins also interact with the cytosolic tails of glycoproteins anchored in the *trans*-Golgi network (72-75). This extensive network of interactions between the tegument and envelope proteins facilitates envelopment of the nucleocapsid for the second time resulting in the enveloped virion inside a vesicle. Finally, the mature virion is transported out of the cell via the secretory pathway (76-78).

Although infection begins in epithelial cells, herpesvirus virions rapidly reach innervating nerve termini and invade the sensory and autonomic ganglia by retrograde axonal transport (79). After entering a neuronal cell, the virion disassembles as in an epithelial cell but now must transport up to a meter in length to deposit the viral genome into the nucleus. In most neuronal nuclei, the viral genome is repressed and latency is established (80). During latency, the viral genome is stably maintained but virion assembly only initiates upon reactivation of lytic infection.

The ability of alphaherpesviruses to routinely invade the nervous system is remarkable. Alphaherpesviruses can directly interact with microtubule-based motors, whereas other neurotropic viruses, such as rabies virus, rely on endosomal trafficking within axons to reach the neuronal cell body (81). Another impressive aspect of herpesvirus neuroinvasion is the ability to enter the nervous system following casual contact with an infected individual. In contrast, rabies virus requires a high dose inoculum, such as that delivered through a bite, to innervate the nervous system. Because of their large, mutable genomes and the unique ability to proficiently

and consistently enter the nervous system, alphaherpesviruses are particularly interesting candidates for gene delivery.

The Nucleocapsid Structure

The herpesvirus nucleocapsid structure is rapidly becoming the most well-understood component of the herpesvirus virion. Recent refinements of cryo-electron microscopy (cryo-EM) reconstruction techniques have pushed nucleocapsid density maps to near-atomic resolution (4-6, 8) with the most well-resolved parts of the HSV-1 nucleocapsid being resolved at 3.5 angstroms (Å) (7). These structures not only inform on the source of the nucleocapsid's mechanical strength but also provide insights into capsid assembly and potential targets for therapeutic intervention (82).

Herpesvirus nucleocapsids are approximately 125 nm in diameter, conform to a T = 16 icosahedral structure (Fig. 1.4), and consist of 162 capsomeres: 150 hexamers (hexon capsomeres), 11 pentamers (penton capsomeres), and one portal vertex (83). The proteinaceous shell is 15 nm thick with an inner diameter of 90 nm. HSV-1 nucleocapsids must withstand an estimated 18 atmospheres of internal pressure exerted by the tightly packed 152 kilobase pair genome until the capsid docks at a nuclear pore and releases the DNA into the nucleus (9, 42).

The herpesvirus nucleocapsid alone weighs in at 200 megadaltons and consists of thousands of viral structural proteins, making herpesviruses easily some of the largest, most complex viruses that infect humans. The majority of the herpesvirus capsid shell mass is comprised of 955 copies of the 149 kilodalton (kDa) major capsid protein (MCP) (84-87), which is arranged into hexamers and pentamers connected by heterotrimeric complexes called triplexes (Table 1.1). MCP pentamers are found at 11 of the capsid vertices while MCP hexamers occupy

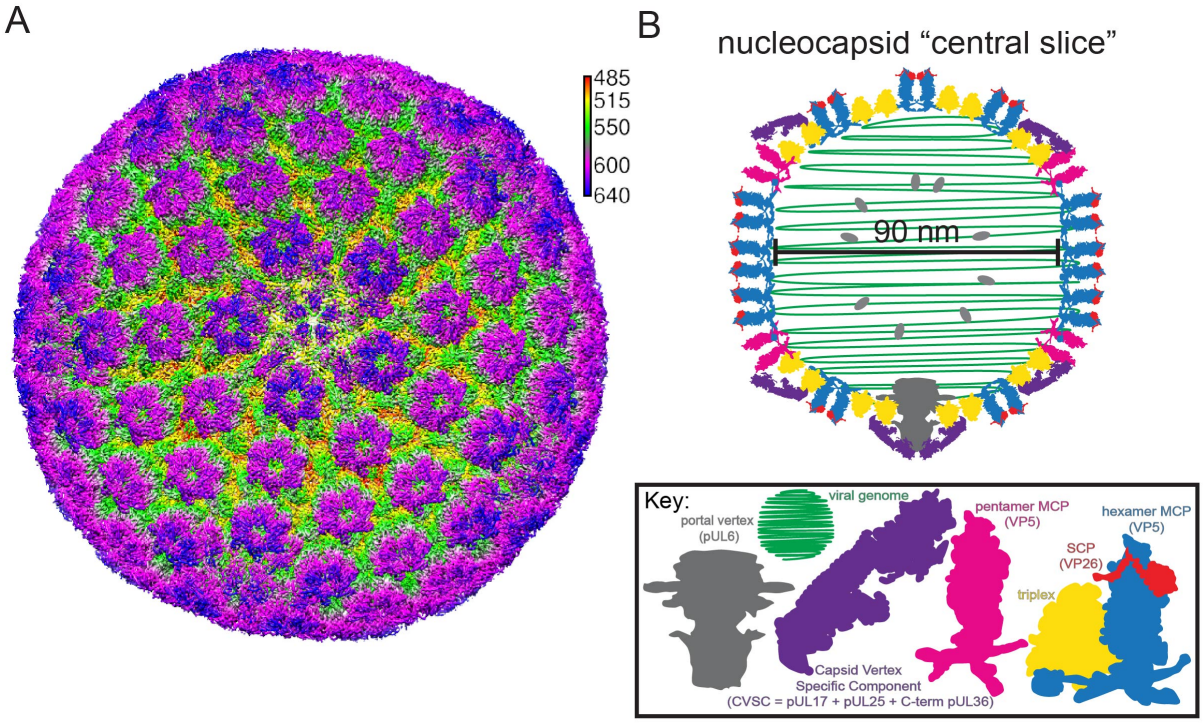

Figure 1.4 The herpesvirus nucleocapsid structure. (A) The 6.8 Å density map of the HSV-1 nucleocapsid (EMD-6386). The capsid is radially colored from the center of the structure. (B) Cartoon representation of a nucleocapsid central slice. Capsid proteins were traced from the highest resolution models published to date (7, 88).

the remainder of the icosahedral lattice, with the exception of the unique portal vertex. Hexamers are crowned with the 12 kDa small capsid protein (SCP), and pentamers are associated with a complex called the capsid vertex specific component (CVSC), five copies of which radiate outward from the pentamers and serve as tegument binding sites (7, 42, 89-92). The CVSC consists of two structural proteins required for encapsidation – pUL17 and pUL25 – and more recently has been expanded to include the large tegument protein, pUL36 (4, 7, 93, 94). However, it is unclear at what step of the infectious cycle pUL36 is added onto the nucleocapsid.

Table 1.1 Structural Components of the Herpesvirus Capsid

Name	Abbreviation	HSV-1 protein(s)	Copies per capsid	Size (kDa)
major capsid protein	MCP	VP5	955	149
portal vertex	-	pUL6	12	74
triplex	-	VP19c, VP23	640, 320	34, 50
small capsid protein	SCP	VP26	900	12
capsid vertex specific component	CVSC	pUL17, pUL25, pUL36	70, 140, ≥ 120	74, 62
small scaffold	-	pUL26.5*	~ 1,900	40
large scaffold	-	VP21*	150	75
protease	-	VP24	150	24

*only present in procapsids (uncleaved form) and B capsids (cleaved form)

The MCP monomer is a large, tower-like protein divided into three domains. The floor domain shares a structural fold coined as nature's favorite building block – the Hawkin 97 (HK97) fold – found in archaeal, bacterial, and eukaryotic viruses (95). This coat protein fold affords the stability and flexibility required for capsid assembly and DNA packaging. The importance of MCP floor domain during formation of the herpesvirus nucleocapsid is well defined. The MCP amino-terminus, which maps to the floor domain, interacts with the carboxyl-terminus of viral scaffold proteins which are required to assemble the capsid shell (96). Mutations disrupting MCP-scaffold interactions prevents the closure of procapsid shells but also have been found to compensate for a lethal mutation blocking scaffold cleavage, a step required for DNA packaging (97-100). Additionally, the MCP floor domains of neighboring monomers form extensive contacts, providing structure and stability to the capsid shell (7, 8, 93). The MCP middle domain also stabilizes the capsid through interactions with other structural components of the capsid shell and closes capsomere channels in mature capsids (101-103).

Perhaps the most substantial difference between the nucleocapsids of herpesviruses is seen in the SCP which differs in size, sequence, and function between the three subfamilies. In

the gammaherpesviruses, stable capsids are not formed in the absence of the SCP (104-106). Additionally, betaherpesvirus replication requires the SCP, which for HCMV anchors the major tegument protein, pp150, to the capsid surface (5, 107, 108). In contrast, the alphaherpesviral SCP is non-essential for capsid formation, although viral production is decreased in a SCP-null mutant. Additionally, more recent work suggests the structural protein influences the incorporation of the CVSC and packaging of DNA (109-111). Lastly, the alphaherpesvirus SCP binding is restricted to hexamers while the beta- and gammaherpesviral SCP binds hexamers and pentamers (4-7). This distinction might be attributed to small structural differences found in the MCP upper domains, primarily where the SCP binds; however, the majority of the MCP tower shows substantial similarity (5, 6). Finally, all herpesviruses exhibit structural differences in MCP hexamers compared to pentamers. MCP pentamers maintain the HK97 fold in the floor domain but also show structural rearrangements compared to MCP hexamers, overall making pentamers taller and less wide than hexamers (5-8).

The structural complexity and mechanical strength of the herpesvirus nucleocapsid is extraordinary. While the most basic viral capsids are comprised of a single structural protein, 11 different structural proteins are required to form the herpesvirus nucleocapsid, eight of which are present in the mature virion. The ability of these viruses to orchestrate over 4,000 structural proteins to self-assemble into such a massive particle is truly a marvel of nature.

Nucleocapsid Assembly and Maturation

Herpesvirus nucleocapsids form through an assembly and maturation pathway that is similar to that of tailed DNA bacteriophages, such as phage P22 and λ. In both viral pathways, an empty, scaffold-dependent precursor structure is built and filled with DNA through a unique

portal vertex. During this process, the capsid undergoes structural changes such as the release of the scaffold proteins from the capsid interior. While some bacteriophage recycle scaffold proteins, others proteolytically process the internal scaffold proteins leaving behind a small fragment (112).

Both bacteriophage and herpesvirus encode powerful terminase complexes which tightly package the viral DNA achieving a liquid-crystalline state which exerts extreme pressure on the capsid shell (9, 113). While some phage like P22 carryout headful packaging, herpesvirus cleave and package the genome at unit length (114). In both cases, the terminase machinery cleaves concatemeric DNA. The terminase machinery of bacteriophage consists of three parts: the portal, and a small and large terminase. The portal is a component of the capsid but the terminase proteins transiently associate with the capsid during packaging. The small terminase recognizes DNA while the large terminase is an ATPase, providing the power needed for genome packaging. The herpesvirus terminase machinery is comprised of proteins similar to bacteriophage: a portal, an ATPase, and a DNA binding protein. However, herpesvirus encodes a fourth terminase protein that interacts with all other components of the terminase machinery and is required for the cleavage and packaging of DNA into capsids (83, 115).

In addition to sharing similar capsid morphogenesis pathways, herpesvirus capsid proteins structurally resemble that of bacteriophage. The herpesvirus MCP is a large extension of the HK97 fold which is found as the major architectural element of icosahedral capsids. Additionally, despite little to no similarity in the primary amino acid sequences of bacteriophage and herpesvirus portal proteins, the products exhibit striking structural similarity.

The extensive knowledge of bacteriophage assembly informs hypothesis-driven studies of herpesvirus capsid morphogenesis. The field's current understanding of herpesvirus capsid

assembly and maturation is educated by findings from both *in vivo* and *in vitro* experiments, which includes analyses of baculovirus and cell-free systems (116-121), temperature-sensitive mutants (122, 123), and three-dimensional reconstructions from cryo-EM (4, 7, 93, 101-103, 124). Although many questions remain, decades of published work provide an overarching model of alphaherpesvirus capsid morphogenesis (Fig. 1.5).

The procapsid outer shell and inner scaffold simultaneously self-assemble to first form an arc-like structure or a partially-formed procapsid. The structure continues to grow until a closed, spherical structure, or fully-formed procapsid, is built (119). The initial building blocks required are the MCP, triplex, portal vertex, and two types of scaffold proteins – large and small. Once assembly of the spherical procapsid is complete, the catalytic activity of the viral protease, housed within the amino-terminus of the large scaffold protein, is triggered (125, 126). The protease autocatalytically releases from the scaffold by cleaving at a release site. Also, the protease disconnects the scaffold from the inner capsid floor by cleaving a second site, called the maturation site, which is located in the carboxyl-terminus of the small and large scaffold proteins (119, 127-131). A small piece – 25 amino acids – of the scaffold protein is required for assembly of closed capsids and, presumably, remains bound to the MPC floor domain (96, 120, 132, 133).

The event that triggers procapsid maturation is unknown, but it is dependent upon activation of the protease which is induced by dimerization *in vitro* (134). Furthermore, it has been observed that *in vitro* procapsids gradually convert to the angularized form and can lose the internal scaffold when incubated long-term at room temperature (119, 124). A temperature-sensitive protease mutant revealed that scaffold cleavage in infected cells requires the activity of the protease but does not require an energy source such as cellular adenosine triphosphate (ATP)

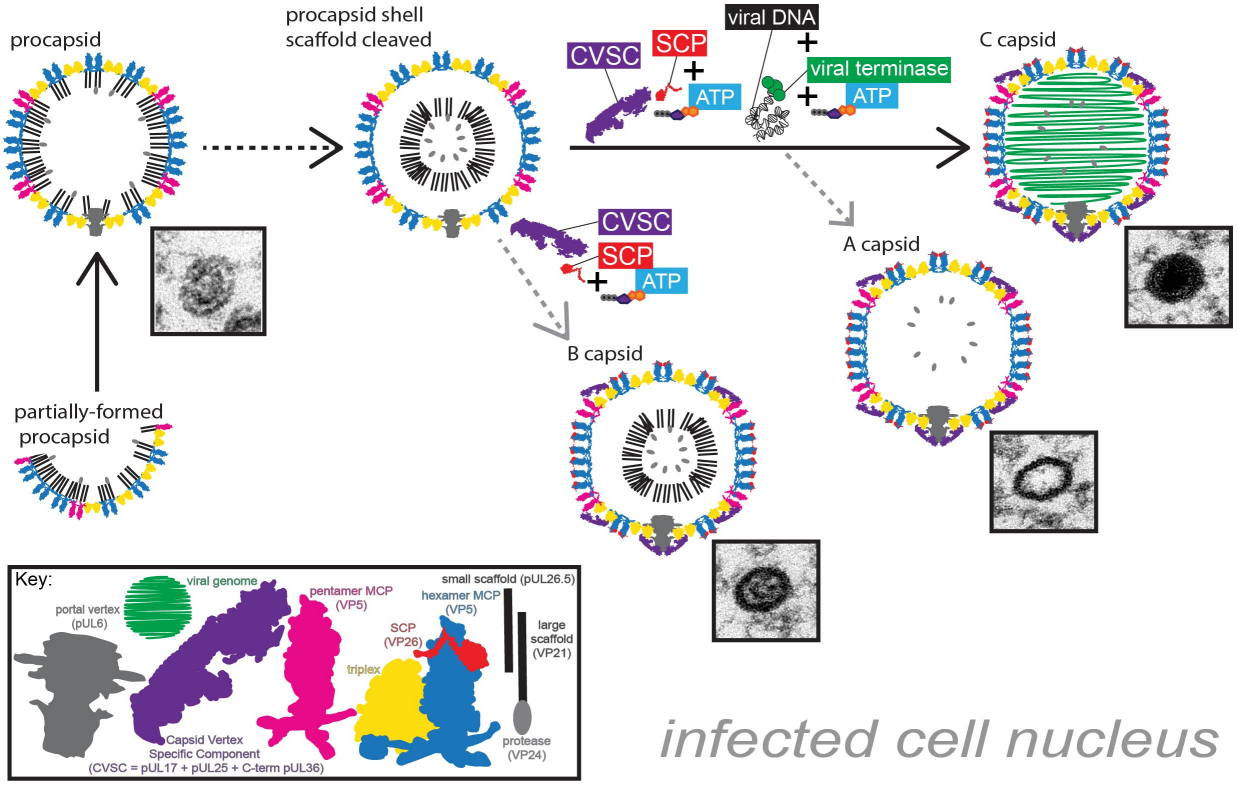

Figure 1.5 A model of herpesvirus nucleocapsid assembly and maturation. Herpesvirus capsid morphogenesis takes place in the infected cell nucleus in which four capsid types are found: procapsids, A, B, and C capsids. An ultrastructural example of each capsid species is shown. Assembly begins as the outer shell and inner scaffold simultaneously self-assemble, giving rise to the partially-formed procapsid. The structure continues to grow until a spherical, closed-shell procapsid is formed. Procapsid maturation is triggered by an unknown mechanism but is dependent on the internal protease which autocatalytically releases from the large scaffold protein and subsequently releases the small and large scaffold fragments by cleavage. This process is ATP-independent and can be decoupled from shell angularization when ATP-hydrolysis is inhibited by azide (dashed black arrow). Transformation of the procapsid shell into the angular form, the recruitment of the SCP, and DNA-packaging are all ATP-dependent and presumed to be coupled. The CVSC is also added after shell angularization. Shell transformation and encapsidation result in three angularized capsids with similar shell exteriors – the CVSC and truncated form of pUL36 are enriched on C capsids. However, with the exception of the

protease, the internal contents of these capsids differ: A capsids are empty, B capsids cleave but retain the scaffold proteins, and C capsids encapsidate the viral genome.

(123, 135). However, other events of capsid morphogenesis – the angularization of the shell, the addition of the SCP, and DNA packaging – require ATP (135, 136).

Angularized capsids are only observed following proteolytic processing of scaffold proteins or loss of scaffold proteins through weakened interactions with the capsid floor (97, 98). These events presumably allow the capsid shell to angularize or transform into a polyhedral shell considering the CVSC, SCP and genome packaging are not required for shell transformation (62, 117, 137, 138). Upon angularization, new epitopes are exposed making the shell surface a substrate for the binding of accessory capsid-surface proteins: the CVSC and the SCP (126, 127, 136, 139). Expulsion of the large and small scaffold proteins is thought to be coupled with DNA packaging but shell angularization can be decoupled from encapsidation (62). The scaffold fragments internal to the capsid are expelled as the viral genome is packaged but the protease is retained (10, 11, 62, 126, 140-142). This process produces three angularized capsid types within infected cell nuclei: capsids that retained the cleaved scaffold proteins and lack DNA (B capsids), capsids that expelled the scaffold but failed to encapsidate the viral genome (A capsids), and nucleocapsids (C capsids).

A total of seven viral proteins are required for the cleavage of the viral DNA to unit length from a replicating concatemer and packaging into the capsid: the portal vertex (pUL6), the CVSC components pUL17 and pUL25, the terminase proteins (pUL15, pUL28, and pUL33), and a putative oxidoreductase (pUL32). The terminase complex associates with procapsids as well as angularized capsids and consists of an ATPase (pUL15), a DNA binding protein (pUL28), and a

bridging protein (pUL33) (126, 143-147). The portal vertex, through which the DNA is inserted, binds the terminase to facilitate encapsidation (143, 146, 148). The role of pUL32 in encapsidation remains elusive: it is required for genome cleavage and packaging, and deletion of UL32 results in fully assembled procapsids that cannot initiate the encapsidation process (64, 149, 150). Although a lack of evidence for capsid or virion association suggests pUL32 does not directly associate with either structure, the protein has been identified in the virion by mass spectrometry (10).

Herpesvirus procapsids undergo dramatic conformational changes during capsid maturation. The procapsid structure is fragile, unstable, and cold-sensitive, making it difficult to isolate by traditional methods used for sturdy, angularized capsids (119, 128). However, successful procapsid isolation has been achieved through the use of procapsid mutants, immuno-precipitation, and carrying out procedures at room temperature, ultimately enabling the visualization of the procapsid structure by cryo-EM. The procapsid is spherical in shape, the MCP monomers make little contact with neighboring monomers in the capsomere except in the floor domain, the capsomere channels are open, and the capsid floor contains gaps (102, 103, 124). Obtaining the procapsid density map further revealed the changes that take place during maturation of the precursor structure into the angularized capsid. In contrast to the procapsid, the angularized capsid is polyhedral in shape, the MCP monomers are tightly clustered within the capsomere, the capsomere channels are mostly closed, and the capsid floor restructures to form a continuous shell.

The appearance of three angularized capsid species within herpesvirus infected cell nuclei is not fully understood but may imply the formation of nucleocapsids (C capsids) is an event that requires significant coordination of viral proteins and cellular ATP. Although B

capsids were originally classified as an intermediate in the maturation pathway, evidence suggests both A and B capsids are defective, or abortive capsids. First, A and B capsids are infrequently found outside of the infected cell nuclei, suggesting they are seldom selected for egress by the viral nuclear egress machinery (86, 123, 151-157). Second, with the exception of pUL25, the absence or disrupted function of the encapsidation proteins results in the accumulation of only B capsids. Therefore, B capsids likely represent capsids that undergo angularization in the absence of encapsidation. Furthermore, B capsids are unlikely to be intermediates that will proceed to DNA packaging considering the scaffold proteins may be trapped inside the shell. Cleaved scaffold proteins presumably must escape the interior through the hexamer and pentamer channels considering DNA is packaged through the opening of the unique portal vertex (158, 159). Procapsid hexamer and pentamer channels are open with diameters of approximately 40 Å and 30 Å, respectively (103, 159). However, in B capsids the hexamer channels have a diameter of 10 Å at their most narrow point and pentamer channels are closed (8). Thus, if scaffold proteins are expelled via hexamer or pentamer channels, these proteins must escape prior to shell angularization. Finally, A capsids appear to be failures of stable DNA encapsidation as they lack the scaffold proteins as well as DNA. A pUL25-null virus successfully cleaves and packages DNA, yet, these capsids are not stable in the absence of the vertex reinforcement protein, and results in an abundance of A capsids isolated from nuclei (65, 137).

The CVSC components, which are largely added after shell angularization, influence each other's incorporation onto the capsid shell, are found in greater abundance on nucleocapsids compared to abortive capsids, and provide the mechanical reinforcement needed to maintain the DNA inside the shell despite the extreme pressure exerted by the tightly packed genome (9, 94,

139, 160-164). The pUL17 component of the CVSC is found on procapsids and is implicated in encapsidation considering a null mutant produces only B capsids in infected cell nuclei (126, 139, 165). Together, the CVSC promotes the escape of nucleocapsids from the nucleus with pUL25 providing a direct link to the machinery that facilitates this translocation, the nuclear egress complex (66, 67).

At a minimum, self-assembly of a HSV-1 capsid shell in baculovirus systems requires the MCP, triplexes, and scaffold (116-118). This differs from beta- and gammaherpesviruses that also require the SCP for shell assembly (104, 105). Protein shells built from these components are incapable of encapsidating the viral genome without the portal vertex but are capable of undergoing shell angularization (119). For alphaherpesviruses, the accessory proteins – the CVSC and the SCP – are not required for the formation of the procapsid or angularized capsid shell, however, these proteins are important in packaging and maintaining the viral genome within the shell (110, 138, 160, 161, 165-167).

The herpesvirus assembly and maturation pathway is essential for viral replication. This process is a target for antiviral development (82, 168-175), which is bolstered by ongoing refinements of cryo-EM reconstruction techniques that have led to herpesvirus capsid models with near-atomic resolution (5-8). Despite a wealth of knowledge, many details of the molecular mechanisms driving procapsid assembly and maturation remain enigmatic.

Interactions at the Capsid Surface

Interactions at the capsid surface are essential during the herpesvirus infectious cycle. Failure of the nucleocapsid to dock and release the viral genome through the nuclear pore terminates the cycle. Similarly, failure of the virus to assemble nascent nucleocapsids that escape

the nucleus and form mature virions limits the infection to the initial host cell, preventing the virus from achieving the lifelong goal of latent infection within the nervous system.

Several structural proteins – the CVSC, the SCP, the MCP, and the portal vertex – decorate the nucleocapsid surface and are available for extrinsic interactions with viral or cellular proteins. The triplexes are buried approximately 100 Å below the tips of the MCP and thus, are not considered to be surface exposed. Figure 1.6 illustrates the surface of the herpesvirus nucleocapsid zoomed in on a vertex. The most prominent feature of the capsid surface is the MCP comprising the hexamers and pentamers which occupy the largest amount of space within the capsid. Hexamers are capped by the SCP, making the accessory protein the most abundant capsid-surface protein of the mature, angularized capsid. Alphaherpesvirus pentamers fail to bind the SCP, leaving the MCP exposed at the capsid vertices. Surrounding the pentamer is five copies of a complex called the CVSC, which sits on top of the buried triplexes and leans on the outer face of the pentamer. The CVSC is comprised of two proteins: pUL17 and pUL25. The pUL25 protein is proximal to the pentamer and is now known to be a dimer, for a total of 10 copies of pUL25 reinforcing each capsid vertex. Recently, it was determined that the CVSC surrounds the portal vertex as well (88).

Capsid surface interactions have been described for most steps of the herpesvirus infectious cycle. However, despite the abundance of proteins reported to interact with capsid constituents, only a handful of these interactions are directly with the intact capsid (Table 1.2). The nucleocapsid surface is mostly covered with the SCP. In the betaherpesvirus HCMV, the SCP anchors the essential large tegument protein to the capsid surface (5, 107). In the alphaherpesviruses, the SCP was proposed to contribute toward nucleocapsid transport due to its interaction with several dynein light chains (176-178). However, support for this role deflated as

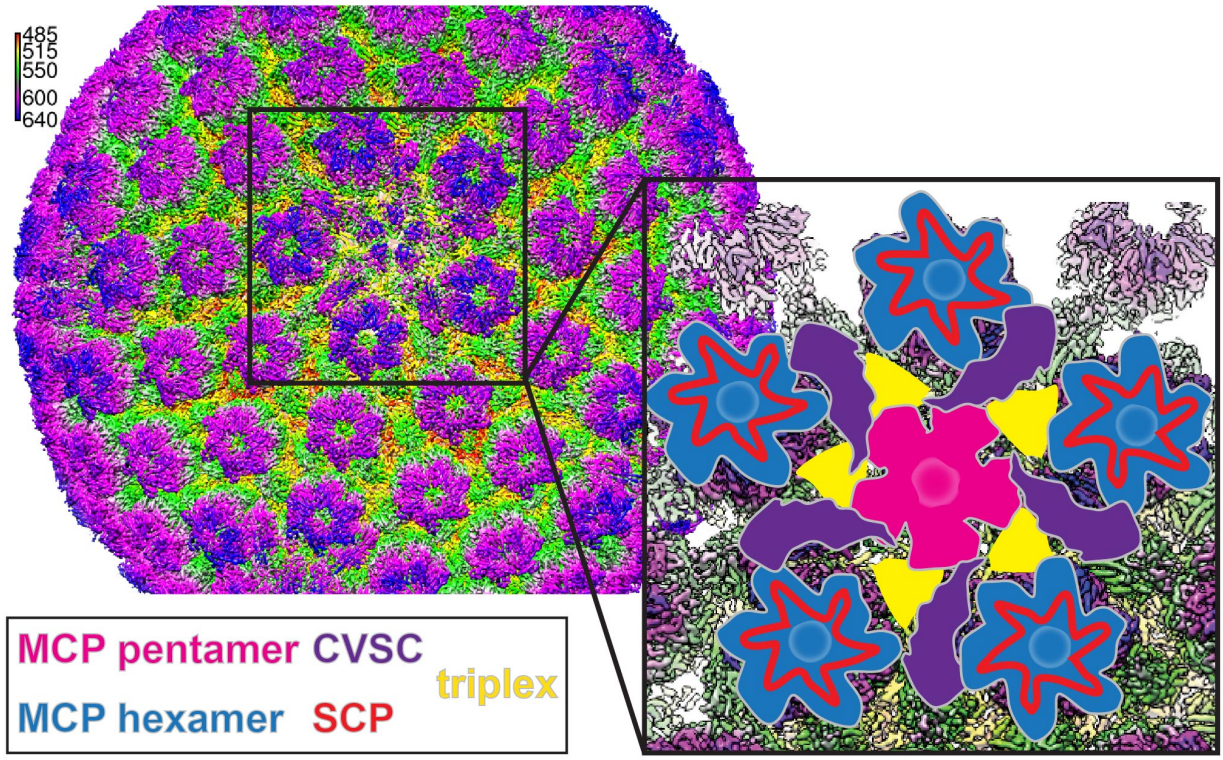

Figure 1.6 The face of the herpesvirus nucleocapsid. The 6.8 Å map of the HSV-1 nucleocapsid (EMD-6386)(93). The capsid is radially colored from the center of the structure and positioned to display a capsid vertex. On the right is a cartoon depiction with a color-coded key to the lower left. At a single vertex of the capsid, the portal replaces the position of the MCP pentamer.

deletion of the SCP does not impact capsid transport (179, 180). The large tegument protein, pUL36, directly binds the capsid vertices through an interaction with the CVSC component pUL25 (181). An additional tegument protein, pUL37, binds pUL36 and together these capsid-bound tegument proteins are effectors of intracellular trafficking, contributing to neuronal transmission and retrograde axonal transport (35, 39-41). A third viral protein, the serine-threonine kinase, pUS3, is also found to cotransport with the capsid following entry and is tethered to the capsid via pUL36 (37, 182, 183).

Table 1.2 Interactions at the Herpesvirus Capsid Surface

Interactor	Capsid binding site	Step of infectious cycle*
pUL36	CVSC (pUL25)	4-5, 10-12, 13
Nucleoporins (CAN/Nup214 and hCG1)	CVSC (pUL25)	5
terminase complex (pUL15 + pUL28 + pUL33)	portal vertex and others?	8
pUL31	CVSC (pUL25) and others?	9-10

*Numbers correspond to Figure 1.3

After entry, the nucleocapsid transports toward the nucleus and docks at a nuclear pore to inject the viral genome. The means by which the nucleocapsid docks at the nuclear pore complex is poorly understood but evidence suggests the CVSC component pUL25 interacts with nucleoporins such as CAN/Nup214 and hCG1 (46). However, how the nucleocapsid positions itself so that the portal vertex faces the nuclear pore opening remains a mystery. The surface anchored large tegument protein, pUL36, serves an additional role with the nucleocapsid post-entry as the cleavage of this protein is required for genome release (47).

Injection of the viral genome into the infected cell nucleus initiates viral gene expression ultimately leading to the production of capsid proteins and the assembly of nascent procapsids. After the procapsid is assembled, DNA is packaged via the viral terminase complex. The terminase complex consists of three proteins, two of which interact with the capsid surface through the portal vertex (143, 146, 148). However, all three terminase components associate with capsids lacking the portal vertex, albeit at reduced levels, suggesting the terminase binds more than one capsid protein (144, 145).

Once the nucleocapsid is formed, the structure must escape the nucleus to form the mature virion within the cytoplasm. Herpesviruses undergo an elaborate two-step egress mechanism that begins with the interaction of the nucleocapsid with the virally encoded nuclear egress machinery which causes budding at the inner nuclear membrane (184-186). The nuclear egress complex consists of, at a minimum, two proteins: pUL31 and pUL34. In HSV-1, the nucleocapsid surface interacts with pUL31 through the CVSC component pUL25 (66, 67). In PRV, this interaction is most evident in the absence of pUL34; however, the capsid-binding site remains unknown as this interaction is not mediated by pUL25, the portal vertex, or the terminase component, pUL33 (65).

A myriad of viral and cellular proteins are implicated as enhancers of nuclear egress, many of which demonstrate interaction with the nuclear egress complex (156, 187-189). However, evidence of a direct link to the capsid exists for two of these proteins: pUL36 and pUL47. The PRV large tegument protein produces a truncated species that associates with nuclear capsids, but is enriched on nucleocapsids, and its binding is dependent on the CVSC component pUL25 (156). The interaction of full-length pUL36 and its binding partner, pUL37, has been demonstrated with HSV-1 nuclear capsids (178, 190), and both proteins appear to influence efficient nuclear egress (191, 192). The highly abundant tegument protein, pUL47, was found to interact with the CVSC component pUL17, however, it is suspected that the pUL17-pUL47 interaction takes place apart from the nucleocapsid considering this interaction is maintained in the absence of capsids (193). Additionally, pUL47 interacts with the nuclear egress complex (pUL31 and pUL34) as well as the kinase, pUS3 (187). It remains unclear if these proteins exclusively form a complex apart from capsids or if this complex directly binds the megastructure surface during nuclear egress.

Finally, capsid surface interactions are essential during viral egress in the cytoplasm. Both pUL36 and pUL37 are required for envelopment with null mutants accumulating unwrapped nucleocapsids in the cytoplasm of infected cells (192, 194). Another protein that associates with cytoplasmic nucleocapsids – independently of pUL36 and pUL37 – and is involved in their proper envelopment, is the tegument-envelope bridging protein, pUL16 (195). This tegument protein exhibits a dynamic interaction with the capsid surface as it is stably bound to cytoplasmic capsids through an unknown capsid-surface protein, yet, this interaction is largely lost in the virion (196, 197). The tegument protein pUL21 is a binding partner of pUL16 and was detected in gradient fractions containing capsids; however, the protein was detected throughout the gradient and was not enriched in capsid-containing fractions (198).

The herpesvirus nucleocapsid has long been viewed as a static protein coat whose only role is to protect the viral genome. The literature demonstrates numerous viral proteins that interact with the nucleocapsid in order to orchestrate the events necessary for its delivery to the nucleus, encapsidation of the viral DNA, and egress from the nucleus and cytoplasm. Thus, the structural components of the capsid surface appear to serve as anchor points for other proteins to attach to and perform their intrinsic functions.

Summary and Contribution to Knowledge

Herpesviruses assemble capsids and encapsidate their genomes by a process that is unlike most other mammalian viruses but is similar to some bacteriophage. Many important aspects of herpesvirus morphogenesis remain enigmatic, including how the capsid shell matures into a stable angularized configuration. The event that initiates procapsid maturation is unknown, but it is dependent upon activation of the internal protease. Scaffold cleavage triggers angularization of

the shell and its decoration with the SCP and CVSC. In both the procapsid and mature angularized capsid, the apical region of the MCP is surface exposed. This dissertation reports on the fortuitous discovery that a region of the major capsid protein that is exposed on the outer surface of the capsid also contributes to capsid maturation, demonstrating that the morphogenesis of the capsid shell from its procapsid precursor to the mature angularized form is dependent upon internal and external components of the megastructure. In addition, this dissertation presents a modified fluorescent fusion design that produced the first described procapsid-specific tag.

CHAPTER 2: Materials and Methods

Structural modeling

Chapter 1 Using UCSF Chimera (199) the previously published density map of HSV-1 (EMDB: EMD-6386) (93) was radially colored.

Chapter 3 Using UCSF Chimera (199) the structure of the upper domain of HSV-1 VP5 (PDB: 1NO7) (158) was fit in both the pentamer and the peripentonal hexamer of the previously published density map of the HSV-1 (EMDB: EMD-6386) (93).

Sequences and alignment

Chapter 4

Major capsid protein amino acid sequences obtained from GenBank are listed in order of appearance from top to bottom of the alignment in Figure 3.1E: GU734771, Z86099, NC_004812, JF797219, AJ004801, AY665713, NC_002686.2, and NC_001348.1. Protein sequences were aligned using the ClustalW alignment tool in MacVector.

Cells and virus

Chapter 3 - 6 Vero (African green monkey kidney epithelial) and Vero cells expressing Cre recombinase (Vero-CRE) were maintained in Dulbecco's Modified Eagle Medium (DMEM) (Invitrogen, Catalog #11965-118) supplemented with 10% bovine growth serum (BGS) (vol/vol) (Rocky Mountain Biologicals, Catalog #FGR-BBT). The latter were generously provided by Dr. David Leib (200). For UL25-null and UL26 S129P mutants, viral stocks were grown on Vero 8-

1 (138) and Vero 26-13 complementing cells, respectively, generously provided by Dr. Fred Homa. Cultured cells were tested for *Mycoplasma* contamination with the PlasmoTest Mycoplasma Detection Kit (InvivoGen, Catalog #rep-pt1). Primary sensory neurons were isolated from the dorsal root ganglion (DRG) of embryonic chicks (E9-10) and cultured as whole explants as previously described (201). Tables 3.1, 4.1, 5.1, and 6.1 detail the recombinant viruses used in this dissertation. Mutation of UL19 (encodes VP5), UL35 (encoded VP26), or insertion of coding sequences for fluorescent proteins was achieved by a two-step RED-mediated recombination method (202). Primers used for BAC mutagenesis are listed in Table 2.1. Mutations were sequence confirmed at the Northwestern University Genomics Core Facility. HSV-1 recombinant viruses were produced by electroporation of the infectious bacterial artificial chromosome (BAC) clone of HSV-1 strain F, pYEbac102, into Vero cells (203). Recombinant viruses were subsequently propagated on Vero-CRE cells to excise the loxP-flanked BAC backbone from the viral genome and produce a working stock of virus. All viral stock titers were determined by plaque assay on Vero cells overlaid with DMEM supplemented with 10 milligram (mg)/milliliter (mL) methyl cellulose (VWR, Catalog #AA36718-36), Penicillin-Streptomycin (Pen-Strep) at 100 U/mL (Invitrogen, Catalog #15140122), and 2% BGS.

Plaque assays

Chapters 3-6 Plaque assays used for plaque diameter measurements were incubated 5 days post infection and then stained with Neutral Red (Santa Cruz, Catalog #sc-281691). Cells were gently rinsed with phosphate buffered saline (PBS) before adding 1 mL of 1:1 Neutral Red and PBS. After 1 hour, stain was replaced with PBS and plaques were imaged on an Epson Perfection V500 Photo scanner at 3,200 dots per inch. Plaque diameters were determined by averaging two

orthogonal diameter measurements for each individual plaque. Plaque diameters were then expressed as percent of wild-type (WT) mean plaque diameter and plotted in Prism 7 (Graphpad). In Chapters 3-5, more than 85 plaques were measured for each virus. In Chapter 6, more than 40 plaques were measured with the exception of the fluorescently-tagged Δ6F10 mutant in which only 13 plaques were visible for measurement. Statistically significant differences were determined by a one-way ANOVA analysis with Tukey's multiple comparisons post-test.

Virus propagation

Chapters 4 Single-step growth curves were determined as previously described (204) with the following changes. In brief, Vero cells seeded in 6-well plates were infected at a multiplicity of infection (MOI) of 10. After 1 hour, unabsorbed virus was inactivated with 1 ml of citrate buffer (pH 3.0), cells were washed, and then incubated in 2 mL of DMEM supplemented with 2% BGS at 37˚C, 5% carbon dioxide (CO_2). Cell-associated and extracellular virus was harvested at 2, 5, 8, 12, 24, and 30 hpi. Titers were determined in duplicate by thawing and sonicating samples and performing plaque assays on Vero cells.

Live-cell fluorescence microscopy

Chapter 3 To monitor capsid retrograde axonal transport, whole-explant chick DRGs were infected, imaged, and analyzed as previously described (205) with the following changes. Imaging began approximately 30 minutes after infecting DRGs with 3-5 x 10^7 plaque forming units (PFU). Live-cell images were captured on an inverted wide-field Nikon Eclipse TE2000-U microscope fitted with a 60x/1.40 numerical aperture (NA) objective and a Cascade II:512

camera. Red fluorescence emissions were captured at 100 millisecond (ms) exposures with the camera's digitizer set 10 megahertz (MHz) with 4,095 electron-multiplying (EM) gain for 250 frames. Run-velocities and run-distances traveled were determined by kymograph analysis. Viral particles with a forward (retrograde) motion > 0.5 micrometers (μm) were plotted on a histogram as fraction of total particles and run-velocities or run-distances were fit to a Gaussian or decaying exponential curve with a non-linear regression, respectively. More than 150 runs were measured for each virus.

For live-cell imaging of infected epithelial cells, Vero cells were seeded on flame-sterilized 22 x 50 millimeter (mm) No. 1.5 cover glass and infected at a MOI of 5. After 1 hour, inoculum was replaced with F12 media supplemented with 2% BGS and Pen-Strep. VALAB chambers were made on 25 x 75 x 1mm slides as previously described (201) at 8.5 hpi – a time when viral capsids can readily be observed in infected cell nuclei (62, 123). Slides were imaged with a 100x lambda/1.49 NA objective on a Nikon Ti inverted microscope housed in an environmental box set at 37˚C (InVivo Scientific) and coupled with a CSU-W1 confocal head (Yokogawa Electric Corporation) and a CascadeII:1024 EM-CCD (Photometrics). Illumination was supplied by a Sapphire 561 nm laser (Coherent) and custom laser launch (Solamere Technology Group, Inc.). Red fluorescence emissions were captured with 4,000 ms exposures with the digitizer set to 1 MHz zero EM gain. Differential interference contrast (DIC) images were captured with 200 ms exposures, 1 MHz zero EM gain.

Chapter 6 For live-cell imaging of infected epithelial cells, Vero cells were seeded on flame-sterilized 22 x 50 mm No. 1.5 cover glass and infected at a MOI of 3. After 1 hour, inoculum was replaced with F12 media supplemented with 2% BGS and Pen-Strep. At 12 hpi, VALAB

chambers were made on 25 x 75 x 1mm slides as previously described (201). Between 12-12.5 hpi, infected Vero cells were imaged by confocal microscopy on a Nikon Ti inverted microscope fitted with a 60x/1.49 NA objective as described above. Red fluorescent protein (RFP) and green fluorescent protein (GFP) emissions were captured sequentially using 5,000 ms and 500 ms exposures, respectively, with 5 MHz digitizer and zero EM gain.

Dual-fluorescent imaging of released particles

Chapter 5 Extracellular viral particles were collected from infected cell supernatant and imaged as previously described (205) with the following modifications. Vero cells were infected at a MOI of 5. Infected cell supernatant was harvested at 18.5 hpi. Particles were diluted 1:10 in PBS and imaged with a 60x/1.40 NA on an inverted wide-field Nikon Eclipse TE2000-U microscope as described above. RFP and GFP emissions were captured sequentially using 1,700 and 1,500 ms exposures, respectively, with 1 MHz digitizer and zero EM gain.

Chapter 6 Extracellular viral particles were collected from infected cell supernatant as previously described (205) with the following modifications. Vero cells were infected at a MOI of 3. Infected cell supernatant was harvested at 22 hpi. Particles were diluted 1:10 in PBS and imaged with a 100x lambda/1.49 NA objective on a Nikon Ti inverted microscope as described above. RFP and GFP emissions were captured sequentially using 200 ms exposures, with 5 MHz digitizer and 4,095 EM gain.

Immunofluorescence assays

Chapter 4 & 5 Vero cells seeded on flame-sterilized cover glass were infected at a MOI of 5 for 1 hour and then incubated in DMEM supplemented with 2% BGS at 37˚C, 5% CO_2. At the indicated time post-infection, infected cells were washed with PBS and then fixed in 4% paraformaldehyde for 15 minutes. Fixed cells were rinsed three times with PBS and then permeabilized in PBST [0.1% Triton X-100 in PBS] for 10 minutes. Permeabilized cells were blocked in 5% bovine serum albumin (BSA) (Sigma, Catalog #A9647) in PBST for 45 minutes at room temperature (RT) or overnight at 4˚C. After blocking, fixed cells were reacted with primary and secondary antibodies each for 1 hour at RT protected from light. Primary antibodies were diluted in 1% BSA in PBST as follows: mouse monoclonal anti-VP5 H1.4 (Meridian Life Science, Inc., Catalog #C05014MA) at 1:30, mouse monoclonal anti-VP5 8F5 (kindly provided by Duncan Wilson) at 1:100, and rabbit anti-VP26 (kindly provided by Prashant Desai) at 1:2,000. Secondary antibodies were diluted in 1% BSA in PBST as follows: goat anti-mouse Alexa Fluor 488 (Thermo Fisher Scientific, Catalog #A-11001) at 1:400 and goat anti-rabbit Alexa Fluor 568 (Thermo Fisher Scientific, Catalog #A-11011) at 1:400. Cover glass was mounted on slides with ProLong Gold with DAPI mounting media (Thermo Fisher Scientific, Catalog #P36931). Slides were imaged by confocal microscopy on a Nikon Ti inverted microscope fitted with a 60x/1.49 NA objective as described above. Blue, green, and red emissions were captured with 1 MHz zero EM gain at the following exposures: DAPI 2,000 ms, αVP5 (H1.4 and 8F5) 200 ms, αVP26 200 ms, mCherry-VP24 4,000 ms, and pUL25/mCherry 5,000 ms. DIC images were captured with 200 ms exposures with 1 MHz digitizer and zero EM gain.

Transmission electron microscopy

Chapter 4 Vero cells seeded in a 10-centimeter (cm) dish were infected at a MOI of 5 for 1 hour and then incubated in DMEM supplemented with 2% BGS and Pen-Strep at 37˚C, 5% CO_2. At the indicated time post-infection, infected cells were rinsed with PBS and fixed in 2.5% glutaraldehyde in 100 millimolar (mM) cacodylate buffer for 60 minutes at RT. After fixation, cells were scraped into fixative and transferred to an Eppendorf tube. Fixed cells were pelleted at 300 x g for 10 minutes. The cell pellet was enrobed in 5% low-melting point agarose (SeaPlaque® Agarose, Catalog #50101) and delivered to Northwestern University's Center for Advanced Microscopy to be processed for transmission electron microscopy. In brief, the agarose plug was post-fixed with 1% Osmium tetroxide, stained with 0.5% uranyl acetate, dehydrated in ascending grades of ethanol from 30-100%, infiltrated with propylenoxide and embedded in hard resin. Blocks were thin sectioned at 50-60 nm and stained with uranyl acetate and Reynolds lead citrate. Slices were mounted on 200 mesh copper grids (Electron Microscopy Sciences). Imaging was performed on a FEI Tecnai Spirit G2 transmission electron microscope at the Northwestern University Center for Advanced Microscopy generously supported by NCI CCSG P30 CA060553 awarded to the Robert H Lurie Comprehensive Cancer Center.

Intranuclear capsid isolation

Chapter 4 & 5 Isolation of intranuclear capsids was performed as previously described (65) with the following changes. Vero cells were seeded in 15-cm dishes and infected at a MOI of 10 with five dishes per virus. Infected cells were harvested between 22-24 hpi. A, B, and C capsid bands were pulled from the 20-50% sucrose gradient using a Gradient Fractionator (BioComp Instruments).

Silver staining of isolated intranuclear capsids

Chapter 4 Each capsid species was subsequently diluted in a total volume of 2 mL of TNE [20 mM Tris pH 7.6, 500 mM sodium chloride, 1 mM ethylenediaminetetraacetic acid] supplemented with 10 microliters (μL) of protease inhibitor cocktail (Sigma, Catalog #P8340) and pelleted in a Beckman SW50.1 rotor at 74,909 x g for 1 hour and 4 minutes at 4˚C. Pelleted capsids were resuspended in 50 μL of 5x final sample buffer (FSB) [60 mM Tris HCl pH 6.8, 2% SDS, 10% glycerol, 0.01% bromophenol blue] supplemented with 5% β-mercaptoethanol and stored at -20˚C. Resuspended capsids were thawed, boiled for 5 minutes, and loaded in equal volumes on a 4-20% Mini-PROTEAN TGX Gel (Catalog #456-1096) with Bio-Rad Dual Color standards (Bio-Rad, Catalog #1610374) diluted 1:100 in 5x FSB supplemented with 5% β-mercaptoethanol. Proteins were then detected using the Pierce Silver Stain Kit (Thermo Fisher Scientific, Catalog #24612). The silver stained gel was imaged on an Epson Perfection V500 Photo scanner at 2,400 dots per inch.

Dual-fluorescent imaging of isolated intranuclear capsids

Chapter 5 Each capsid species was diluted 1:30 in PBS and pipetted into chamber slides comprised of plasma-cleaned 22 x 50 mm No. 1.5 cover glass and 25 x 75 x 1mm slide separated by pedestals, or four small shards of coverslip glass. Chambers were sealed with VALAB and imaged with a 60x/1.40 NA on an inverted wide-field Nikon Eclipse TE2000-U microscope as described above. RFP and GFP emissions were captured sequentially using 1,700 and 1,500 ms exposures, respectively, with 1 MHz digitizer and zero EM gain.

Preparation of cell lysates

Chapter 4 Vero cells seeded in a 10-cm dish were infected at a MOI of 5. After 1 hour, inoculum was replaced with DMEM supplemented with 2% BGS. At 8 hpi, cells were washed with 10 mL of ice cold PBS and lysed in 300 µL of RIPA buffer [50 mM Tris pH 8, 150 mM sodium chloride, 1% NONIDET P40 substitute, 0.5% sodium deoxycholate, 0.1% sodium dodecyl sulfate] supplemented with 5 mM dithiothreitol and protease inhibitors [2.5 mM sodium fluoride, 1 mM sodium orthovanadate, 0.5 mM phenylmethylsulfonyl fluoride, 100 µL of protease inhibitor cocktail (Sigma, Catalog #P8340)]. Cells were scraped into lysis buffer, transferred to an Eppendorf tube, and set on ice for 15 minutes. Lysates were then sonicated for three 1.5 second pulses and set on ice for an additional 15 minutes. Lysates were spun at 13,201 x g for 20 minutes and the supernatants were harvested. Total protein concentration of cell lysates was determined using the Pierce 660 nm Protein Assay Reagent (Thermo Fisher Scientific, Catalog #22660). Lysate absorbances were read at 650 nm wavelength on a Molecular Devices SpectraMax M5 Microplate Reader. Sample protein concentration was calculated from the standard curve of Pierce Pre-Diluted Protein Assay Standards: Bovine Serum Albumin Set (Thermo Fisher Scientific, Catalog #23208). Samples were diluted in 5x FSB supplemented with 5% β-mercaptoethanol and stored at -20˚C.

Western blot and densitometry analysis

Chapter 4 Cell lysates were thawed, boiled for 5 minutes, and loaded as three-fold dilutions in equal concentrations across samples on a 4-20% mini-PROTEAN TGX Gel (Catalog #456-1096). Bio-Rad Dual Color standards (Bio-Rad, Catalog #1610374) were also loaded to mark

molecular weights. Proteins were separated and transferred to a PVDF membrane (Millipore, Catalog #IPFL00010). The membrane was blocked in 5% milk for 80 minutes and then incubated overnight with primary antibodies diluted in 1% milk in PBST [0.1% Tween 20 in PBS] as follows: mouse monoclonal anti-VP5 H1.4 (Meridian Life Science, Inc., Catalog #C05014MA) at 1:1,000 and rabbit polyclonal anti-pUL37 (kindly provided by Frank Jenkins) at 1:500. The next day, the membrane was washed and incubated for 1 hour at RT with secondary antibodies diluted in 1% milk in PBST as follows: goat anti-mouse IRDye 800 CW (LI-COR Biosciences, Catalog #926-32210) at 1:10,000 and donkey anti-rabbit IRDye 680 RD (LI-COR Biosciences, Catalog #926-68073) at 1:10,000. The membrane was imaged on a LI-COR Odyssey FC imaging system at 700 nm and 800 nm wavelengths for 3 minutes and 30 seconds each wavelength. Next, the membrane was blocked again with 5% milk in PBS for 80 minutes and then incubated for 1 hour at RT with primary antibody mouse monoclonal αGAPDH [clone 6C5] (Abcam, Catalog #ab8245) diluted 1:500 in 1% milk in PBS. The membrane was washed and then incubated at RT for 1 hour with secondary antibody goat αmouse IRDye 800 CW at 1:10,000 and imaged on the LI-COR Odyssey FC imaging system at 700 nm for 3 minutes and 30 seconds.

Densitometry analysis was carried out using Image Studio Lite software. In brief, rectangles were added around each VP5 and pUL37 signal band with background subtraction set to median with a border width of 3 pixels on top and bottom. Boxes were adjusted, if needed, based on the profiles shape and intensity tools. The signal values for VP5 bands were calculated as a ratio to their corresponding pUL37 signal value. These ratio values were then normalized to wild-type samples.

Table 2.1 Primers Used to Construct Viruses Used in this Dissertation

Strain	Template	Primer Pair
HSVF-GS5798	pEP-KanS2	5’ TACGCCACCCTGCAGAACATGGTGGTCCCGGCGATCGCCCCCGGCGCGGAGTGCCCCAGCGA C**AGGATGACGACGATAAGTAGGG** 3’
		5’ GTGCAGGGGGTGCGCGGGGTCCGTCACGGGGTCGCTGGGGCACTCCGCGCCGGGGGCGATC GC**CAACCAATTAACCAATTCTGATTAG** 3’
HSVF-GS5799	pEP-KanS2	5’ GTGACGGACCCCGCGCACCCCCTGCACCCGGCCAATCTGGTGGCCGCGACCGTGGCCGCCAT GTTTCACAAC**AGGATGACGACGATAAGTAGGG** 3’
		5’ CATGGCGGGCCCGTCCACTACCACGCGCCCGTTGTGAAACATGGCGGCCACGGTCGCGGCCAC CAGATTGGC**CAACCAATTAACCAATTCTGATTAG** 3’
HSVF-GS5801	pEP-KanS2	5’ CCCCGGCGAGGAGTGCCCCAGCGACCCCGTGACGGACCCCGCGGCGCCGCTAGCCCCGGCCA ATCTGGTG**AGGATGACGACGATAAGTAGGG** 3’
		5’ GTTGTGAAACATGGCGTTGACCGTGTTGGCCACCAGATTGGCCGGGGCTAGCGGCGCCGCGG GGTCCGTCAC**CAACCAATTAACCAATTCTGATTAG** 3’
HSVF-GS5905	pEP-KanS2	5’ CCAGCGACCCCGTGACGGACCCCGCGGCGCCGCTAGCCCCGGCCGCTGCAGCGGCAAACGCG GTCAACGCCATGTTT**AGGATGACGACGATAAGTAGGG** 3’
		5’ CCGTCCACTACCACGCGCCCGTTGTGAAACATGGCGTTGACCGCGTTTGCCGCTGCAGCGGCC GGGGCTAGCGGCAAC**CAATTAACCAATTCTGATTAG** 3’
HSVF-GS6276	pEP-KanS2	5’ CCCCGGCGAGGAGTGCCCCAGCGACCCCGTGACGGACCCCGGAGGCAGCGGAGGATCCACG GTCAACGCCATG**AGGATGACGACGATAAGTAGGG** 3’
		5’ GTCCACTACCACGCGCCCGTTGTGAAACATGGCGTTGACCGTGGATCCTCCGCTGCCTCCGGG GTCCGTCACGGG**CAACCAATTAACCAATTCTGATTAG** 3’
HSVF-GS5748	pEP-mCherry-in	5’ GACCGTTGCGCCTTTTTTTTTTTTCGTCCACCAAAGTCTCTGTGGGTGCGCGCATG**GTGAGCAAG GGCGAGGAG** 3’
		5’ CAGGGGCTCCTCCATCCGGTCTCCCGGGGCATCGGCTGCACCACCTCCGCCACC**CTTGTACAGC TCGTCCATGC** 3’
HSVF-GS6460	pEP-mCherry-in	5’ GACCGTTGCGCCTTTTTTTTTTTTCGTCCACCAAAGTCTCTGTGGGTGCGCGCATG**GTGAGCAAG GGCGAGGAG** 3’
		5’ CAGGGGCTCCTCCATCCGGTCTCCCGGGGCATCGGCTGCACCACCTCCGCCACC**CTTGTACAGC TCGTCCATGC** 3’
HSVF-GS6493	pEP-mCherry-in	5’ GACCGTTGCGCCTTTTTTTTTTTTCGTCCACCAAAGTCTCTGTGGGTGCGCGCATG**GTGAGCAAG GGCGAGGAG** 3’
		5’ CAGGGGCTCCTCCATCCGGTCTCCCGGGGCATCGGCTGCACCACCTCCGCCACC**CTTGTACAGC TCGTCCATGC** 3’
HSVF-GS6197	pEP-KanS2	5’ CACCCTGCAGAACATGGTGGTCCCGGAGATCGCGCCCGGGGCGGAGTGCCCCAGCGAC**AGGA TGACGACGATAAGTAGGG** 3’
		5’ GGGGTGCGCGGGGTCCGTCACGGGGTCGCTGGGGCACTCCGCCCCGGGCGCGATCTCCAAC**C AATTAACCAATTCTGATTAG** 3’
HSVF-GS6434	pEP-KanS2	5’ CGCTTCGACCGCGTATACGCCACCCTGCAGAACATGGTGGTCCCGGCGATCGCCCCCGGCGAG **AGGATGACGACGATAAGTAGGG** 3’
		5’ GGGGTCCGTCACGGGGTCGCTGGGGCACTCCTCGCCGGGGGCGATCGCCGGGACCACCATGT TCAAC**CAATTAACCAATTCTGATTAG** 3’
HSVF-GS6462	pEP-KanS2	5’ TACGCCACCCTGCAGAACATGGTGGTCCCGGAGATCGCGCCCGGGGAGGAGTGCCCCAGCGA C**AGGATGACGACGATAAGTAGGG** 3’
		5’ GTGCAGGGGGTGCGCGGGGTCCGTCACGGGGTCGCTGGGGCACTCCTCCCCGGGCGCGATCT C**CAACCAATTAACCAATTCTGATTAG** 3’
HSVF-GS6410	pEP-KanS2	5' CGCTTCGACCGCGTATACGCCACCCTGCAGAACATGGTGGTCCCGAGGATCGCGCCCGGGGAG **AGGATGACGACGATAAGTAGGG 3'**
		5' GGGGTCCGTCACGGGGTCGCTGGGGCACTCCTCCCCGGGCGCGATCCTCGGGACCACCATGTT **CAACCAATTAACCAATTCTGATTAG 3'**
HSVF-GS6278	pEP-KanS2	5' CACCCTGCAGAACATGGTGGTCCCGGAGATCGCGCCCGGGCGGGAGTGCCCCAGCGAC**AGGA TGACGACGATAAGTAGGG** 3'
		5' GGGGTGCGCGGGGTCCGTCACGGGGTCGCTGGGGCACTCCCGCCCGGGCGCGATCTC**CAACC AATTAACCAATTCTGATTAG** 3'
HSVF-GS5396	pEP-KanS2	5' CGACCGCAGTTCTCGTGTGTTATTTTCGCTCTCCGCCTCTCGCAGTAGTGGGTGGTGGGC**AGGA TGACGACGATAAGTAGGG 3'**
		5' TTTTTTCTCCCTAATGCCCCCTCCCCCCTCGCCCACCACCCACTACTGCGAGAGGCGGAG**CAACC AATTAACCAATTCTGATTAG** 3'
HSVF-GS6199	pEP-KanS2	5' CCCCATATCGCTTCCCGACCTCCGGTCCCGATGGCCGTCCCGCAATGAGGCCCAGGGAGT**AGG ATGACGACGATAAGTAGGG** 3'

HSVF-GS5748	pEP-mCherry-in	5’ GACCGTTGCGCCTTTTTTTTTTTTCGTCCACCAAAGTCTCTGTGGGTGCGCGCATG**GTGAGCAAG GGCGAGGAG** 3’ 5’ CAGGGGCTCCTCCATCCGGTCTCCCGGGGCATCGGCTGCACCACCTCCGCCACC**CTTGTACAGC TCGTCCATGC** 3’
HSVF-GS6460	pEP-mCherry-in	5’ GACCGTTGCGCCTTTTTTTTTTTTCGTCCACCAAAGTCTCTGTGGGTGCGCGCATG**GTGAGCAAG GGCGAGGAG** 3’ 5’ CAGGGGCTCCTCCATCCGGTCTCCCGGGGCATCGGCTGCACCACCTCCGCCACC**CTTGTACAGC TCGTCCATGC** 3’
HSVF-GS4553	pEP-mCherry-in	5' GTCGCCCGTCTTTAACCTCCCCCGGGAGACGGCGGCGGAG**GTGAGCAAGGGCGAGGAG** 3' 5' CGGCAGCCGCTGTGCGCTGGGCCTGTAGGACGACCACCTG**CTTGTACAGCTCGTCCATGC** 3'
HSVF-GS5797	pEP-KanS2	5’ TACGCCACCCTGCAGAACATGGTGGTCCCGGCGATCGCCCCCGGCGCGGAGTGCCCCAGCGA C**AGGATGACGACGATAAGTAGGG** 3’ 5’ GTGCAGGGGGTGCGCGGGGTCCGTCACGGGGTCGCTGGGGCACTCCGCGCCGGGGGCGATC GC**CAACCAATTAACCAATTCTGATTAG** 3’
HSVF-GS6601	pEP-EGFP-in	5' GACCGTTGCGCCTTTTTTTTTTTTCGTCCACCAAAGTCTCTGTGGGTGCGCGCATG**GTGAGCAAG GGCGAGGAG** 3' 5' CAGGGGCTCCTCCATCCGGTCTCCCGGGGCATCGGCTGCACCACCTCCGCCACC**CTTGTACAGC TCGTCCATGC** 3'
HSVF-GS6661	pEP-EGFP-in	5' GACCGTTGCGCCTTTTTTTTTTTTCGTCCACCAAAGTCTCTGTGGGTGCGCGCATG**GTGAGCAAG GGCGAGGAG** 3' 5' CAGGGGCTCCTCCATCCGGTCTCCCGGGGCATCGGCTGC- ACTACTAGCATTCACCAGAGCTCCACCTCCGCCACC**CTTGTACAGCTCGTCCATGC** 3'
HSVF-GS6672	pEP-EGFP-in	5' GACCGTTGCGCCTTTTTTTTTTTTCGTCCACCAAAGTCTCTGTGGGTGCGCGCATG**GTGAGCAAG GGCGAGGAG** 3' 5' CAGGGGCTCCTCCATCCGGTCTCCCGGGGCATCGGCTGCACTACTAGCATTCACCAGAGCTCCA CCTCCGCCACC**CTTGTACAGCTCGTCCATGC** 3'
HSVF-GS5471	pEP-EGFP-in	5' GACCGTTGCGCCTTTTTTTTTTTTCGTCCACCAAAGTCTCTGTGGGTGCGCGCATG**GTGAGCAAG GGCGAGGAG** 3' 5' CAGGGGCTCCTCCATCCGGTCTCCCGGGGCATCGGCTGCACCACCTCCGCCACC**CTTGTACAGC TCGTCCATGC** 3'
HSVF-GS6684	pEP-mCherry-in	5' GTCGCCCGTCTTTAACCTCCCCCGGGAGACGGCGGCGGAG**GTGAGCAAGGGCGAGGAG** 3' 5' CGGCAGCCGCTGTGCGCTGGGCCTGTAGGACGACCACCTG**CTTGTACAGCTCGTCCATGC** 3'
HSVF-GS5747	pEP-EGFP-in	5' ATATCGCTTCCCGACCTCCGGTCCCGATGGCCGTCCCGCACTCGACCATG**GTGAGCAAGGGCG AGGAGC** 3' 5' AAGCGCCCGGACGCTATCGGTGGTAACGGTGCTGGGGCGGCTCGAG**TTGTACAGCTCGTCCAT GCCG** 3'
HSVF-GS5934	pEP-EGFP-in	5' ATATCGCTTCCCGACCTCCGGTCCCGATGGCCGTCCCGCACTCGACCATG**GTGAGCAAGGGCG AGGAGC** 3' 5' AAGCGCCCGGACGCTATCGGTGGTAACGGTGCTGGGGCGGCTCGAG**TTGTACAGCTCGTCCAT GCCG** 3'

Bold nucleotides denote primer homology to the template

CHAPTER 3: Basic Characterization of VP5 Apical Region Mutants

This chapter appeared as the published article: Ruhge LL, Huet AGE, Conway JF, Smith GA. 2018. J Virol. Accepted manuscript posted online 5 July 2018 doi:10.1128/JVI.00821-18.

INTRODUCTION

The majority of the herpesvirus capsid shell mass is comprised of 955 copies of the 149 kDa the major capsid protein (VP5) (84-87), which is arranged into hexamers and pentamers. Pentamers are found at 11 of the capsid vertices while hexamers occupy the remainder of the icosahedral lattice, with the exception of the unique portal vertex. Hexamers are crowned with the 12 kDa small capsid protein (VP26), and pentamers are associated with five copies of the CVSC (pUL25 and pUL17), which radiate outward from the pentamers and serve as tegument binding sites (7, 42, 89-92). The VP5 monomer is a large, tower-like protein divided into three domains: the upper, middle, and floor. The apical region of the upper domain, which consists of a polyproline loop plus an adjacent sequence that serves as an antibody binding epitope (206), is surface exposed in hexamers and pentamers and does not participate in subunit interactions within the capsid shell. Instead, the apical region is proposed to be important for binding VP26 onto hexamers and tegument onto pentamers (158).

The large tegument protein, pUL36, binds the capsid vertices through an interaction with pUL25 (181). An additional tegument protein, pUL37, binds pUL36, and together these capsid-bound tegument proteins cotransport with the capsid, contributing to neuronal transmission and

retrograde axonal transport (35, 39-41). To examine if the capsid surface participates in these processes, a collection of HSV-1 encoding mutations in the VP5 apical region was made. Initial characterization of these viruses in cell culture revealed only modest changes in propagation, with the exception of a virus mutated at two conserved acidic residues in the polyproline loop. Neither the polyproline loop mutant nor a mutant lacking the majority of the antibody epitope was impacted for retrograde axonal transport. However, localization of VP5 during infection was impacted not in the antibody epitope mutant but the polyproline loop mutant.

RESULTS

The majority of the HSV-1 major capsid protein, VP5, is integral to the capsid icosahedral structure and its constituent capsomeres. An exception is a small apical region within the VP5 upper domain that is exposed on the capsid surface (Fig. 3.1A-D) and consists of a polyproline loop and a binding site for a capsid-specific antibody (158, 206). The accessibility of the apical domain indicates it may interface with cellular or viral proteins to promote infection. To assess the importance of the apical region during HSV-1 infection, an alignment of eight alphaherpesviruses was used to inform a mutational approach (Fig. 3.1E). Based on sequence conservation, five VP5 mutants were made by two-step RED-mediated recombination in the F strain of HSV-1 (Fig. 3.1F). The recombinant viruses exhibited a reduction in cell-cell spread as evidenced by decreased plaque diameters compared to wild-type (WT) virus (Fig. 3.2). The most severe decrease in plaque size occurred when two glutamic acid residues in the polyproline loop, E846 and E851, were mutated to alanines (EE>AA). These glutamic acid residues, shown on the VP5 crystal structure in magenta and blue in Figure 3.1A-D, are located in the most apical region of the VP5 monomer (Fig. 3.1C-D).

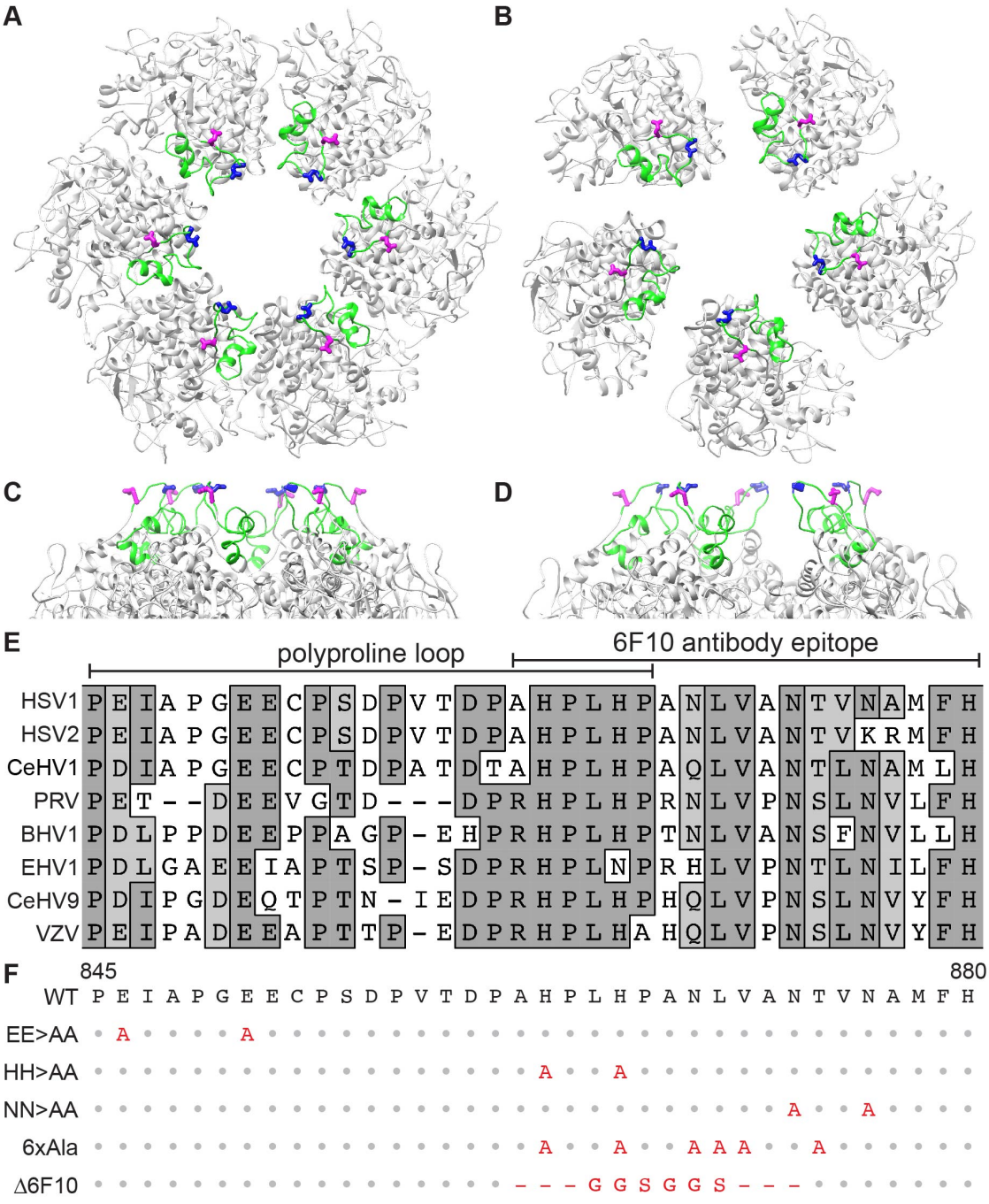

Figure 3.1 Targeted mutation of the VP5 apical region. (A-D) Representation of the HSV-1 VP5 upper domain crystal structures as arranged in a top view of (A) a peripentonal hexamer, (B) a pentamer, and a side view of (C) a peripentonal hexamer, and (D) a pentamer. C and D are

rotated arbitrarily to best display the glutamic acid residues. The apical region is colored green and side chains of residues E846 (magenta) and E851 (blue) are shown as sticks. (E) Alignment of the apical region of eight alphaherpesvirus major capsid proteins. Amino acid positions for the HSV-1 sequence are indicated below. (F) HSV-1 VP5 apical region mutants used in this study. Predicted amino acid changes are in red.

Table 3.1 Viruses Used in Chapter 3

Strain	Fluorescent fusion	Mutations	Titer (PFU/mL)
HSVF-GS2695	-	-	2.59×10^8
HSVF-GS5798	-	UL19 E846A/E851A	4.72×10^7
HSVF-GS5799	-	UL19 N873A/N876A	9.81×10^7
HSVF-GS5801	-	UL19 H863A/H866A	1.31×10^8
HSVF-GS5905	-	UL19 H863A/H866A/N869A/L870A/V871A/T874A	7.56×10^7
HSVF-GS6276	-	UL19 A862-N873 > GGSGGS	1.07×10^8
HSVF-GS5748	mCherry-5xG-UL26	-	2.95×10^8
HSVF-GS6460	mCherry-5xG-UL26	UL19 E846A/E851A	8.06×10^7
HSVF-GS6493	mCherry-5xG-UL26	UL19 A862-N873 > GGSGGS	1.32×10^7

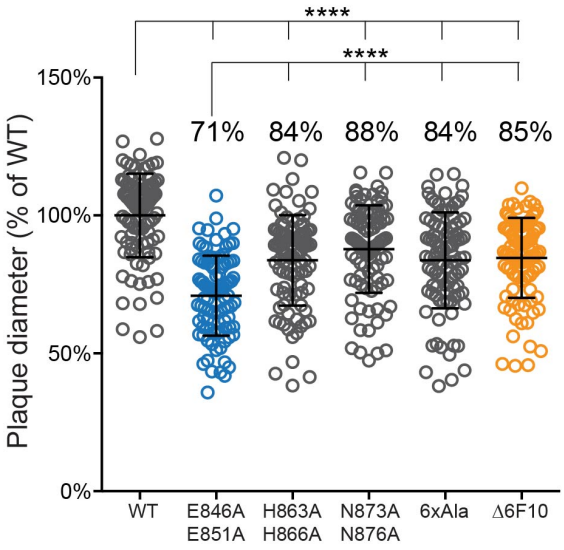

Figure 3.2 Impact of the VP5 mutations on plaque size. Vero cells were infected with VP5 apical region mutants. Plaque diameters were measured 5 days post-infection. Diameters are

represented as a percent of the mean plaque diameter of wild-type HSV-1 strain F (WT). Error bars indicate the standard deviation of three independent experiments. Asterisks indicate a statistically significant difference from WT or VP5 EE>AA (****, $p \leq 0.0001$) as determined by Tukey's multiple comparison test.

The capsid-bound tegument proteins, pUL36 and pUL37, are effectors of intracellular capsid transport (39-44). To examine if the capsid surface-exposed region of VP5 contributes to its transport on microtubules, primary sensory neurons were infected with the EE>AA and Δ6F10 mutant viruses (Fig. 3.1F). To visualize individual capsids in the process of retrograde axonal transport by time-lapse fluorescence microscopy, the viruses were further modified to encode an amino-terminal mCherry fusion to the maturation protease, VP24 (62). The mCherry-VP24 fusion was chosen because the internal location of VP24 inside the capsid shell predicts that the mCherry tag should not interplay with the mutations introduced into the VP5 apical region. Capsid dynamics were monitored during the first hour post-infection (hpi) and continuous periods of retrograde motion (runs) were analyzed for average velocity and distance traveled. The distribution of run velocities were consistently Gaussian for the wild-type, EE>AA, and Δ6F10 viruses ($R^2 \geq 0.96$ for each) and run distances were decaying exponential ($R^2 \geq 0.98$ for each), the latter being consistent with processive motion (Fig. 3.3). These transport dynamics were consistent between the WT and mutant viruses, demonstrating that mutation of the VP5 apical region did not impair microtubule-based retrograde axonal transport.

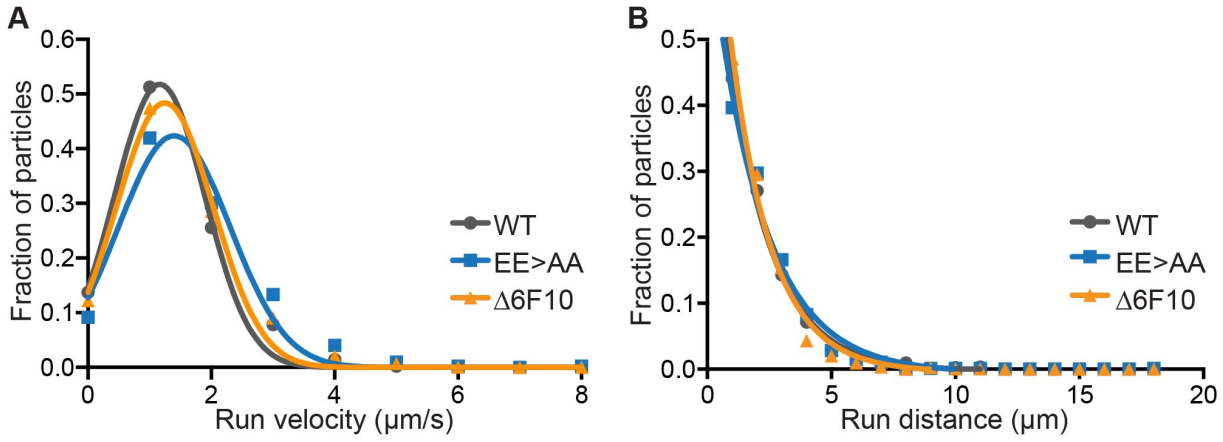

Figure 3.3 Mutation of the VP5 upper domain did not impair retrograde axonal transport. Primary sensory neurons were infected with derivatives of the VP5 wild-type (WT), glutamic acid mutant (EE>AA), and Δ6F10 mutant that encode a mCherry-VP24 fusion to allow for tracking of individual capsids in axons. Intracellular capsid transport was monitored by time-lapse fluorescence microscopy during the first hour of infection. Run velocity (A) and run distance (B) profiles of individual capsids are representative of three independent experiments.

Because the defect underlying the reduction in plaque diameter was not ascribed to defects in retrograde trafficking, *de novo* capsid production was next examined. Vero cells infected with the mCherry-VP24 variants of the EE>AA and Δ6F10 mutants were examined by live-cell microscopy at 8.5 hpi. As is seen in wild-type infection, the nuclei of cells infected with either mutant virus filled with diffraction-limited punctae consistent with high loads of dispersed capsids (62); however, the EE>AA mutant also produced large intranuclear structures (Fig. 3.4).

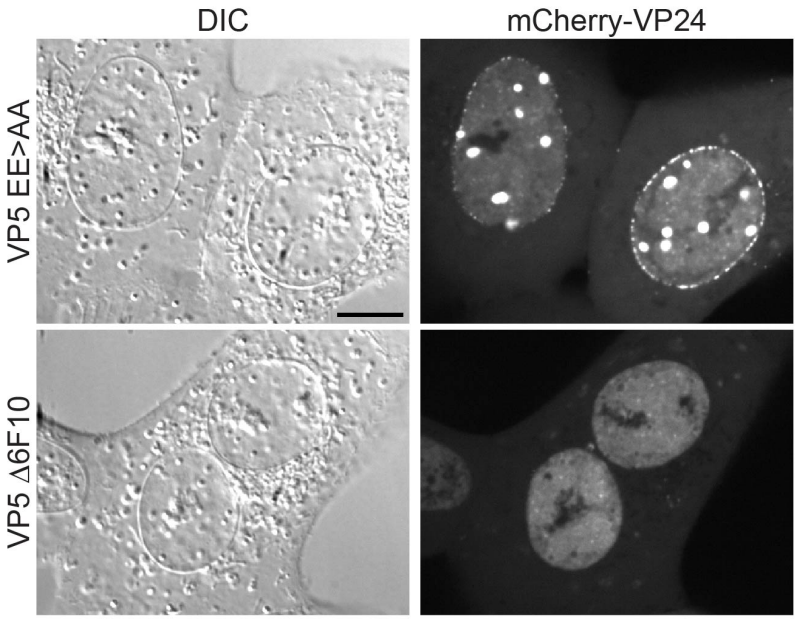

Figure 3.4 The VP5 EE>AA mutant forms intranuclear clusters of VP24. Vero cells were infected at a MOI of 5 with derivatives of HSV-1 encoding mCherry-VP24 and either VP5 EE>AA or Δ6F10. Live-cells were imaged at 8.5 hpi. Scale bars are 10 μm.

DISCUSSION

The surface of the procapsid is decorated by the apical region of the VP5 major capsid protein, which constitutes the tips of the 11 pentamers (accounting for 11 of the icosahedral vertices, with the 12th vertex consisting of 12 copies of pUL6 portal protein) and 150 hexamers that make up the majority of the icosahedral shell. Following maturation, the procapsid acquires the pUL25 and VP26 accessory proteins, the latter of which selectively covers the apical regions of the hexamers. Thus, the procapsid displays 955 copies of the apical region on its surface, which is reduced to 55 exposed copies upon maturation and decoration with VP26. The exposure of the VP5 apical region on the mature capsid led me to investigate whether it contributes to the

retrograde axonal transport of capsids that leads to the establishment of latent infections in the nervous system.

Although no functions have formally been ascribed to the apical region, fitting of the VP5 upper domain crystal into the herpesvirus capsid map reveals the close association of the VP5 apical region with densities attributed to pUL25 and pUL36 (4, 7). As a result, I hypothesized that the VP5 apical region participated in retrograde transport of the DNA-filled capsid following entry. However, the data demonstrates the glutamic acid residues of the polyproline loop were dispensable for retrograde axonal transport in primary sensory neurons, as was the antibody epitope portion of the apical region (based on analysis of the Δ6F10 mutant). Given that the VP26 protein is also dispensable for axonal transport (179, 180), I conclude that the bulk of exposed outer capsid surface does not promote this critical component of the HSV-1 neuroinvasion mechanism. While the scope of the mutagenesis included in this study does not entirely rule out a role for capsid surface epitopes that contribute to the transport mechanism, it seems likely that the previously identified interaction between pUL25 and the pUL36 tegument protein may be sufficient to confer these dynamic properties to the virus particle (181). These results support a model in which the herpesvirus capsid is a dormant cargo that requires the action of attached tegument proteins to produce the dynamics that underlie productive infection.

ACKNOWLEDGEMENTS

I thank Sarah Antinone for providing embryonic chick DRGs and Ekaterina Heldwein for her assistance designing the VP5 Δ6F10 mutant.

CHAPTER 4: VP5 Glutamic Acid Residues Promote Capsid Assembly and Maturation

Figures 4.1A, 4.3-4.7, and 4.9 of this chapter appeared as the published article: Ruhge LL, Huet AGE, Conway JF, Smith GA. 2018. J Virol. Accepted manuscript posted online 5 July 2018 doi:10.1128/JVI.00821-18.

INTRODUCTION

Extensive efforts have been undertaken to understand herpesvirus capsid assembly and maturation, which includes analyses of baculovirus and cell-free systems (116-121), temperature-sensitive mutants (122, 123), and three-dimensional reconstructions from cryo-EM (4, 7, 93, 101-103, 124). While many details remain unclear, this work provides an overarching model of HSV-1 capsid morphogenesis. The major capsid protein (VP5), triplexes (VP19c and VP23), portal vertex (pUL6), and internal scaffold proteins self-assemble into a spherical procapsid within the cell nucleus. There are two types of scaffold proteins: small (pUL26.5) and large (VP24 + VP21). Once assembly of the procapsid is complete the catalytic activity of the VP24 protease, housed within the amino-terminus of the large scaffold protein, is triggered (125). VP24 cleaves itself from the scaffold and cleaves a release site in the carboxyl-terminus of the small and large scaffold proteins, disconnecting them from the shell floor (119, 127, 128). These events cause the capsid shell to angularize into a stable form and become a substrate for the binding of two accessory capsid surface proteins: pUL25 and VP26 (126, 127, 136, 139). The scaffold fragments internal to the capsid are expelled as the viral genome is packaged, but VP24

is retained (10, 11, 62, 126, 140-142). This process produces three angularized capsid types within infected cell nuclei: capsids that retained the scaffold and lack DNA (B capsids), capsids that expelled the scaffold but failed to stably encapsidate the viral genome (A capsids), and nucleocapsids (C capsids).

In the previous chapter, I investigated whether the VP5 apical region contributes to intracellular transport dynamics following entry into primary sensory neurons. In this chapter, I test the hypothesis that conserved negatively-charged amino acids in the apical region contribute to VP26 acquisition. To my surprise neither hypothesis proved true. Instead, mutation of glutamic acid residues in the apical region delayed viral propagation and induced focal capsid accumulations in nuclei. Examination of capsid morphogenesis based on epitope unmasking, capsid composition, and ultrastructural analysis indicated that these clusters consisted of procapsids. The results demonstrate that, in addition to established events that occur inside the capsid, the exterior capsid shell promotes capsid morphogenesis and maturation.

RESULTS

Of the VP5 apical region mutants assessed in Chapter 3, the mutation of two conserved acid charges resulted in the greatest impairment of propagation in cell culture. The decrease in plaque size was only observed when both glutamic acid residues were mutated, and the defect was rescued when both mutations were repaired (Fig. 4.1A).

Additional glutamic acid mutants were made to test if the defect in viral propagation was a result of changing the negatively charged residues to hydrophobic residues. To address this concern, the negatively charged residues, E846 and E851, were reversed in their charge by mutating the residues singly or combined to arginines. The E846R mutant demonstrated a

decrease in plaque size similar to the EE>AA mutant while the E851R mutant produced a more severe decrease (Fig 4.1B). The EE>RR mutant failed to propagate in cell culture.

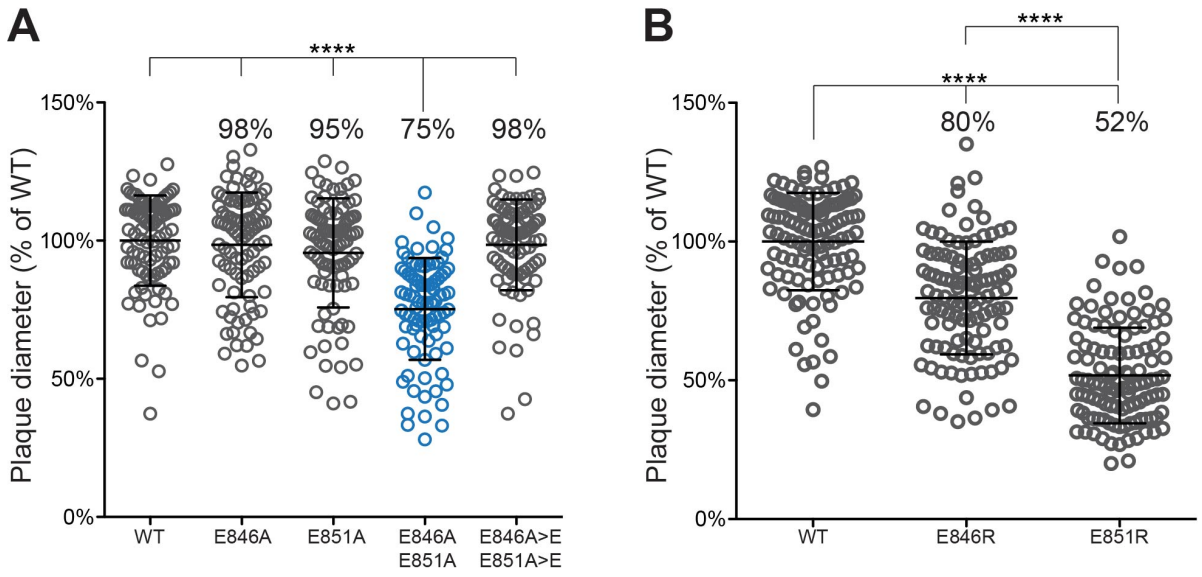

Figure 4.1 Impact of the VP5 mutations on plaque size. Vero cells were infected with VP5 glutamic acid mutants. Polyproline loop glutamic acid residues were mutated to (A) alanine or (B) arginine residues. Plaque diameters were measured 5 days post infection. Diameters are represented as a percent of the mean plaque diameter of wild-type HSV-1 strain F (WT). Error bars indicate the standard deviation of three independent experiments. Asterisks indicate a statistically significant difference from WT, VP5 E846A/E851A, or E851R (****, $p \leq 0.0001$) as determined by Tukey's multiple comparison test.

Next, the VP5 localization during infection was assessed for each of the glutamic acid mutants. Vero cells were infected at a MOI of 5 and fixed and stained for VP5 at 8 hpi. As previously observed with the mCherry-VP24 tag, the EE>AA mutant formed intranuclear foci which reacted with a VP5 antibody. Because these foci were evident by a fusion protein (Fig.

3.4) and antibody staining (Fig. 4.2), it suggests these foci were not artifacts of either the VP24 fluorescent tag or fixation. The E846R and E851R mutants also formed intranuclear foci but the E>A single mutants did not impact VP5 localization during infection (Fig 4.2).

Table 4.1 Viruses Used in Chapter 4

Strain	Fluorescent fusion	Mutations	Titer (PFU/mL)
HSVF-GS2695	-	-	2.59×10^8
HSVF-GS5798	-	UL19 E846A/E851A	4.72×10^7
HSVF-GS6197	-	UL19 E846A	1.45×10^8
HSVF-GS6434	-	UL19 E851A	1.93×10^8
HSVF-GS6462	-	UL19E846A>E/E851A>E	3.06×10^8
HSVF-GS6410	-	UL19 E846R	1.57×10^8
HSVF-GS6278	-	UL19 E851R	1.52×10^7
HSVF-GS5396	-	ΔUL25	6.25×10^7
HSVF-GS6199	-	ΔUL35	1.59×10^8
HSVF-GS5748	mCherry-5x-VP24	-	2.95×10^8
HSVF-GS6460	mCherry-5x-VP24	UL19 E846A/E851A	8.06×10^7
HSVF-GS4553	pUL25/mCherry	-	7.65×10^7
HSVF-GS5797	pUL25/mCherry	UL19 E846A/E851A	3.70×10^7

The EE>AA mutant was chosen for further study given the following consideration: the phenotype was observed with the mutation of two residues, as opposed to a single point mutation, reducing the likelihood of genotypic reversion. Additionally, reversion of the EE>AA mutant may be readily identified considering E846A and E851A mutations were not sufficient to induce the phenotype of VP5 intranuclear foci (Fig. 4.2). Next, a time course was carried out with cells infected with HSV-1 WT, EE>AA, or a repair of the EE>AA mutant. Intranuclear foci were observed at all time points evaluated in EE>AA infected cells but were not evident with

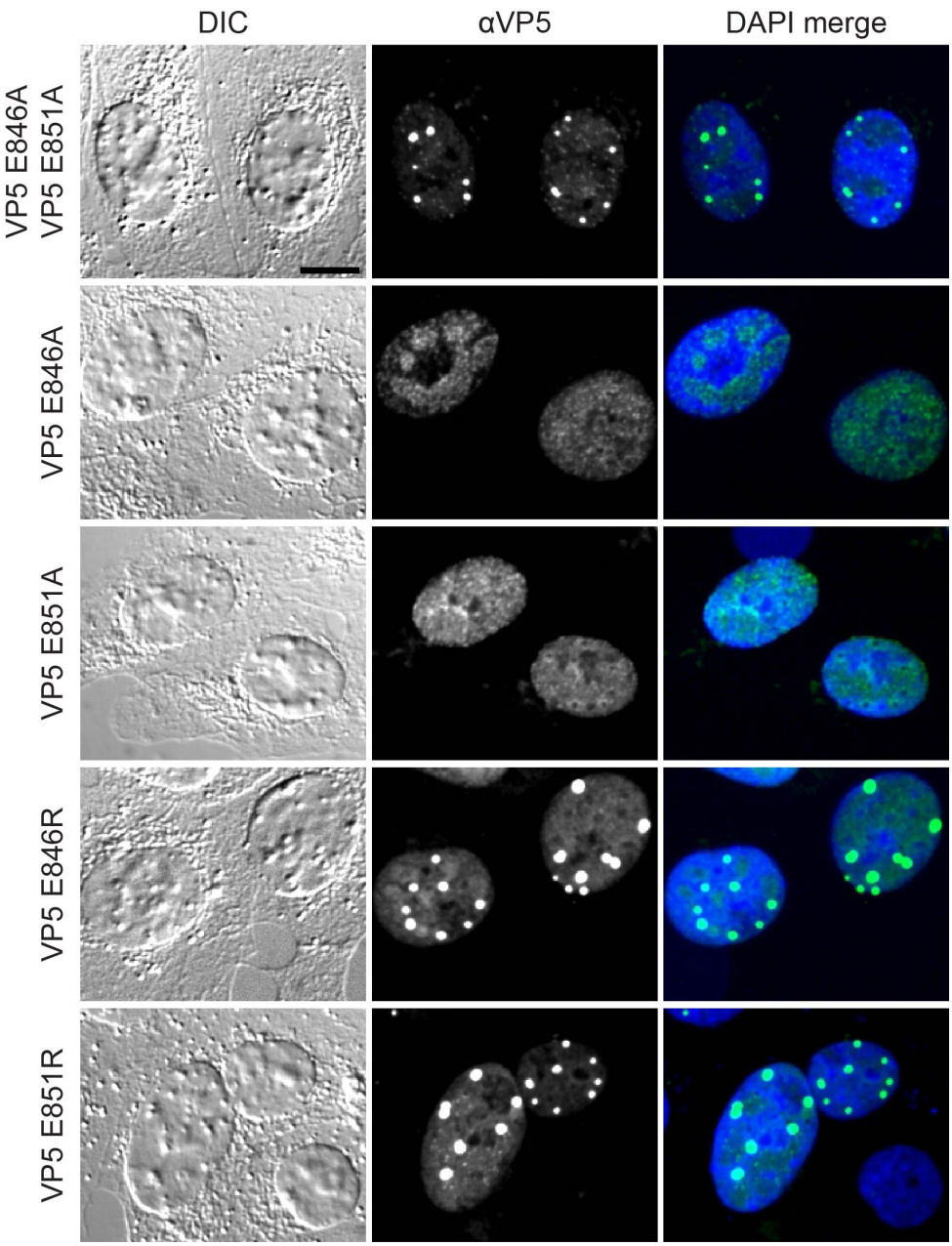

Figure 4.2 Formation of VP5 intranuclear foci requires mutation of both VP5 glutamic acid residues or a swap in charge. Vero cells were infected at a MOI of 5 with HSV-1 glutamic acid mutants. Infected cells were fixed at 8 hpi and processed for immunofluorescence using the αVP5 H1.4 antibody and DAPI stain.

WT HSV-1 or a repair of the EE>AA mutant (Fig. 4.3), demonstrating that the EE>AA mutations induced intranuclear clusters of the capsid VP24 and VP5 capsid proteins.

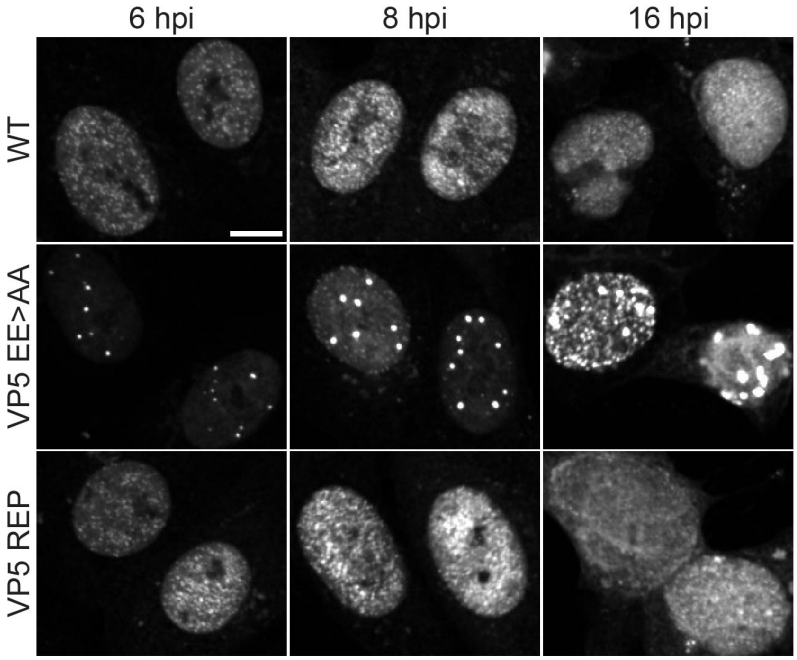

Figure 4.3 The VP5 EE>AA intranuclear foci persist throughout infection. Vero cells were infected at a MOI of 5 with unmodified HSV-1 (WT), VP5 glutamic acid mutant (EE>AA), and VP5 repair (REP). Cells were fixed at the indicated time post infection and stained with the αVP5 H1.4 antibody. Scale bar is 10 μm.

In order to assess the impact of these intranuclear clusters of capsid proteins on viral propagation, single-step growth kinetics were evaluated. The EE>AA mutant was attenuated relative to the wild-type and repair viruses (Fig. 4.4). At 8 and 12 hpi, the EE>AA mutant exhibited a decrease in both cell-associated and supernatant PFU, but attained titers approaching the wild-type by 30 hpi. The delays in PFU production were confirmed in triplicate: the EE>AA mutant cell-associated titers were consistently 6% ± 1.6% of the repaired virus at 8 hpi, and the supernatant titers were 8% ± 3.8% of the repaired virus at 12 hpi. I conclude that the aberrant

nuclear foci correlated to decreased rates of virus propagation, as well as plaque size (Fig. 3.2 and Fig. 4.1) but had limited impact on the number of plaque-forming units per cell (burst size).

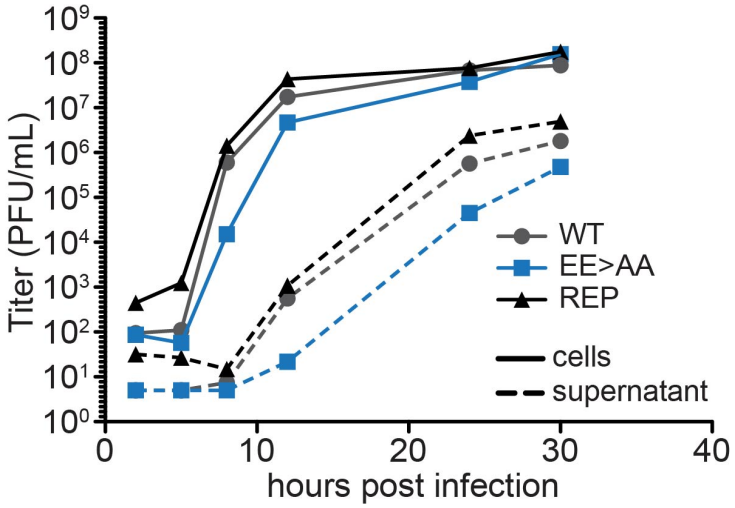

Figure 4.4 VP5 glutamic acid residues support HSV-1 propagation. Single-step replication kinetics of HSV-1 WT, VP5 glutamic acid mutant (EE>AA), and the VP5 repair in Vero cells are shown following infection at a MOI of 10. Cells (solid lines) and supernatants (dashed lines) were collected at indicated times and titers were determined by plaque assay on Vero cells.

Negatively-charged residues within the VP5 polyproline loop were predicted to mediate binding of the VP26 capsid protein onto the surface of capsid hexamers (158). To test this hypothesis, intranuclear capsids were isolated at 22 hpi from Vero cells infected with wild-type HSV-1 (WT) or the glutamic acid mutant (EE>AA). A VP26-null mutant (Δ26) was included as a control. A, B, and C capsids were separated by density ultracentrifugation and visualized by light scattering. The EE>AA and VP26-null viruses produced each capsid species similar to the

wild-type (Fig. 4.5A). The protein compositions of the A, B, and C capsids produced from the wild-type and EE>AA viruses were indistinguishable from one another; notably, capsids of the EE>AA virus possessed wild-type levels of VP26, which was identified by its 12 kDa molecular weight and its absence from the VP26-null samples (Fig. 4.5B). This data indicates that the VP5 EE>AA mutant assembles A, B, and C capsids and that E846 and E851 are dispensable for VP26 incorporation.

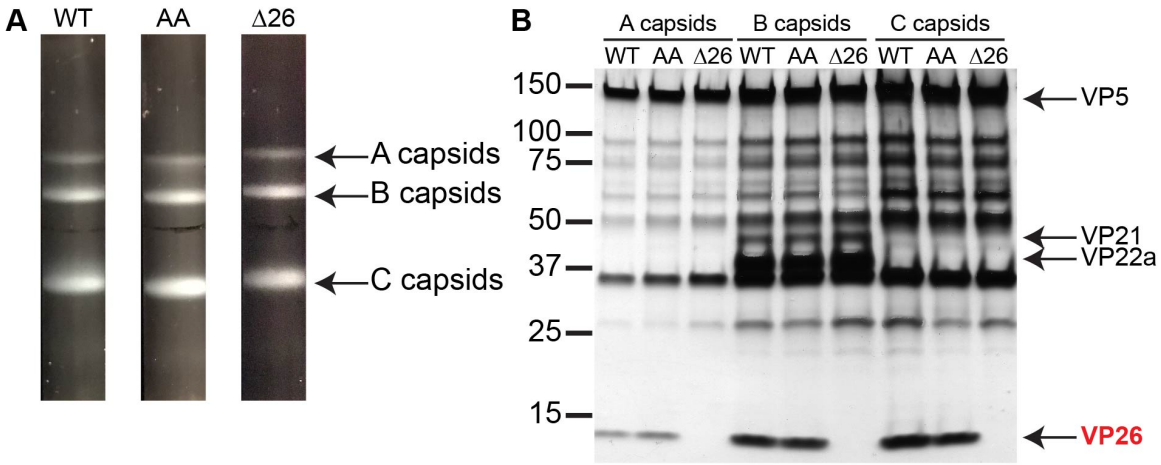

Figure 4.5 VP5 EE>AA capsids acquire VP26. A) A, B, and C capsids were isolated from nuclei of Vero cells infected with HSV-1 over a 20-50% sucrose gradient and visualized by light scattering. B) Protein profiles of the capsids observed by silver staining of a 4-20% gradient denaturing gel. HSV-1 strains used were wild-type (WT), the glutamic acid mutant (AA), and a VP26-null mutant (Δ26). The latter serves to identify VP26 in the denaturing gel.

The capsid profiles from the previous experiment were consistent with the expression of capsid proteins and their assembly. Nevertheless, the potential impact of the EE>AA mutation on VP5 expression warranted further inspection. Western blot detection of VP5 from cell lysates

was performed at 8 hpi. VP5 was detected as a 149 kDa band in both HSV-1 WT and EE>AA but not mock-infected cell lysates (Fig. 4.6A). The expression of VP5 was normalized to the pUL37 tegument protein as a loading control following densitometry analysis. The analysis revealed no significant change in the amount of VP5 produced by the EE>AA mutant (Fig. 4.6B). Therefore, the impact of EE>AA mutation on capsid morphogenesis was next examined.

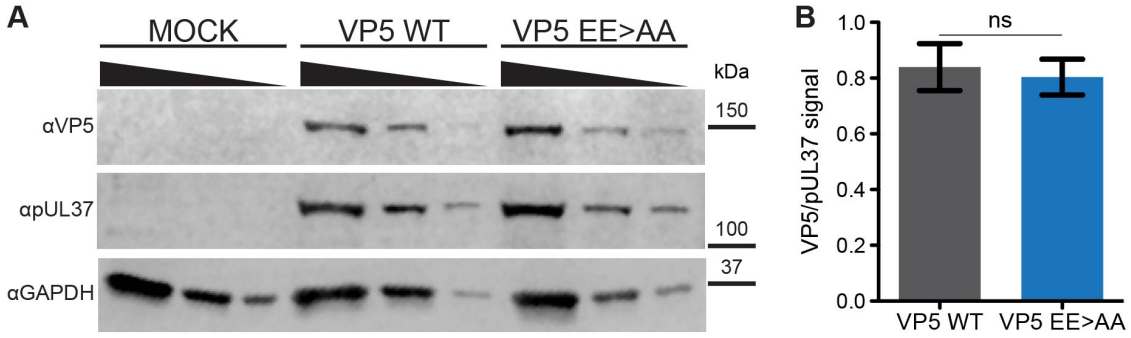

Figure 4.6 VP5 expression is not impacted by glutamic acid mutations. (A) Western blots of cell lysates prepared from mock or infected cells. Vero cells were infected with HSV-1 encoding the wild-type (WT) or EE>AA VP5 allele at a MOI of 5. Threefold dilutions of cell lysates, prepared at 8 hpi, were probed by western blot. The HSV-1 tegument protein, pUL37, and cellular GAPDH served as loading controls. The image shown is representative of three independent experiments. (B) VP5 expression was quantitated by densitometry analysis. Individual measurements are normalized to the pUL37 loading control. The difference was not statistically significant (ns) by an unpaired t-test. Error bars represent the standard error of the mean.

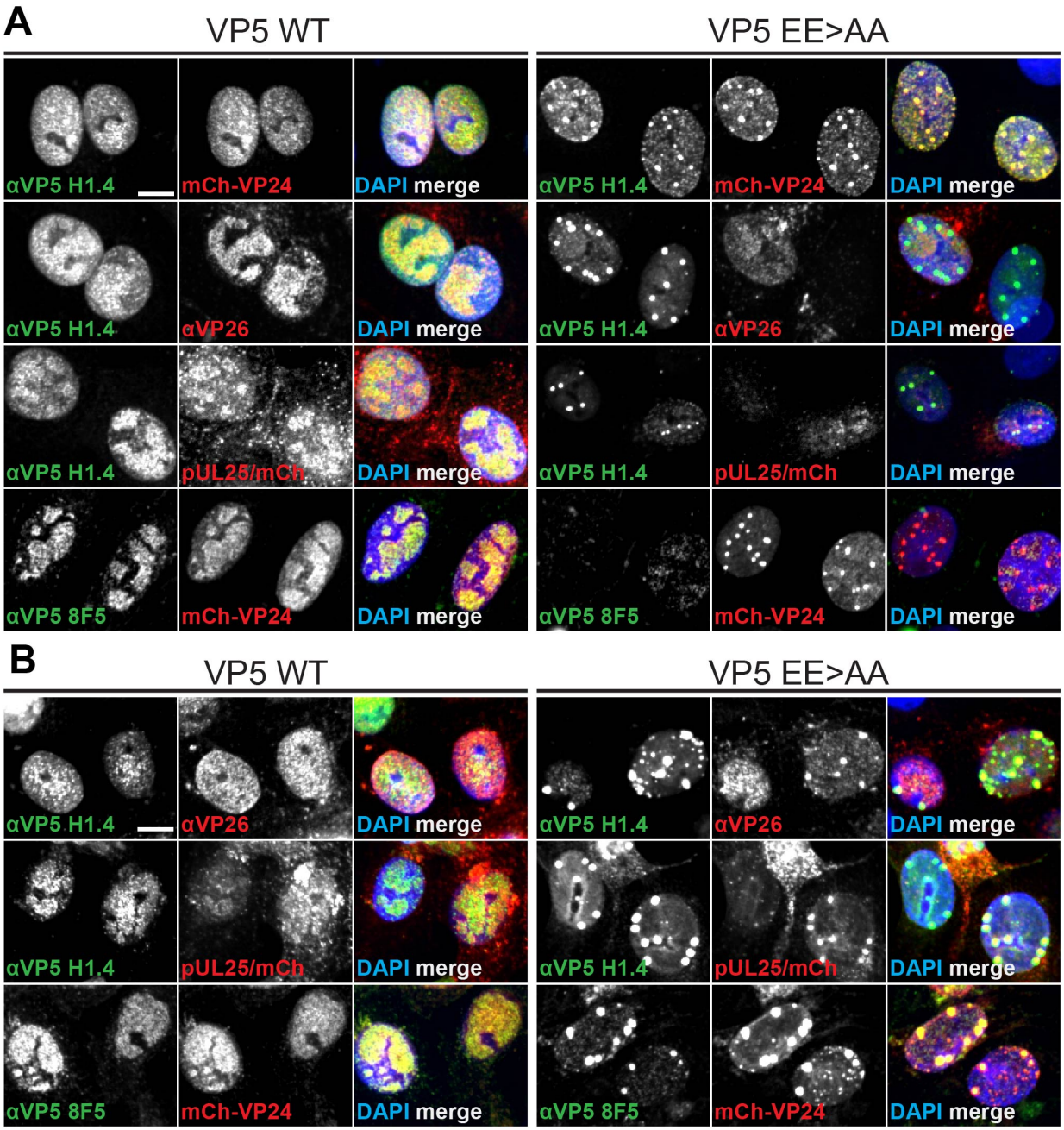

Figure 4.7 VP5 EE >AA foci composition is initially consistent with that of procapsids.

Vero cells were infected with HSV-1 encoding WT or EE>AA VP5 at a MOI of 5 were fixed at (A) 8 hpi or (B) 16 hpi and processed for immunofluorescence using αVP5 and αVP26 antibodies. In some instances, the viruses encoded mCherry-VP24 or pUL25/mCherry fusions, as

indicated. Scale bar is 10 μm.

To better understand the protein composition of EE>AA foci, Vero cells were infected, fixed at 8 hpi, and processed for fluorescence imaging. Cells infected with HSV-1 encoding wild-type VP5 had capsids dispersed throughout the nuclei, which colocalized with VP24, VP26, pUL25, and with reactivity to the maturation-specific VP5 antibody, 8F5 (Fig. 4.7A). In contrast, the EE>AA nuclear foci colocalized only with VP24. Because the VP26 and pUL25 capsid proteins are acquired upon shell angularization (126, 127, 136, 139), and the VP5 8F5 epitope (207) is exposed on the tips of hexamers after internal scaffold cleavage by the maturation protease (132, 208), I conclude the EE>AA nuclear foci did not contain mature capsids. However, by 16 hpi, the foci acquired each of these markers (Fig. 4.7B).

Recently, intranuclear foci of VP5 were observed in nuclei infected with HSV-1 VP26-null virus (110, 209). To test if the absence of either of the angularized shell proteins, VP26 or pUL25, was sufficient to induce foci formation, Vero cells were infected with HSV-1 VP26-null or UL25-null and processed for immunofluorescence with a VP5 antibody. In contrast to the Kawaguchi group's observations, the VP26-null virus did not result in intranuclear foci of VP5. Additionally, VP5 foci did not form in UL25-null infected cells (Fig 4.8). Thus, I conclude that nuclear foci formation results from the VP5 glutamic acid mutations and not the lack of VP26 or pUL25.

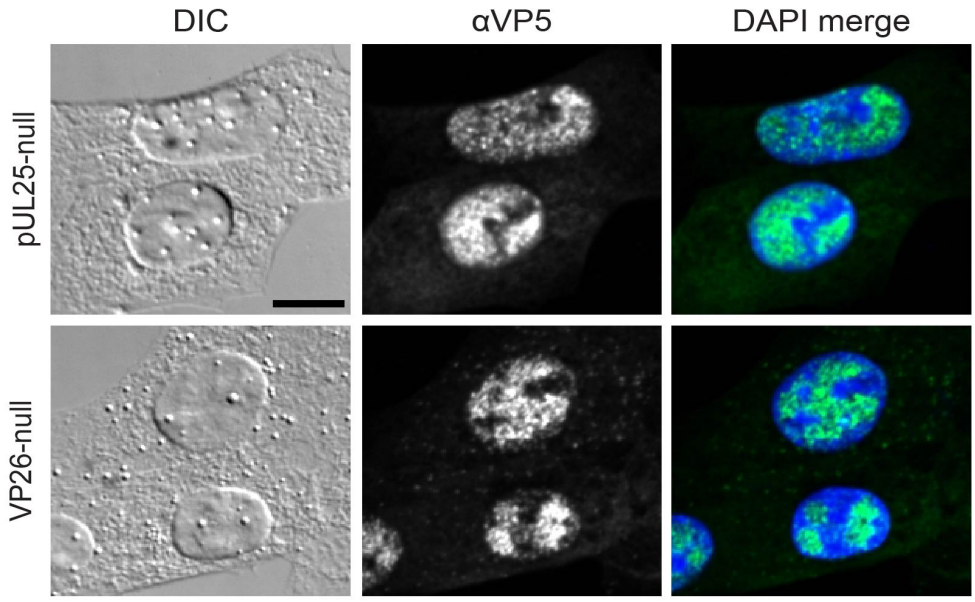

Figure 4.8 VP26- and UL25-null viruses do not form foci. Vero cells infected with HSV-1 deleted for the gene encoding VP26 (UL35) or pUL25 (UL25) at a MOI of 5 were fixed at 8 hpi and processed for immunofluorescence using the αVP5 H1.4 antibody and DAPI stain.

Next, transmission electron microscopy was used to visualize the glutamic acid mutant foci. Vero cells infected with HSV-1 VP5 EE>AA and fixed at 8 hpi contained nuclear foci of electron-dense material surrounding partially- and fully-formed procapsids (Fig. 4.9A and B). Consistent with the production of infectious EE>AA virions (Fig. 4.4), mature capsid species were detected throughout these nuclei but always apart from the foci (Fig. 4.9C-F). At 16 hpi, the intranuclear foci persisted but now contained mixtures of procapsids and B capsids (Fig. 4.9G-H). Interestingly, only scaffold-containing capsids were observed within the EE>AA foci with C capsids found outside the foci (Fig 4.9I). To further analyze this data, intranuclear capsids were quantified at 8 and 16 hpi (Table 4.2). While B capsids were the predominant capsid species

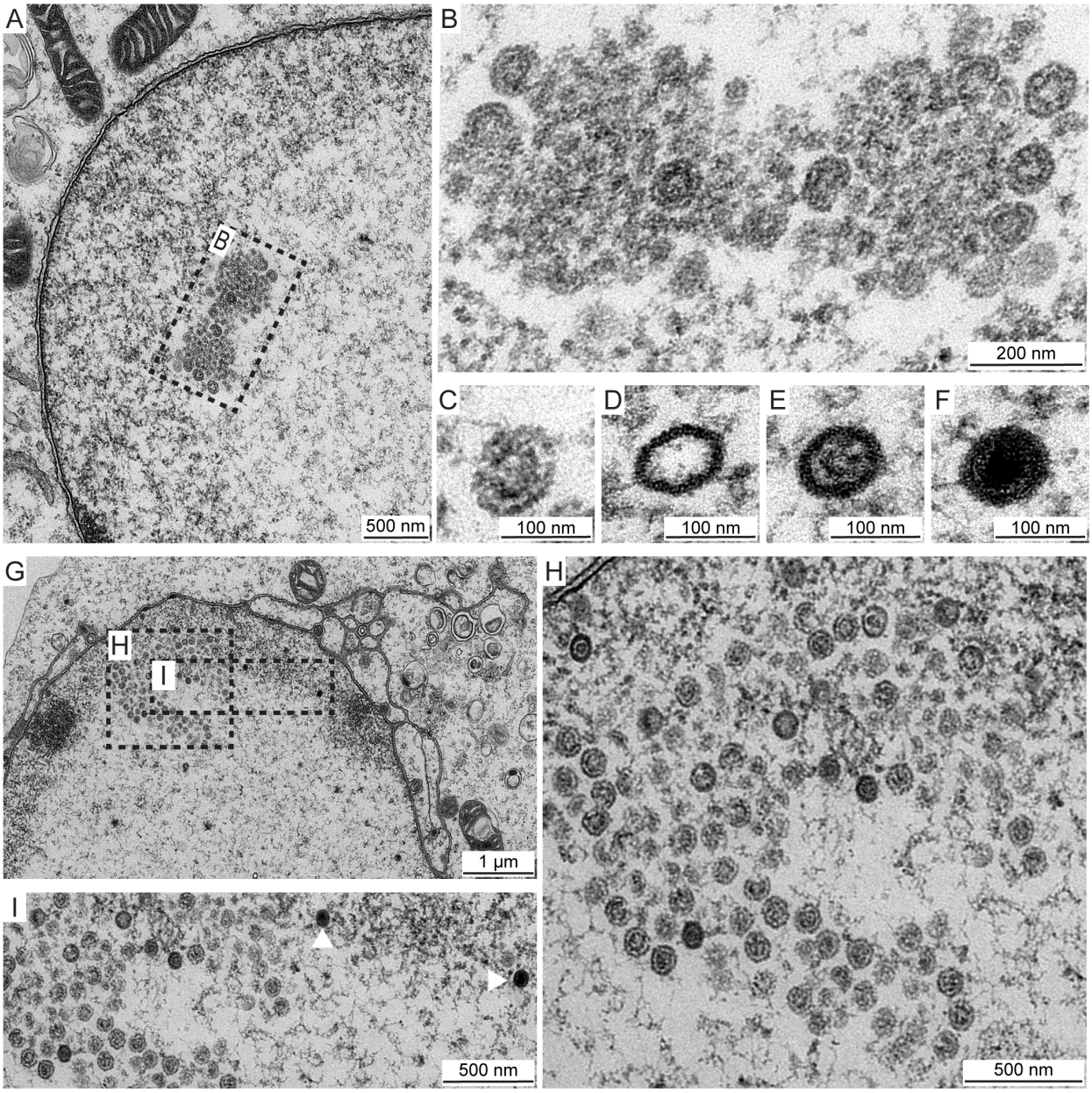

Figure 4.9 VP5 EE>AA foci contain clusters of procapsids. HSV-1 VP5 EE>AA infected Vero cells (MOI of 5) were fixed at 8 hpi (A-F) or 16 hpi (G-I) and imaged by transmission electron microscopy. A and B) Foci ultrastructure reveals fully- and partially-formed capsids containing large-core scaffolds consistent with procapsids. C, D, E, F) Infected cells exhibit all capsid species: C) procapsid, D) A capsid, E) B capsid, and F) C capsid. G and H) Procapsids persist in

foci and B capsids are now evident as small-core capsids. I) C capsids (white arrowheads) are present in nuclei but are excluded from foci.

found in wild-type infected nuclei, partially- or fully-formed procapsids were most frequently observed. Collectively, the data indicate that mutations of the E846 and E851 residues on the capsid surface delays procapsid maturation.

Table 4.2 Quantification of Intranuclear Capsid Species

		Capsid species % of total (no. of capsids)				
Time	Virus	Pro *	A	B	C	n value
8 hpi	WT	9.1 (5)	0.0 (0)	81.8 (45)	9.1 (5)	9
	EE>AA	82.8 (48)	1.7 (1)	10.3 (6)	5.2 (3)	10
16 hpi	WT	4.2 (8)	8.5 (16)	77.2 (146)	10.1 (19)	9
	EE>AA	66.0 (198)	3.3 (10)	24.7 (74)	6 (18)	7

*Includes partially- and fully-formed procapsids

DISCUSSION

Although no functions have formally been ascribed to the apical region, two conserved glutamic acids within the polyproline loop of the apical region (E846 and E851) were proposed as potential sites for recruitment of VP26 upon shell maturation (93, 158). While residues within the VP5 upper domain are undoubtedly important for the VP26-VP5 interaction, the data presented here demonstrated that the two glutamic acid residues are not required for VP26 binding to capsids.

Despite these findings, mutation of VP5 apical region glutamic acid residues to hydrophobic or positively charged amino acids produced small plaques in cell culture, indicating the apical region was not fully dispensable. Although the EE>AA mutant was further studied, the more severely attenuated E851R mutant may provide insight toward the mechanism driving foci formation. In the future, this mutant should be serially passaged and revertant viruses identified. Further analysis of the EE>AA mutant correlated the propagation defect with the formation of focal structures in infected cell nuclei that consisted of clusters of procapsids. This observation was unexpected because it indicated that capsid maturation was delayed: a process dependent on proteolytic processing of the interior scaffold. While the VP5 floor domain faces the interior of the capsid and interacts with the scaffold proteins (96-100), the exterior location of the apical region is inconsistent with it promoting scaffold processing. Furthermore, the VP5 apical region does not participate in inter-capsomeric interactions (7, 8, 93, 101-103). Importantly, the persistence of procapsids that was initially indicated by the absence of maturation markers (pUL25, VP26, and exposure the 8F5 epitope) was verified by ultrastructural analysis. The latter revealed the foci to consist of capsids containing large scaffold cores, which are indicative of procapsids (117, 123, 210). While the acquisition of surface markers could be sterically restricted within foci, the large scaffold cores indicate that the VP24 maturation protease was inefficiently activated within these procapsids: an event that does not require any known extrinsic interactions, including those with pUL25 or VP26, or genome encapsidation (62, 117, 137, 138).

Notably, the procapsid foci of the polyproline mutant were associated with electron-dense material when imaged by transmission electron microscopy, and in this way resembled procapsids in cell-free assembly systems (119, 211). The procapsid foci were also reminiscent of foci observed when VP24 activity is disrupted through deletion or a temperature-sensitive

mutation (122, 123, 212). In contrast, a recently report detailed a catalytically-inactive VP24 mutant which did not form procapsid foci (62), suggesting these foci are induced by some but not all VP24 mutations. Thus, the mechanism driving procapsids to cluster in foci is of interest, as the clusters may represent sites of capsid assembly or serve to further inform about procapsid maturation. Of greater interest is why capsid maturation is sensitive to mutations in the polyproline loop of the VP5 apical region. While procapsids in the mutant foci were often seen in a partially assembled state, the defect is inconsistent solely with an assembly defect, as seeing accumulations of procapsids is atypical of wild-type infections. Because angularization of the capsid shell under physiological conditions is dependent solely on VP24 activation, which occurs independently of genome encapsidation (62, 119, 150, 213), it can be inferred that mutation of the apical region has affected VP24 activation. Although speculative, the results are consistent with VP24 activation being enhanced by a cue external of the capsid. Capsids require ATP for shell maturation (135), and the apical domain could respond to ATP or interface with another factor such as the putative chaperone of preassembled capsids, pUL32 (64). Interestingly, the mutant foci exclusively consisted of procapsids and B capsids, the two capsid species containing the internal scaffold. While A and C capsids could be found in proximity to the foci, there was no evidence of DNA-packaging occurring within them.

Despite a wealth of knowledge, the details of the molecular mechanisms driving procapsid assembly and maturation remain enigmatic. Viral mutants are a valuable resource to better understanding the complex assembly and maturation of nucleocapsids (123, 135). To the best of my knowledge, this report presents the first attribution of function to the VP5 apical region and documents that the exterior of the capsid contributes to shell maturation.

ACKNOWLEDGEMENTS

I thank Duncan Wilson and Prashant Desai for generously providing antibodies. I also thank Lennell Reynolds, Jr. for processing the transmission electron microscopy samples in Northwestern University's Center for Advanced Microscopy and providing training on the facility's FEI Tecnai Spirit G2 transmission electron microscope.

CHAPTER 5: Development and Characterization of a Procapsid-Specific Fluorescent Fusion

INTRODUCTION

Studies of capsid assembly and maturation are hindered by the short-lived, unstable nature of procapsids. Although baculovirus and cell-free systems (116-121), temperature-sensitive mutants (122, 123), and three-dimensional reconstructions from cryo-electron microscopy (4, 7, 93, 101-103, 124) have provided insights into capsid morphogenesis, our understanding suffers from the lack of a procapsid-specific label. Fluorescent fusions to the capsid proteins VP26 and pUL25, although invaluable toward studying capsid dynamics in live-infected cells, fail to inform on procapsid dynamics since these proteins are added upon maturation. The angularized capsid consists of 8 structural proteins, 2 of them absent from procapsids. The only structural feature unique to the procapsid is uncleaved scaffold proteins.

There are two types of scaffold proteins encoded by the HSV-1 UL26 gene: small (pUL26.5) and large (VP24 + VP21). The large scaffold protein is transcribed from the start methionine at codon 1 producing the maturation protease, VP24, connected to the larger scaffold fragment, VP21. The small scaffold protein transcribes from a second start methionine at amino acid position 307, producing a scaffold protein nearly identical to VP21 (Fig 5.1A). After the capsid assembles a closed shell around the scaffold proteins, VP24 is activated and releases itself from VP21 and then cleaves the carboxyl-terminus of the scaffold proteins, disconnecting them from the inner capsid floor (119, 125-128). In an attempt to create a procapsid specific tag, Maier et al. introduced GFP into four different positions within the UL26 and overlapping UL26.5 open

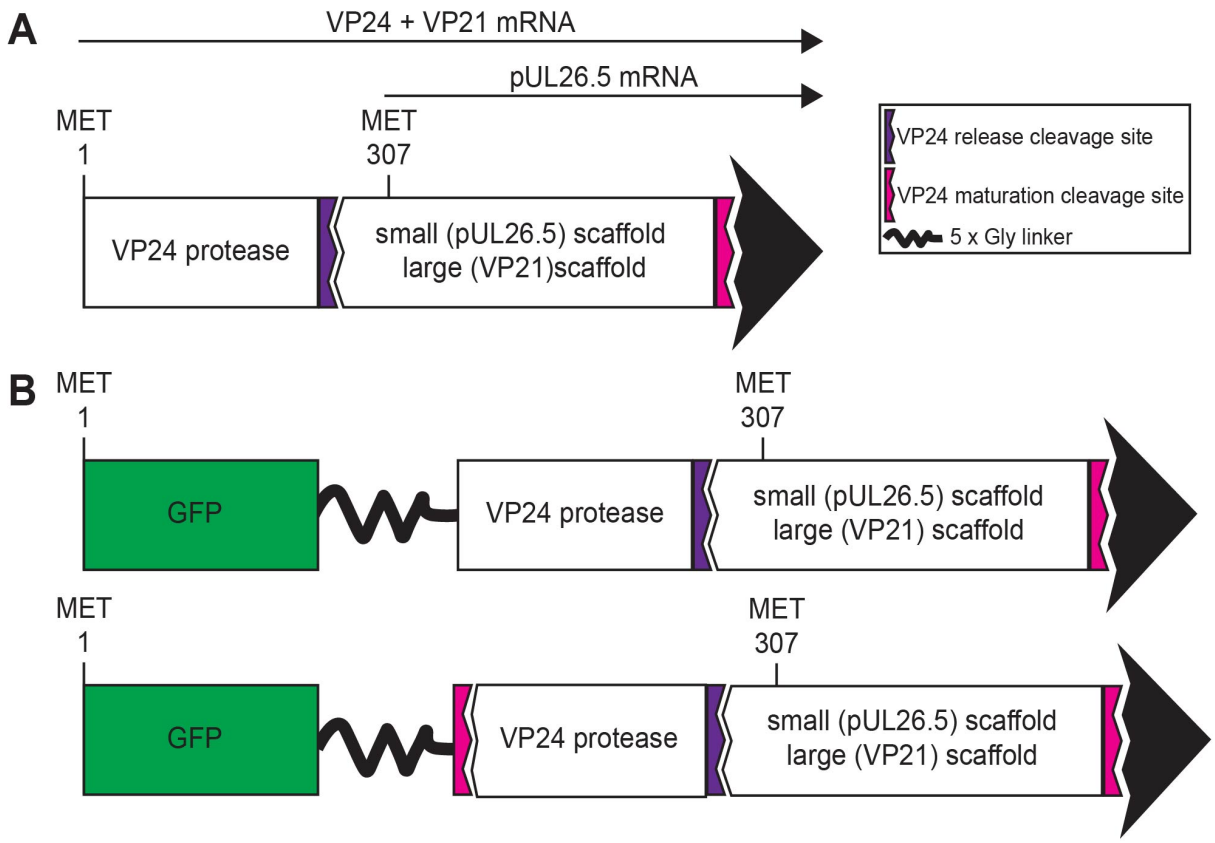

Figure 5.1 Design of a procapsid-specific translational fluorescent fusion protein. (A) Schematic of the HSV-1 UL26 and overlapping UL26.5 open reading frames. (B) Schematic of the GFP-VP24 (upper) and GFP-cut-VP24 (lower) fusion designs.

reading frame. Of these four, only one virus was viable: one in which the fluorescent protein open reading frame was introduced after the first codon of UL26, producing an amino-terminal fusion to the protease, VP24.

Unlike the scaffold proteins, VP24 is retained inside the capsid shell after maturation (10, 11, 126, 140-142). As a result, the GFP-VP24 fusion labels all capsid species: procapsids, A, B,

and C capsids (62). Although this approach allows procapsid dynamics to be studied in live-infected cells for the first time, it requires a second fluorescent capsid protein in order to distinguish procapsids from angularized capsids. In an attempt to further modify this approach and achieve the goal of a procapsid-specific label, the previous design was modified to encode the protease cut site between the green fluorescent protein and the protease (Fig. 5.1B). The prediction was that procapsids, in which VP24 is not yet activated, would exhibit green fluorescence while angularized capsids, in which VP24 has been activated, would lose GFP in a manner similar to the loss of scaffold proteins in most capsid species.

The resulting tag, termed GFP-cut-VP24, produced green fluorescence in a procapsid mutant and little to no fluorescence in angularized capsids or released particles. This work produced the first described procapsid-specific fluorescent fusion which also serves as a fluorescent readout of VP24 activation.

RESULTS

The previously described amino-terminal fusion of GFP in-frame of the HSV-1 UL26 gene was modified to include the sequence of the VP24 cleavage site following the 5 x glycine linker sequence (Fig. 5.1B). Mono-fluorescent and dual-fluorescent viruses were made by two-step RED mediated recombination with or without the VP24 maturation cleavage site, referred to as the cut site in this chapter. To assess the impact of these modifications on viral propagation, plaque diameters were compared to wild-type virus by Neutral Red staining. Mono-fluorescent virus plaque diameters demonstrated no significant change while dual-fluorescent viruses impaired spread in cell-culture (Fig. 5.2). This decrease, although significant, is comparable to the frequently used fusion to pUL25 (Fig. 6.2).

Table 5.1 Viruses Used in Chapter 5

Strain	Fluorescent fusion	Mutations	Titer (PFU/mL)
HSVF-GS2695	-	-	2.59×10^8
HSVF-GS6601	GFP-5xG-VP24	-	
HSVF-GS6661	GFP-5xG-cut*-VP24	-	2.47×10^8
HSVF-GS6672	GFP-5xG-cut*-VP24	UL26 S129P	1.50×10^8
HSVF-GS5471	GFP-5xG-VP24 UL25/mCherry	-	1.60×10^8
HSVF-GS6684	GFP-5xG-cut*-VP24 UL25/mCherry	-	2.64×10^8

*VP24 maturation cleavage site

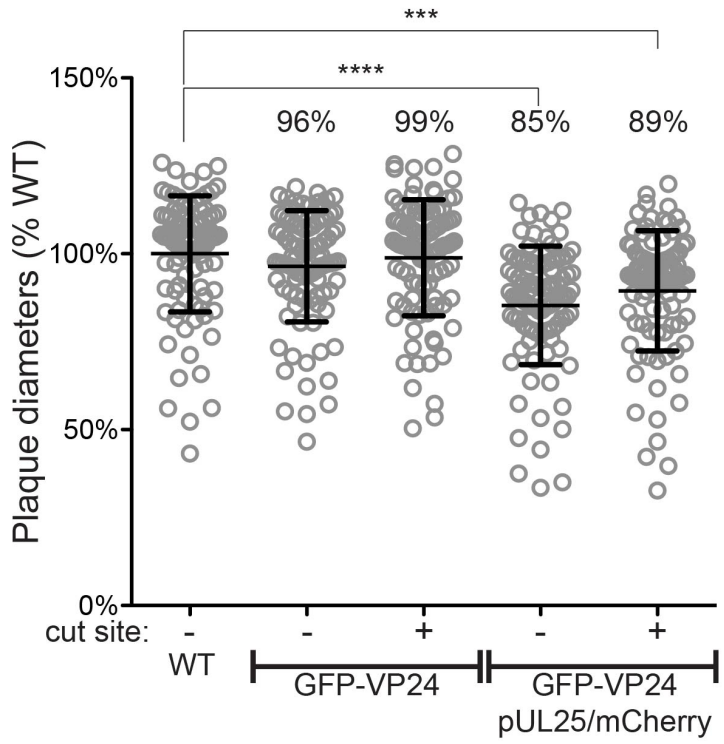

Figure 5.2 Impact of fluorescent fusions on plaque size. Vero cells were infected with mono- and dual-fluorescent viruses encoding or lacking the VP24 cleavage site after the GFP and 5 x glycine linker sequence (cut site). Plaque diameters were measured 5 days post infection.

Diameters are represented as a percent of the mean plaque diameter of wild-type HSV-1 strain F (WT). Error bars indicate the standard deviation of three independent experiments. Asterisks indicate a statistically significant difference from WT (***, $p \leq 0.001$ and ****, $p \leq 0.0001$) as determined by Tukey's multiple comparison test.

In order to initially characterize the GFP-cut-VP24 tag, a catalytically inactive VP24 mutant, UL26 S129P, was used to test the incorporation of the fluorescent tag. Vero cells were infected with HSV-1 encoding the GFP-cut-VP24 tag and the UL26 S129P mutation. At 16 hpi, infected cells were fixed and stained with a VP5 antibody and imaged by confocal microscopy. The nuclei of infected cells exhibited numerous GFP positive diffraction limited puncta that colocalized with VP5 (Fig. 5.3A).

Next, Vero cells were infected with HSV-1 encoding pUL25/mCherry and GFP-VP24 with or without the cut site. Released particles were collected from the infected cell supernatant and spotted on plasma cleaned cover glass for fluorescence microscopy. Particles released from cells infected with the virus lacking the cut site produced red and green diffraction-limited puncta that colocalized while particles released from cells infected with the virus encoding the cut site lacked green fluorescence (Fig. 5.3B). These results demonstrate that GFP is incorporated into capsids when VP24 is inactive but absent from particles released from infected cells, suggesting the GFP-cut-VP24 tag functions as anticipated.

To further characterize and understand the limitations of this new approach, angularized capsid species were next examined. A, B, and C capsids were isolated by density gradient ultracentrifugation from the nuclei of cells infected with dual-fluorescent HSV-1 with or without the cut site. Capsids were spotted on cover glass and imaged by fluorescence microscopy. All

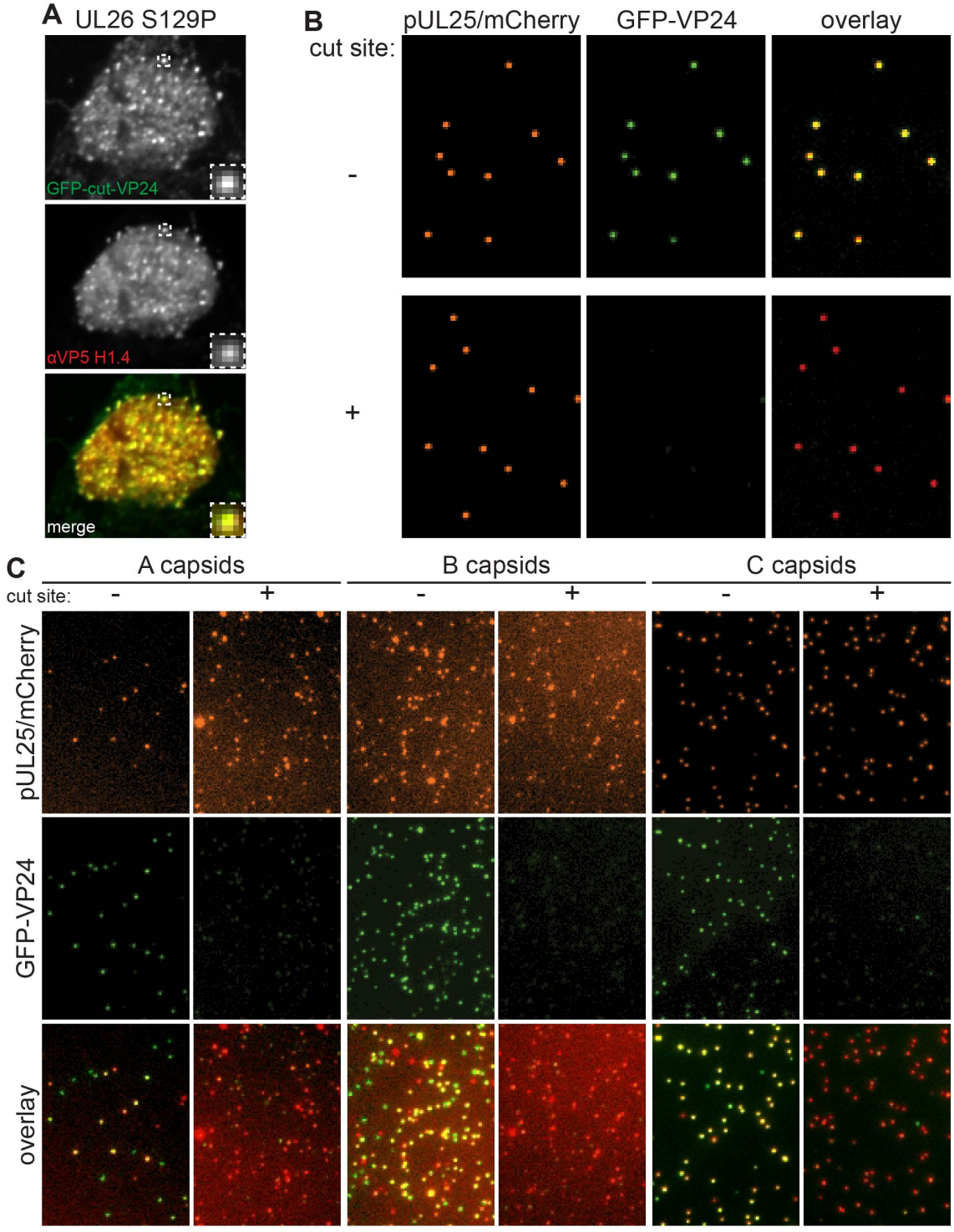

Figure 5.3 Characterization of the GFP-cut-VP24 tag. (A) Vero cells were infected at a MOI of 5 and fixed at 16 hpi. Fixed cells were processed for immunofluorescence using the αVP5 H1.4

antibody and DAPI stain. (B) Vero cells were infected at a MOI of 5 and infected-cell supernatant was harvested at 18.5 hpi. Released particles were collected from the infected-cell supernatant and spotted on cover glass for fluorescence microscopy. (C) Vero cells were infected at a MOI of 10 and intranuclear capsids isolated from nuclei of infected cells over a 20-50% sucrose gradient and visualized by light scattering. Each capsid species was pulled from the gradient and spotted on cover glass for fluorescence microscopy.

---

capsid species lacking the cut site produced diffraction-limited puncta with green fluorescence that substantially colocalized with the pUL25/mCherry signal. In contrast, capsids carrying the cut site exhibited little to no green fluorescence (Fig 5.3 C). Interestingly, the pUL25/mCherry signal on A and B capsids showed more heterogeneity when compared to that of C capsids, suggesting pUL25/mCherry is more tightly bound to DNA-filled capsids and less sensitive to stripping during isolation. Together, the results demonstrate the GFP-cut-VP24 tag labels procapsids in which VP24 is not active but is absent from angularized and mature capsids, making it a procapsid-specific fluorescent label.

DISCUSSION

The procapsid-specific tag, GFP-cut-VP24, presents a new opportunity to study procapsids using fluorescence microscopy. Prior to this development, identification of procapsids required examination of two capsid proteins at a minimum (62). Now, a mono-fluorescent virus is sufficient to monitor procapsid dynamics by fluorescence microscopy in live-infected cells.

The data demonstrate that GFP remains fused to VP24 when the protease is rendered inactive, yet, is absent from capsid species and released particles in which scaffold cleavage has already taken place. This dual-fluorescent virus demonstrated a reduced ability to spread in cell-

culture compared to untagged HSV-1. However, the decrease is modest with respect to other mono-fluorescent capsid tags. Tagging the amino-terminus of VP26 in PRV is akin to deleting VP26, reducing plaque diameters ~25% and titers 10-fold in cell-culture (111). In HSV-1, the impact of various amino-terminal VP26 tags ranges from inducing nuclear aggregates of capsid proteins to impairing nuclear egress and the production of infectious virions (180, 214, 215).

In addition to studying procapsid dynamics, the GFP-cut-VP24 tag could prove invaluable in identifying the events required for VP24 activation. Although it is known that VP24 activation initiates procapsid maturation, the cue required for VP24 to cleave itself from the scaffold and begin disconnecting the scaffold from the inner capsid shell is unknown. The GFP-cut-VP24 tag is a tool that could shed light on enigmatic aspects of herpesvirus capsid morphogenesis.

ACKNOWLEDGEMENTS

I thank Greg Smith for the GFP-cut-VP24 primer design.

CHAPTER 6: Proceed with Caution – The Dangers of Fluorescent Fusion Proteins

INTRODUCTION

Since the discovery of GFP in 1962 (216), fluorescent fusion proteins have become a widely used tool across diverse disciplines to understand the localization and dynamics of proteins of interest. More than 30 years after its discovery, GFP was fused to the herpesvirus small capsid protein, VP26, to create the first fluorescent fusion protein incorporated into the herpesvirus virion structure (217). The GFP-VP26 tag enabled the study of herpesvirus capsid dynamics in living cells and is used to this day.

As the arsenal of fluorescent proteins available increases, herpesviruses are commonly studied with multiple fluorescent fusion proteins encoded by one virus. Bohannon et al. used a panel of dual-fluorescent viruses to dissect the protein composition and architecture of the herpesvirus virion (218). Monomeric red fluorescent protein was fused to VP26 providing a copy-controlled fluorescent marker of capsids, and GFP was fused to a second protein of interest, such as pUL25. Extending this dual-fluorescent approach, I sought to determine residues of the VP5 apical region required for VP26 incorporation on capsids. The results highlighted potential pitfalls of fluorescent fusion proteins as the data directly contradicts data collected from an untagged virus.

RESULTS

When the crystal structure of the VP5 upper domain was solved, glutamic acid residues in the apical region were predicted to mediate binding of VP26, a protein extremely basic in nature (158). Chapters 3 and 4 describe a VP5 glutamic acid mutant, EE>AA, which accumulates intranuclear foci of procapsids that exhibit delayed maturation. Initially, the EE>AA mutant was made in a dual-fluorescent background of HSV-1 with fusions to the structural proteins VP26 and pUL25 (Table 6.1). To test the importance of VP5 glutamic acid residues toward VP26 incorporation on the capsid surface, Vero cells were infected with HSV-1 encoding pUL25/mCherry and GFP-VP26 with VP5 WT or EE>AA. Released particles were isolated from the infected cell supernatant and spotted on cover glass for fluorescence microscopy. pUL25/mCherry puncta colocalized with GFP-VP26 emissions from wild-type capsids. In contrast, the majority of EE>AA capsids lacked GFP-VP26 (Fig. 6.1A).

Table 6.1 Viruses Used in Chapter 6

Strain	Fluorescent fusion	Mutations	Titer (PFU/mL)
HSVF-GS5747	pUL25/mCherry GFP-VP26	-	2.19×10^7
HSVF-GS5934	pUL25/mCherry GFP-VP26	UL19 E846A/E851A	8.61×10^6
HSVF-GS2695	-	-	2.59×10^8
HSVF-GS5798	-	UL19 E846A/E851A	4.72×10^7
HSVF-GS6276	-	UL19 A862-N873 > GGSGGS	1.07×10^8
HSVF-GS4553	pUL25/mCherry	-	7.65×10^7
HSVF-GS5797	pUL25/mCherry	UL19 E846A/E851A	3.70×10^7
HSVF-GS6133	pUL25/mCherry	UL19 A862-N873 > GGSGGS	5.99×10^6

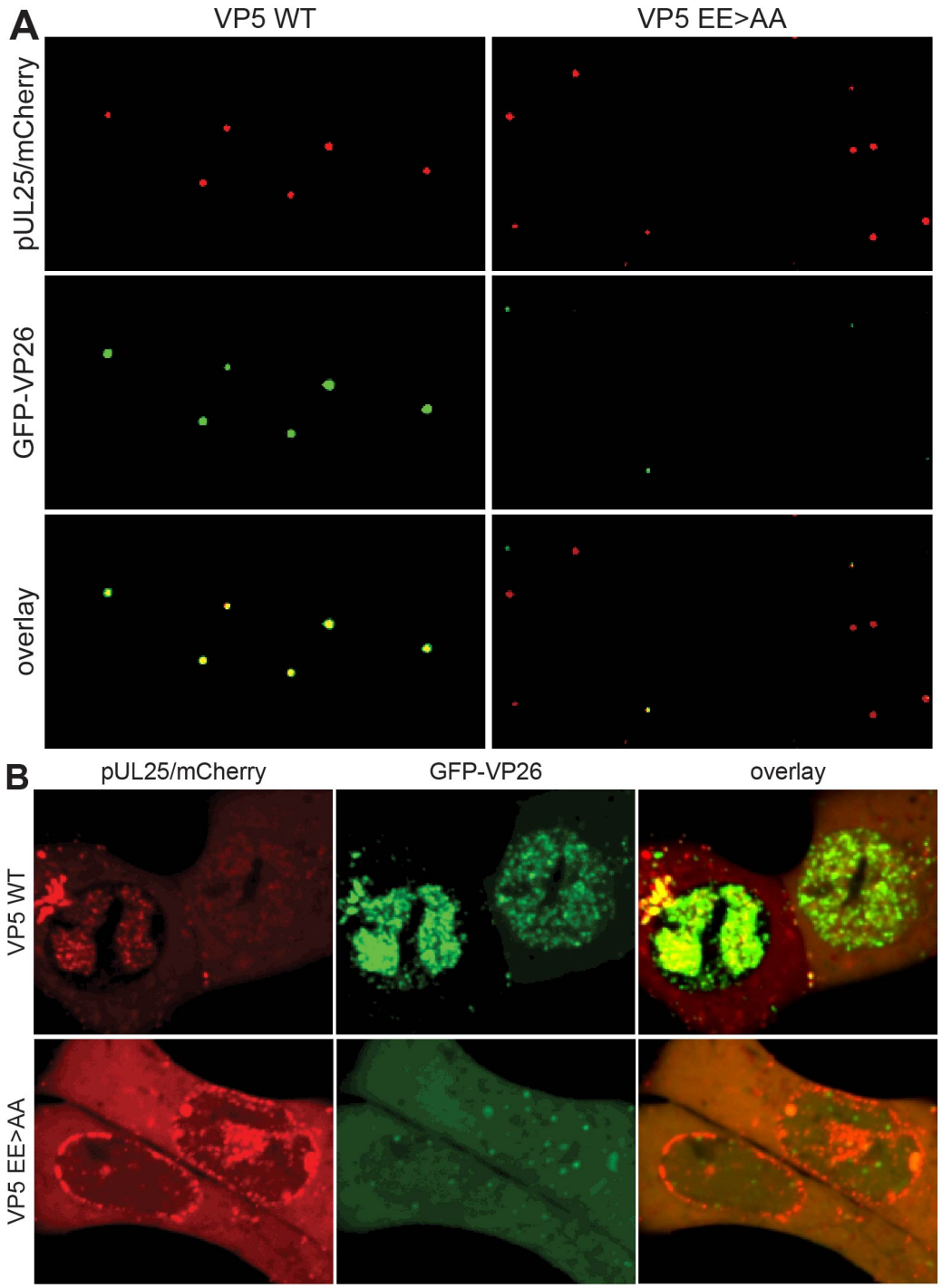

Figure 6.1 Examination of VP5 EE>AA mutant with dual-fluorescent HSV-1. (A) Vero cells were infected at a MOI of 3 and infected-cell supernatant was harvested at 22 hpi. Released particles were collected from the infected-cell supernatant and spotted on cover glass for fluorescence

microscopy. (B) Vero cells were infected at a MOI of 3 and subjected to live-cell microscopy at 12 hpi.

Next, capsid assembly was examined by live-cell confocal microscopy. Vero cells were infected with the above viruses and imaged at 12 hpi. The nuclei of cells infected with HSV-1 wild-type VP5 accumulated GFP-VP26 puncta that significantly overlapped with pUL25/mCherry puncta. However, VP5 EE>AA infected cells demonstrated diffuse GFP-VP26 fluorescence throughout the cell with nuclear aggregates that failed to colocalize with pUL25/mCherry signal (Fig 6.1B). Taken together, the results suggest that the EE>AA mutations disrupt VP26 incorporation, yet this conclusion directly conflicts with the protein profiles of untagged EE>AA capsids, which clearly incorporate VP26 (Fig. 4.5).

In order to assess the impact of a mono-fluorescent capsid surface tag combined with a capsid surface mutation, the plaque diameters of untagged and pUL25/mCherry tagged HSV-1 VP5 EE>AA and Δ6F10 mutants were compared to wild-type virus by Neutral Red staining. The addition of the pUL25/mCherry tag alone significantly reduced plaque diameters, but a more severe decrease was observed when combined with mutations in the VP5 apical region (Fig. 6.2). The synergistic effect between the pUL25/mCherry tag and Δ6F10 mutations was the most dramatic with the fluorescent mutant producing plaques more than 70% smaller than wild-type HSV-1 strain F.

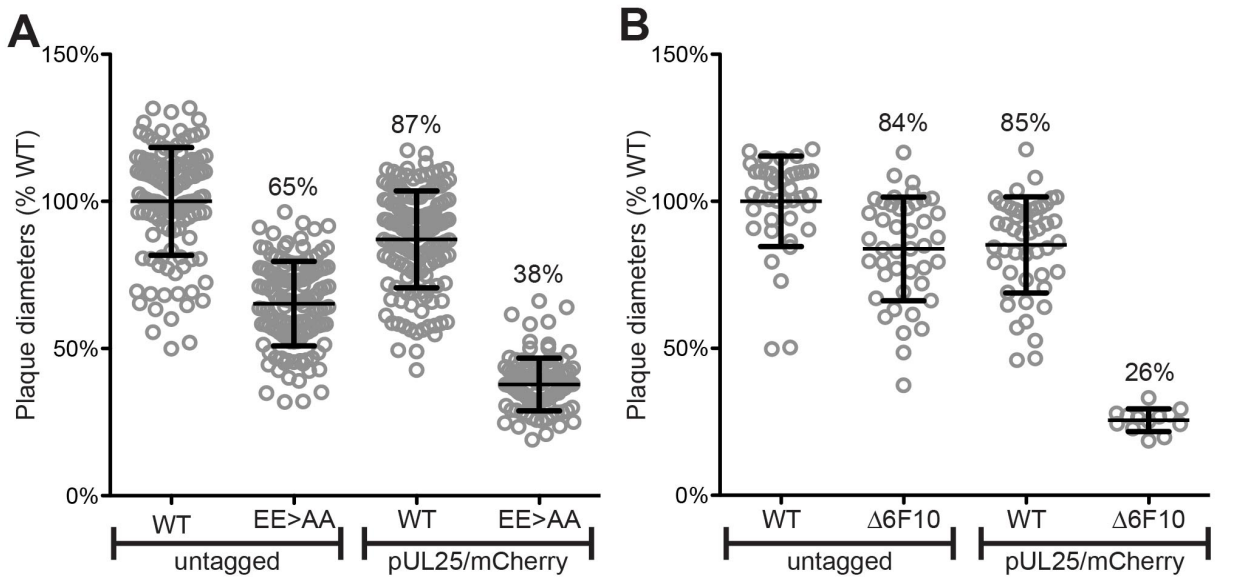

Figure 6.2 Synergistic effects between the VP5 apical region mutations and mCherry tagging pUL25. Vero cells were infected with VP5 EE>AA or Δ6F10 mutants carrying pUL25/mCherry as indicated. Plaque diameters were measured 5 days post infection. Diameters are represented as a percent of the mean plaque diameter of untagged wild-type HSV-1 strain F (WT). Error bars indicate the standard deviation of three independent experiments.

DISCUSSION

The fusion of GFP to the amino-terminus of VP26 produced the first fluorescently labeled herpesvirus capsid (217). Due to its abundance on the capsid, the GFP-VP26 tag is an attractive fluorescent fusion for monitoring viral capsids during infection. Although the fusion design is widely used for its bright signal, consequences accompany attaching a ≥ 25 kDa fluorescent protein to the 12 kDa small capsid protein, VP26. Amino-terminal fusions are reported to reduce viral propagation *in vitro* and *in vivo*, and the copy number of VP26 per

capsid drops from 900 to 300 (111, 180, 205, 214, 215). Additionally, the viral genome undergoes increased mutations when VP26 is tagged (Prashant Desai, personal communication with Greg Smith). However, a newly designed carboxyl-terminal fusion to VP26 in PRV promises greater functionality compared to the long-used amino-terminal tag (219).

The second-generation capsid tag was an in-frame fusion to pUL25 (205, 220). Although this fusion protein is present in a lower quantity, approximately 70 copies per capsid, the pUL25 in-frame fusion less significantly impacts viral propagation compared to the amino-terminal VP26 tag (205). The combination of these two capsid tags is well tolerated in PRV and was used to approximate the copy number of a variety of virion constituents (218). However, the work presented here suggests the two capsid fusions together are less well tolerated in HSV-1. Although the capsid proteins exhibit copy-controlled incorporation, the released particles from HSV-1 encoding pUL25/mCherry and GFP-VP26 appear to have heterogenous signals of each fluorescent protein (Fig. 6.1A), which was not observed with PRV. Additionally, the dual-fluorescent viruses used in this chapter propagated poorly and spontaneously lost fluorescence during passage in cell-culture. These concerns, combined with the results in Chapter 4, suggest the phenotype of the dual-fluorescent VP5 EE>AA mutant is likely an artifact of combining three mutations on the capsid surface.

This chapter also discusses the Δ6F10 mutant which has a dramatic phenotype when combined with the pUL25/mCherry tag. As discussed, the pUL25 fusion alone only modestly impacts viral propagation. However, recent advances in cryo-EM reconstructions has produced near-atomic resolution of the herpesvirus capsid, allowing for more reliable fitting of crystal structures and revealing an intimate association of a pUL25 dimer with the VP5 apical region of

pentamers (4, 7). Therefore, the further decreased ability of the tagged Δ6F10 mutant to spread in cell-culture may indicate a true biological phenotype and be of interest for further study.

Fluorescent proteins have revolutionized virology, opening doors to deeper microscopic exploration. Amidst the excitement, the field fails to call viral fluorescent fusion proteins for what they truly are: mutants. Although a powerful tool, fluorescent tags can easily disrupt a protein of interest's folding, localization, and function (221, 222). Scientists must always acknowledge the caveats of introducing a fluorescent fusion, analyze the data with caution, and confirm the results with alternative methods. As for this scientist's words of advice: only use a fluorescent fusion to a viral protein when necessary.

ACKNOWLEDGEMENTS

I thank basic research for teaching me hard lessons and refining me into a better version of myself.

CHAPTER 7: Discussion and Future Direction

Assembly of herpesvirus virions begins with the formation of spherical procapsid shells in infected cell nuclei. These short-lived structures are unstable but angularize into rigid, stable capsids during maturation (62, 123). When shell maturation is accompanied by genome encapsidation, the resulting product is a C capsid or nucleocapsid. This critical process is a target for antiviral development (82, 168-175), which is bolstered by ongoing refinements of cryo-EM reconstruction techniques that have led to herpesvirus capsid models with near-atomic resolution (5-8).

The surface of the procapsid is decorated by the apical region of the MCP (VP5), which constitutes the tips of the 11 pentamers (accounting for 11 of the icosahedral vertices, with the 12th vertex occupied by the portal) and 150 hexamers that make up the majority of the icosahedral shell. Following maturation, the procapsid acquires the accessory proteins – the CVSC component pUL25 and the SCP (VP26) – the latter of which selectively covers the apical regions of the hexamers. Thus, the procapsid displays 955 copies of the apical region on its surface, which is reduced to 55 exposed copies upon maturation and decoration with the SCP. The exposure of the MCP apical region on the mature capsid led me to investigate whether it contributes to the retrograde axonal transport of capsids that leads to the establishment of latent infections in the nervous system. Although the mutational analysis presented in Chapter 3 cannot rule out the entirety of the MCP apical region, retrograde analysis shows nearly half of the apical region's residues are dispensable for capsid transport. Considering the most abundant surface protein of the mature capsid, the SCP, is also dispensable for transport, it appears that the bulk of

exposed outer capsid surface does not promote this critical component of the HSV-1 neuroinvasion mechanism.

Despite these negative results, the polyproline (EE>AA) mutant produced small plaques in cell culture, indicating the apical region was not fully expendable. Further analysis correlated the propagation defect with the formation of focal structures in infected cell nuclei that consisted of clusters of procapsids. This observation was unexpected because it indicated that capsid maturation was delayed: a process dependent on proteolytic processing of the interior scaffold. While the MCP floor domain faces the interior of the capsid and interacts with the scaffold proteins (96-100), the exterior location of the apical region is inconsistent with it promoting scaffold processing. Furthermore, the MCP apical region does not participate in inter-capsomeric interactions (7, 8, 93, 101-103). Importantly, the persistence of procapsids that was initially indicated by the absence of maturation markers (pUL25, VP26, and exposure the 8F5 epitope) was verified by ultrastructural analysis. The latter revealed the foci to consist of capsids containing large scaffold cores, which are indicative of procapsids (117, 123, 210). While the acquisition of surface markers could be sterically restricted within foci, the large scaffold cores indicate that the maturation protease was inefficiently activated within these procapsids: an event that does not require any known extrinsic interactions including with pUL25, the SCP, or genome encapsidation (62, 117, 137, 138).

Notably, the foci of the polyproline mutant consisted of partially- and fully-formed procapsids which were associated with electron-dense material when imaged by transmission electron microscopy, and in this way resembled procapsids in cell-free assembly systems (119, 211). In transmission electron micrographs of HSV-1 infected cells, partially-formed procapsids are not observed, even at 7 hpi (123). Additionally, foci of procapsids are not observed in wild-

type infection as evidenced by ultrastructural analysis as early as 8 hpi. These observations suggest the EE>AA mutant might exhibit delayed capsid assembly kinetics.

The procapsid self-assembles presumably from protomers, or assembly units, which join together to first form an arc-like structure or a partially-formed procapsid. The structure continues to grow until a closed, spherical structure, or fully-formed procapsid, is built (119). Based on *in vitro* assembly studies, the protomers were suggested to be pre-formed triplexes that interact with MCP-scaffold complexes (223). More recently, the protomer was proposed to consist of one triplex surrounded by three MCP monomers each of which may interact with a dimer of scaffold proteins (102, 224). Perhaps MCP apical region glutamic acid residues aid in positioning MCP towers within the protomer or relative to other protomers, and mutation of these residues causes protomers to assemble more slowly. Although the field lacks finely-tuned *in vitro* assembly assays, such those used for bacteriophage (95, 225-227), a comparison of wild-type and EE>AA MCP in a baculovirus system may provide initial insights toward understanding the impact of the glutamic acid mutations on procapsid assembly. An additional point of interest is to understand the composition of the electron-dense matrix surrounding EE>AA procapsids. This matrix might consist of capsid proteins or even protomers. Immunogold labeling should be carried out to identify proteins contained within this matrix.

The EE>AA procapsid foci were also reminiscent of foci observed when the maturation protease activity is disrupted through mutation or deletion (122, 123, 212). However, in contrast, a previously reported catalytically-inactive protease mutant that did not produce procapsid foci (62). Thus, the mechanism driving procapsids to cluster in foci is of interest, as the clusters may represent sites of capsid assembly. Other herpesviruses with slower replication cycles compared to PRV or HSV-1 form clusters of capsids which are thought to be sites of assembly and

maturation. The alphaherpesvirus, VZV, exhibits dynamic capsid aggregates in the nuclei of infected cells during the height of PFU production (63), and EBV capsid assembly is reported to take place within nuclear domains known as PML bodies (228). However, evidence of preferential sites of capsid assembly have not been observed for HSV-1 or PRV (62).

At one time, it was proposed that HSV-1 capsid assembly and maturation was modeled within assemblons, or large paracrystalline arrays of capsids observed within the nucleus during late (~16 hpi) infection (229). While assemblons have been used to determine the ability of a protein to associate with capsid structures (181, 230), it is questionable whether these structures inform on productive capsid morphogenesis considering the cell-associated PFU production tapers around 16 hpi and capsid maturation in the nucleus must precede virion formation in the cytoplasm. In contrast, the EE>AA mutant exhibits a kinetic delay with cell-associated PFU still increasing at the latest time examined (30 hpi). Whether EE>AA foci represent dynamic sites of capsid assembly remains to be determined. Using a the photoconvertible protein mEOS fused to the internal protease, I examined EE>AA foci by live-cell microscopy. While photoconversion of foci was successful, the foci exhibited dynamic motion during infection, frequently moving in and out of the plane of view, making it difficult to track photoconverted foci and individual capsids prior to bleaching of the fluorescent signal. Furthermore, mEOS presumably matured with a delayed kinetic, considering foci were evident by MCP antibody staining prior to mEOS fluorescence. In the future, advanced microscopy techniques such as fluorescence recovery after photobleaching or photoactivation with an alternative fluorescent protein might serve to investigate this possibility.

Of greater interest is why capsid maturation is sensitive to mutations in the polyproline loop of the MCP apical region. While procapsids in the mutant foci were often seen in a partially

assembled state, the defect is inconsistent solely with an assembly defect, as seeing accumulations of procapsids is atypical of wild-type infections. Because angularization of the capsid shell under physiological conditions is dependent solely on protease activation, which occurs independently of genome encapsidation (62, 119, 150, 213), it can be inferred that mutation of the apical region has affected protease activation. Although speculative, the results are consistent with protease activation being enhanced by a cue external of the capsid. Capsids require ATP for shell maturation (135), and the apical domain could respond to ATP. Interestingly, the mutant foci exclusively consisted of procapsids and B capsids, with procapsids being the predominant species at 8 hpi and B capsids accumulating by 16 hpi. While A and C capsids could be found in proximity to the foci, there was no evidence of DNA-packaging occurring within them.

Instead of ATP, the external cue could be the binding of a cellular or viral protein. Future work should investigate two encapsidation proteins of particular interest: pUL32 and pUL17. As a putative chaperone of preassembled capsids that has been demonstrated to modify disulfide bonds of viral structural proteins, pUL32 might function to modify the capsid in preparation for encapsidation by striking the balance between flexibility and rigidity found in the DNA-filled megastructure (64, 149). Furthermore, a pUL32-null mutant accumulates procapsids unable to initiate maturation (150). The encapsidation role of the CVSC component pUL17 is also somewhat muddled. Although it is clear this component of the vertex affords the capsid mechanical strength, it is not yet appreciated why a null virus accumulates only B capsids – a capsid species thought to have an unproductive relationship with the DNA packaging machinery. The other vertex reinforcement protein, pUL25, is not required for the encapsidation process as the nuclei of cells infected with a null mutant accumulate DNA-filled capsids. Thus, pUL32 and

pUL17 stand out as interesting candidates that perhaps must localize to procapsids within EE>AA foci for maturation to proceed.

Although no functions have formally been ascribed to the MCP apical region, two conserved glutamic acids within the polyproline loop of the apical region (E846 and E851) were proposed as potential sites for recruitment of the SCP upon shell maturation (93, 158). While residues within the MCP upper domain are undoubtedly important for the SCP-MCP interaction, the data demonstrated that the two glutamic acid residues are not required for SCP binding to capsids. In the beta and gammaherpesviruses, the SCP binds hexamers and pentamers. The MCP of these viruses show structural differences in the upper domain where the MCP binds, and for KSHV, four MCP hydrophobic residues were required for interactions with the SCP *in vitro* (5, 6).

Despite the high-level of SCP observed on EE>AA mutant capsids, it cannot be assumed the SCP is present at full occupancy in the absence of quantitative analysis. For the most part, the EE>AA mutant phenotype does not appear to mimic observations of SCP-null mutants (111, 179, 180). It does bear similarity to SCP-null and SCP-phosphorylation mutants described by one research group. In this work, deletion of the SCP or mutation of a critical phosphorylation site induced intranuclear accumulations of the MCP at 12 hpi (209). However, in a follow-up study, these accumulations were found to consist of all three angularized capsid species (110), while EE>AA MCP foci contain no evidence of DNA-packaging, consisting only of procapsids and B capsids. Furthermore, a SCP-null mutant constructed in our laboratory failed to reproduce the result of intranuclear MCP accumulations, suggesting the phenotypes are likely unrelated. However, in the future, densitometry analysis of the SCP levels on isolated capsids could determine if EE>AA mutations reduce SCP incorporation.

In addition to assessing the contribution of the MCP apical region toward infection, this dissertation presents a modified fluorescent fusion design that produced the first described procapsid-specific tag. The design fuses a fluorescent protein open reading frame to the amino-terminus of the protease and includes the protease cleavage site immediately following the fluorescent protein's sequence. As a result, the fluorescent protein is cleaved from the protease upon its activation during capsid maturation and the fluorescent signal is lost from the megastructure. This procapsid-specific tag not only allows for the identification of procapsids in living cells but also might serve as a fluorescent readout of protease activity. The procapsid-specific tag, GFP-cut-VP24, presents a new opportunity to study procapsids using fluorescence microscopy. Prior to this development, identification of procapsids required examination of two capsid proteins at a minimum (62). Now, a mono-fluorescent virus is sufficient to monitor procapsid dynamics by fluorescence microscopy in live-infected cells.

Further characterization of the GFP-cut-VP24 tag should be carried out in order to understand the limitations of this approach. First, Western Blot analysis of procapsids versus angularized capsids and virions should be performed to detect the amount of GFP present in each capsid species population. Additionally, single-particle analysis of a dual-fluorescent virus (GFP-cut-VP24 and pUL25/mCherry) could be used to quantify the average copy number of GFP found in each capsid type.

An additional point of interest is to determine the means by which GFP is able to escape the capsid shell following cleavage from the protease. It was interesting to find GFP was absent from B capsids while the scaffold is trapped, demonstrating the scaffold is somehow specifically retained in this capsid species. It led me to wonder if the restriction mechanism was simply protein size considering the GFP fused to the protease is 27 kDa with a diameter of 40 Å – just

small enough to theoretically fit through the approximated size of the portal vertex opening of 40 Å – while the cleaved small and large scaffold proteins are approximately 40 kDa and 75 kDa, respectively (231). To test this, a mutant virus encoding the GFP-cut-VP24 tag should be modified to lack the portal vertex and the resultant capsid structures assessed in combination with a second capsid marker such as a MCP antibody or the pUL25/mCherry fusion. Although this point may be a curiosity, it would provide additional understanding of the herpesvirus capsid structure and the GFP-cut-VP24 tag.

Despite a wealth of knowledge accrued from decades of research, the details of the molecular mechanisms driving herpesvirus nucleocapsid assembly and maturation remain enigmatic. Viral mutants, including viruses encoding fluorescent fusion proteins, are a valuable resource to better understanding the complex assembly and maturation of nucleocapsids (123, 135). With its delayed propagation kinetics, perhaps further examination of the EE>AA mutant will provide additional insights into capsid morphogenesis. To the best of my knowledge, this report presents the first attribution of function to the MCP apical region and documents that the exterior of the capsid contributes to shell maturation.

REFERENCES

1. Davison AJ. 2011. Evolution of sexually transmitted and sexually transmissible human herpesviruses. Ann N Y Acad Sci 1230:E37-49.

2. Nishiyama Y. 2004. Herpes simplex virus gene products: the accessories reflect her lifestyle well. Rev Med Virol 14:33-46.

3. Kornfeind EM, Visalli RJ. 2018. Human herpesvirus portal proteins: Structure, function, and antiviral prospects. Rev Med Virol 28:e1972.

4. Liu YT, Jiang J, Bohannon KP, Dai X, Gant Luxton GW, Hui WH, Bi GQ, Smith GA, Hong Zhou Z. 2017. A pUL25 dimer interfaces the pseudorabies virus capsid and tegument. J Gen Virol 98:2837-2849.

5. Yu X, Jih J, Jiang J, Zhou ZH. 2017. Atomic structure of the human cytomegalovirus capsid with its securing tegument layer of pp150. Science 356.

6. Dai X, Gong D, Lim H, Jih J, Wu TT, Sun R, Zhou ZH. 2018. Structure and mutagenesis reveal essential capsid protein interactions for KSHV replication. Nature 553:521-525.

7. Dai X, Zhou ZH. 2018. Structure of the herpes simplex virus 1 capsid with associated tegument protein complexes. Science 360.

8. Yuan S, Wang J, Zhu D, Wang N, Gao Q, Chen W, Tang H, Wang J, Zhang X, Liu H, Rao Z, Wang X. 2018. Cryo-EM structure of a herpesvirus capsid at 3.1 A. Science 360.

9. Bauer DW, Huffman JB, Homa FL, Evilevitch A. 2013. Herpes virus genome, the pressure is on. J Am Chem Soc 135:11216-21.

10. Kramer T, Greco TM, Enquist LW, Cristea IM. 2011. Proteomic characterization of pseudorabies virus extracellular virions. J Virol 85:6427-41.

11. Loret S, Guay G, Lippe R. 2008. Comprehensive characterization of extracellular herpes simplex virus type 1 virions. J Virol 82:8605-18.

12. Johannsen E, Luftig M, Chase MR, Weicksel S, Cahir-McFarland E, Illanes D, Sarracino D, Kieff E. 2004. Proteins of purified Epstein-Barr virus. Proc Natl Acad Sci U S A 101:16286-91.

13. Bradley H, Markowitz LE, Gibson T, McQuillan GM. 2014. Seroprevalence of herpes simplex virus types 1 and 2--United States, 1999-2010. J Infect Dis 209:325-33.

14. Britt WJ. 2018. Maternal Immunity and the Natural History of Congenital Human Cytomegalovirus Infection. Viruses 10.

15. Eliassen E, Krueger G, Luppi M, Ablashi D. 2018. Lymphoproliferative Syndromes Associated with Human Herpesvirus-6A and Human Herpesvirus-6B. Mediterr J Hematol Infect Dis 10:e2018035.

16. Staras SAS, Dollard SC, Radford KW, Flanders WD, Pass RF, Cannon MJ. 2006. Seroprevalence of Cytomegalovirus Infection in the United States, 1988-1994. Clin Infect Dis 43.

17. Pellett PE, Ablashi DV, Ambros PF, Agut H, Caserta MT, Descamps V, Flamand L, Gautheret-Dejean A, Hall CB, Kamble RT, Kuehl U, Lassner D, Lautenschlager I, Loomis KS, Luppi M, Lusso P, Medveczky PG, Montoya JG, Mori Y, Ogata M, Pritchett JC, Rogez S, Seto E, Ward KN, Yoshikawa T, Razonable RR. 2012. Chromosomally integrated human herpesvirus 6: questions and answers. Rev Med Virol 22:144-55.

18. Ablashi DV, Berneman ZN, Kramarsky B, Asano Y, Choudhury S, Pearson GR. 1994. Human Herpesvirus-7 (HHV-7). In Vivo 8:549-554.

19. Mesri EA, Cesarman E, Boshoff C. 2010. Kaposi's sarcoma herpesvirus/ Human herpesvirus-8 (KSHV/ HHV8), and the oncogenesis of Kaposi's sarcoma. Nat Rev Cancer 10:707-19.

20. Choi R, Kim GM, Jo IJ, Sim MS, Song KJ, Kim BJ, Na DL, Huh HJ, Kim JW, Ki CS, Lee NY. 2014. Incidence and clinical features of herpes simplex viruses (1 and 2) and varicella-zoster virus infections in an adult Korean population with aseptic meningitis or encephalitis. J Med Virol 86:957-62.

21. Jaques DA, Bagetakou S, L'Huillier AG, Bartoli A, Vargas MI, Fluss J, Kaiser L. 2016. Herpes simplex encephalitis as a complication of neurosurgical procedures: report of 3 cases and review of the literature. Virol J 13:83.

22. Kaye S, Choudhary A. 2006. Herpes simplex keratitis. Prog Retin Eye Res 25:355-80.

23. Tsatsos M, MacGregor C, Athanasiadis I, Moschos MM, Hossain P, Anderson D. 2016. Herpes simplex virus keratitis: an update of the pathogenesis and current treatment with oral and topical antiviral agents. Clin Exp Ophthalmol 44:824-837.

24. Rasche L, Kapp M, Einsele H, Mielke S. 2014. EBV-induced post transplant lymphoproliferative disorders: a persisting challenge in allogeneic hematopoetic SCT. Bone Marrow Transplant 49:163-7.

25. Chen YC, Sheng J, Trang P, Liu F. 2018. Potential Application of the CRISPR/Cas9 System against Herpesvirus Infections. Viruses 10.

26. Steiner I, Kennedy PGE, Pachner AR. 2007. The neurotropic herpes viruses: herpes simplex and varicella-zoster. The Lancet Neurology 6:1015-1028.

27. Knipe DM, Cliffe A. 2008. Chromatin control of herpes simplex virus lytic and latent infection. Nat Rev Microbiol 6:211-21.

28. Grinde B. 2013. Herpesviruses: latency and reactivation - viral strategies and host response. J Oral Microbiol 5.

29. Wilson AC, Mohr I. 2012. A cultured affair: HSV latency and reactivation in neurons. Trends Microbiol 20:604-11.

30. Schiffer JT, Corey L. 2013. Rapid host immune response and viral dynamics in herpes simplex virus-2 infection. Nat Med 19:280-90.

31. Zhang J, Liu H, Wei B. 2017. Immune response of T cells during herpes simplex virus type 1 (HSV-1) infection. J Zhejiang Univ Sci B 18:277-288.

32. Akhtar J, Shukla D. 2009. Viral entry mechanisms: cellular and viral mediators of herpes simplex virus entry. FEBS J 276:7228-36.

33. Reske A, Pollara G, Krummenacher C, Chain BM, Katz DR. 2007. Understanding HSV-1 entry glycoproteins. Rev Med Virol 17:205-15.

34. Aggarwal A, Miranda-Saksena M, Boadle RA, Kelly BJ, Diefenbach RJ, Alam W, Cunningham AL. 2012. Ultrastructural visualization of individual tegument protein dissociation during entry of herpes simplex virus 1 into human and rat dorsal root ganglion neurons. J Virol 86:6123-37.

35. Luxton GW, Haverlock S, Coller KE, Antinone SE, Pincetic A, Smith GA. 2005. Targeting of herpesvirus capsid transport in axons is coupled to association with specific sets of tegument proteins. Proc Natl Acad Sci U S A 102:5832-7.

36. Kelly BJ, Fraefel C, Cunningham AL, Diefenbach RJ. 2009. Functional roles of the tegument proteins of herpes simplex virus type 1. Virus Research 145:173-186.

37. Granzow H, Klupp BG, Mettenleiter TC. 2005. Entry of pseudorabies virus: an immunogold-labeling study. J Virol 79:3200-5.

38. Antinone SE, Smith GA. 2010. Retrograde axon transport of herpes simplex virus and pseudorabies virus: a live-cell comparative analysis. J Virol 84:1504-12.

39. Zaichick SV, Bohannon KP, Hughes A, Sollars PJ, Pickard GE, Smith GA. 2013. The herpesvirus VP1/2 protein is an effector of dynein-mediated capsid transport and neuroinvasion. Cell Host Microbe 13:193-203.

40. Richards AL, Sollars PJ, Pitts JD, Stults AM, Heldwein EE, Pickard GE, Smith GA. 2017. The pUL37 tegument protein guides alpha-herpesvirus retrograde axonal transport to promote neuroinvasion. PLoS Pathog 13:e1006741.

41. Huffmaster NJ, Sollars PJ, Richards AL, Pickard GE, Smith GA. 2015. Dynamic ubiquitination drives herpesvirus neuroinvasion PNAS 112:12818-12823.

42. Sodeik B, Ebersold MW, Helenius A. 1997. Microtubule-mediated Transport of Incoming Herpes Simplex Virus 1 Capsids to the Nucleus. The Journal of Cell Biology 136:1007-1021.

43. Shanda SK, Wilson DW. 2008. UL36p is required for efficient transport of membrane-associated herpes simplex virus type 1 along microtubules. J Virol 82:7388-94.

44. Krautwald M, Fuchs W, Klupp BG, Mettenleiter TC. 2009. Translocation of incoming pseudorabies virus capsids to the cell nucleus is delayed in the absence of tegument protein pUL37. J Virol 83:3389-96.

45. Copeland AM, Newcomb WW, Brown JC. 2009. Herpes simplex virus replication: roles of viral proteins and nucleoporins in capsid-nucleus attachment. J Virol 83:1660-8.

46. Pasdeloup D, Blondel D, Isidro AL, Rixon FJ. 2009. Herpesvirus capsid association with the nuclear pore complex and viral DNA release involve the nucleoporin CAN/Nup214 and the capsid protein pUL25. J Virol 83:6610-23.

47. Jovasevic V, Liang L, Roizman B. 2008. Proteolytic cleavage of VP1-2 is required for release of herpes simplex virus 1 DNA into the nucleus. J Virol 82:3311-9.

48. Huffman JB, Daniel GR, Falck-Pedersen E, Huet A, Smith GA, Conway JF, Homa FL. 2017. The C Terminus of the Herpes Simplex Virus UL25 Protein Is Required for Release of Viral Genomes from Capsids Bound to Nuclear Pores. J Virol 91.

49. Abaitua F, Daikoku T, Crump CM, Bolstad M, O'Hare P. 2011. A single mutation responsible for temperature-sensitive entry and assembly defects in the VP1-2 protein of herpes simplex virus. J Virol 85:2024-36.

50. Preston VG, Murray J, Preston CM, McDougall IM, Stow ND. 2008. The UL25 gene product of herpes simplex virus type 1 is involved in uncoating of the viral genome. J Virol 82:6654-66.

51. Batterson W, Furlong D, Roizman B. 1983. Molecular Genetics of Herpes Simplex Virus VIII. Further Characterization of a Temperature-Sensitive Mutant Defective in Release of Viral DNA and in Other Stages of the Viral Reproductive Cycle. J Virol 45:397-407.

52. Lehman IR, Boehmer PE. 1999. Replication of Herpes Simplex Virus DNA. J Biol Chem 274:28059-28062.

53. Smiley JR, Lavery C, Howes M. 1992. The Herpes Simplex Virus Type 1 (HSV-1) a Sequence Serves as a Cleavage/Packaging Signal but Does Not Drive Recombinational Genome Isomerization When It Is Inserted into the HSV-2 Genome. J Virol 66:7505-7510.

54. Honess RW, Roizman B. 1974. Regulation of Herpesvirus Macromolecular Synthesis. I. Cascade Regulation of the Synthesis of Three Groups of Viral Proteins. J Virol 14:8-19.

55. Jones PC, Roizman B. 1979. Regulation of Herpesvirus Macromolecular Synthesis VIII. The Transcription Program Consists of Three Phases During Which Both Extent of Transcription and Accumulation of RNA in the Cytoplasm Are Regulated. J Virol 31:299-314.

56. Holland LE, Anderson KP, Shipman CJ, Wagner EK. 1979. Viral Synthesis Is Required for the Efficient Expression of Specific Herpes Simplex Virus Type 1 mRNA Species. Virology 101:10-24.

57. Pomeranz LE, Reynolds AE, Hengartner CJ. 2005. Molecular biology of pseudorabies virus: impact on neurovirology and veterinary medicine. Microbiol Mol Biol Rev 69:462-500.

58. Everett RD. 2000. ICP0, a regulator of herpes simplex virus during lytic and latent infection. BioEssays 22:761-770.

59. Monier K, Arma JCG, Etteldorf S, Ghazal P, Sullivan KF. 2000. Annexation of the interchroomosomal space during viral infection. Nat Cell Biol 2:661-665.

60. Liptak LM, Uprichard SL, Knipe DM. 1996. Functional Order of Assembly of Herpes Simplex Virus DNA Replication Proteins into Prereplicative Site Structures. J Virol 70:1759-1767.

61. Everett RD, Sourvinos G, Leiper C, Clements JB, Orr A. 2004. Formation of Nuclear Foci of the Herpes Simplex Virus Type 1 Regulatory Protein ICP4 at Early Times of Infection: Localization, Dynamics, Recruitment of ICP27, and Evidence for the De Novo Induction of ND10-Like Complexes. Journal of Virology 78:1903-1917.

62. Maier O, Sollars PJ, Pickard GE, Smith GA. 2016. Visualizing Herpesvirus Procapsids in Living Cells. J Virol 90:10182-10192.

63. Lebrun M, Thelen N, Thiry M, Riva L, Ote I, Conde C, Vandevenne P, Di Valentin E, Bontems S, Sadzot-Delvaux C. 2014. Varicella-zoster virus induces the formation of dynamic nuclear capsid aggregates. Virology 454-455:311-27.

64. Lamberti C, Weller SK. 1998. The Herpes Simplex Virus Type 1 Cleavage/Packaging Protein, UL32, Is Involved in Efficient Localization of Capsids to Replication Compartments. J Virol 72:2463-2473.

65. Leelawong M, Guo D, Smith GA. 2011. A physical link between the pseudorabies virus capsid and the nuclear egress complex. J Virol 85:11675-84.

66. Yang K, Baines J. 2011. Selection of HSV capsids for envelopment involves interaction between capsid surface components pUL31, pUL17, and pUL25. PNAS 108:14276-14281.

67. Yang K, Wills E, Lim HY, Zhou ZH, Baines JD. 2014. Association of Herpes Simplex Virus pUL31 with Capsid Vertices and Components of the Capsid Vertex Specific Complex. J Virol doi:10.1128/JVI.03175-13.

68. Reynolds AE, Ryckman BJ, Baines JD, Zhou Y, Liang L, Roller RJ. 2001. UL31 and UL34 Proteins of Herpes Simplex Virus Type 1 Form a Complex That Accumulates at the Nuclear Rim and Is Required for Envelopment of Nucleocapsids. Journal of Virology 75:8803-8817.

69. Fuchs W, Klupp BG, Granzow H, Osterrieder N, Mettenleiter TC. 2002. The Interacting UL31 and UL34 Gene Products of Pseudorabies Virus Are Involved in Egress from the Host-Cell Nucleus and Represent Components of Primary Enveloped but Not Mature Virions. Journal of Virology 76:364-378.

70. Henaff D, Remillard-Labrosse G, Loret S, Lippe R. 2013. Analysis of the early steps of herpes simplex virus 1 capsid tegumentation. J Virol 87:4895-906.

71. Loret S, Lippe R. 2012. Biochemical analysis of infected cell polypeptide (ICP)0, ICP4, UL7 and UL23 incorporated into extracellular herpes simplex virus type 1 virions. J Gen Virol 93:624-34.

72. Granzow H, Klupp BG, Fuchs W, Veits J, Osterrieder N, Mettenleiter TC. 2001. Egress of alphaherpesviruses: comparative ultrastructural study. J Virol 75:3675-84.

73. van Genderen IL, Brandimarti R, Torrisi MR, Campadelli G, van Meer G. 1994. The Phospholipid Composition of Extracellular Herpes Simplex Virions Differs from That of Host Cell Nuclei. Virology 200:831-836.

74. Turcotte S, Letellier J, Lippe R. 2005. Herpes simplex virus type 1 capsids transit by the trans-Golgi network, where viral glycoproteins accumulate independently of capsid egress. J Virol 79:8847-60.

75. Diefenbach RJ. 2015. Conserved tegument protein complexes: Essential components in the assembly of herpesviruses. Virus Res 210:308-317.

76. Antinone SE, Zaichick SV, Smith GA. 2010. Resolving the assembly state of herpes simplex virus during axon transport by live-cell imaging. J Virol 84:13019-30.

77. Favoreel HW. 2006. The why's of Y-based motifs in alphaherpesvirus envelope proteins. Virus Res 117:202-8.

78. Henaff D, Radtke K, Lippe R. 2012. Herpesviruses exploit several host compartments for envelopment. Traffic 13:1443-9.

79. Smith G. 2012. Herpesvirus transport to the nervous system and back again. Annu Rev Microbiol 66:153-76.

80. Thellman NM, Triezenberg SJ. 2017. Herpes Simplex Virus Establishment, Maintenance, and Reactivation: In Vitro Modeling of Latency. Pathogens 6.

81. Salinas S, Schiavo G, Kremer EJ. 2010. A hitchhiker's guide to the nervous system: the complex journey of viruses and toxins. Nat Rev Microbiol 8:645-55.

82. Taylor LF, Yuan Y. 2018. Structure of Herpesvirus Capsid Sheds Light on Drug Discovery. Trends Microbiol doi:10.1016/j.tim.2018.03.003.

83. Baines JD. 2011. Herpes simplex virus capsid assembly and DNA packaging: a present and future antiviral drug target. Trends Microbiol 19:606-13.

84. Newcomb WW, Brown JC, Booy FP, Steven AC. 1989. Nucleocapsid Mass and Capsomer Protein Stoichiometry in Equine Herpesvirus 1: Scanning Transmission Electron Microscopic Study. J Virol 64:3777-3783.

85. Newcomb WW, Trus BL, Booy FP, Steven AC, Wall JS, Brown JC. 1993. Structure of the Herpes Simplex Virus Capsid. Molecular Composition of the Pentons and the Triplexes.

86. Gibson W, Roizman B. 1972. Proteins Specified by Herpes Simplex Virus. VIII. Characterization and Composition of Multiple Capsid Forms of Subtypes 1 and 2. J Virol 10:1044-1052.

87. Newcomb WW, Brown JC. 1991. Structure of the Herpes Simplex Virus Capsid: Effects of Extraction with Guanidine Hydrochloride and Partial Reconstitution of Extracted Capsids. J Virol 65:613-620.

88. McElwee M, Vijayakrishnan S, Rixon F, Bhella D. 2018. Structure of the herpes simplex virus portal-vertex. PLoS Biol 16:e2006191.

89. Zhou ZH, He J, Jakana J, Tatman JD, Rixon FJ, Chiu W. 1995. Assembly of VP26 in herpes simplex virus-1 inferred from structures of wild-type and recombinant capsids. Nature Struct Biol 2:1026-1030.

90. Booy FP, Trus BL, Newcomb WW, Brown JC, Conway JF, Steven AC. 1994. Finding a needle in a haystack: Detection of a small protein (the 12-kDa VP26) in a large complex (the 200-MDa capsid of herpes simplex virus). PNAS 91:5652-5656.

91. Chen DH, Jakana J, McNab D, Mitchell J, Zhou ZH, Dougherty M, Chiu W, Rixon FJ. 2001. The pattern of tegument-capsid interaction in the herpes simplex virus type 1 virion is not influenced by the small hexon-associated protein VP26. J Virol 75:11863-7.

92. Zhou ZH, Chen DH, Jakana J, Rixon FJ, Chiu W. 1999. Visualization of Tegument-Capsid Interactions and DNA in Intact Herpes Simplex Virus Type 1 Virions. JVirol 73:3210.

93. Huet A, Makhov AM, Huffman JB, Vos M, Homa FL, Conway JF. 2016. Extensive subunit contacts underpin herpesvirus capsid stability and interior-to-exterior allostery. Nat Struct Mol Biol doi:10.1038/pj.2016.37.

94. Fan WH, Roberts AP, McElwee M, Bhella D, Rixon FJ, Lauder R. 2015. The large tegument protein pUL36 is essential for formation of the capsid vertex-specific component at the capsid-tegument interface of herpes simplex virus 1. J Virol 89:1502-11.

95. Suhanovsky MM, Teschke CM. 2015. Nature's favorite building block: Deciphering folding and capsid assembly of proteins with the HK97-fold. Virology 479-480:487-97.

96. Hong Z, Beaudet-Miller M, Durkin J, Zhang R, Kwong AD. 1996. Identification of a Minimal Hydrophobic Domain in the Herpes Simplex Virus Type 1 Scaffolding Protein Which Is Required for Interaction with the Major Capsid Protein. J Virol 70:533-540.

97. Desai P, Person S. 1999. Second Site Mutations in the N-Terminus of the Major Capsid Protein (VP5) Overcome a Block at the Maturation Cleavage Site of the Capsid Scaffold Proteins. Virology 261:357-366.

98. Warner SC, Desai P, Person S. 2000. Second-site mutations encoding residues 34 and 78 of the major capsid protein (VP5) of herpes simplex virus type 1 are important for overcoming a blocked maturation cleavage site of the capsid scaffold proteins. Virology 278:217-26.

99. Walters JN, Sexton GL, McCaffery JM, Desai P. 2003. Mutation of Single Hydrophobic Residue I27, L35, F39, L58, L65, L67, or L71 in the N Terminus of VP5 Abolishes Interaction with the Scaffold Protein and Prevents Closure of Herpes Simplex Virus Type 1 Capsid Shells. Journal of Virology 77:4043-4059.

100. Huang E, Perkins EM, Desai P. 2007. Structural features of the scaffold interaction domain at the N terminus of the major capsid protein (VP5) of herpes simplex virus type 1. J Virol 81:9396-407.

101. Zhou ZH, Dougherty M, Jakana J, He J, Rixon FJ, Chiu W. 2000. Seeing the Herpesvirus Capsid at 8.5 A. Science 288:877-880.

102. Aksyuk AA, Newcomb WW, Cheng N, Winkler DC, Fontana J, Heymann JB, Steven AC. 2015. Subassemblies and asymmetry in assembly of herpes simplex virus procapsid. MBio 6:e01525-15.

103. Trus BL, Booy FP, Newcomb WW, Brown JC, Homa FL, Thomsen DR, Steven AC. 1996. The Herpes Simplex Virus Procapsid: Structure, Conformational Changes Upon

Maturation, and Roles of the Triplex Proteins VP19c and VP23 in Assembly. J Mol Biol 263:447-462.

104. Perkins EM, Anacker D, Davis A, Sankar V, Ambinder RF, Desai P. 2008. Small capsid protein pORF65 is essential for assembly of Kaposi's sarcoma-associated herpesvirus capsids. J Virol 82:7201-11.

105. Henson BW, Perkins EM, Cothran JE, Desai P. 2009. Self-assembly of Epstein-Barr virus capsids. J Virol 83:3877-90.

106. Dai X, Gong D, Xiao Y, Wu TT, Sun R, Zhou ZH. 2015. CryoEM and mutagenesis reveal that the smallest capsid protein cements and stabilizes Kaposi's sarcoma-associated herpesvirus capsid. Proc Natl Acad Sci U S A 112:E649-56.

107. Dai X, Yu X, Gong H, Jiang X, Abenes G, Liu H, Shivakoti S, Britt WJ, Zhu H, Liu F, Zhou ZH. 2013. The smallest capsid protein mediates binding of the essential tegument protein pp150 to stabilize DNA-containing capsids in human cytomegalovirus. PLoS Pathog 9:e1003525.

108. Borst EM, Mathys S, Wagner M, Muranyi W, Messerle M. 2001. Genetic evidence of an essential role for cytomegalovirus small capsid protein in viral growth. J Virol 75:1450-8.

109. Desai P, DeLuca NA, Person S. 1998. Herpes Simplex Virus Type 1 VP26 is Not Essential for Replication in Cell Culture but Influences Production of Infectious Virus in the Nervous System of Infected Mice. Virology 247:115-124.

110. Kobayashi R, Kato A, Sagara H, Watanabe M, Maruzuru Y, Koyanagi N, Arii J, Kawaguchi Y. 2017. Herpes Simplex Virus 1 Small Capsomere-Interacting Protein VP26 Regulates Nucleocapsid Maturation. J Virol doi:10.1128/JVI.01068-17.

111. Krautwald M, Maresch C, Klupp BG, Fuchs W, Mettenleiter TC. 2008. Deletion or green fluorescent protein tagging of the pUL35 capsid component of pseudorabies virus impairs virus replication in cell culture and neuroinvasion in mice. J Gen Virol 89:1346-51.

112. Dokland T. 1999. Scaffolding proteins and their role in viral assembly. Cell Mol Life Sci 56:580-603.

113. Booy FP, Newcomb WW, Trus BL, Brown JC, Baker TS, Steven AC. 1991. Liquid-Crystalline, Phage-like Packing of Encapsidated DNA in Herpes Simplex Virus. Cell 64:1007-1015.

114. Veesler D, Johnson JE. 2012. Virus maturation. Annu Rev Biophys 41:473-96.

115. Beilstein F, Higgs MR, Stow ND. 2009. Mutational analysis of the herpes simplex virus type 1 DNA packaging protein UL33. J Virol 83:8938-45.

116. Newcomb WW, Homa F, Thomsen DR, Ye Z, Brown JC. 1994. Cell-Free Assembly of the Herpes Simplex Virus Capsid. J Virol 68:6059-6063.

117. Tatman JD, Preston VG, Nicholson P, Elliott RM, Rixon FJ. 1994. Assembly of herpes simplex virus type 1 capsids using a panel of recombinant baculoviruses. J Gen Virol 75:1101-1113.

118. Thomsen DR, Roof LL, Homa FL. 1994. Assembly of Herpes Simplex Virus (HSV) Intermediate Capsids in Insect Cells Infected with Recombinant Baculoviruses Expressing HSV Capsid Proteins. J Virol 68:2442-2457.

119. Newcomb WW, Homa F, Thomsen DR, Booy FP, Trus BL, Steven AC, Spencer JV, Brown JC. 1996. Assembly of the Herpes Simplex Virus Capsid: Characterization of Intermediates Observed During Cell-free Capsid Formation. J Mol Biol 263:432-446.

120. Thomsen DR, Newcomb WW, Brown JC, Homa FL. 1995. Assembly of the Herpes Simplex Virus Capsid: Requirement for the Carboxyl-Terminal Twenty-Five Amino Acids of the Proteins Encoded by the UL26 and UL26.5 Genes. J Virol 69:3690-3703.

121. Kennard J, Rixon FJ, McDougall IM, Tatman JD, Preston VG. 1995. The 25 amino acid residues at the carboxy terminus of the herpes simplex virus type 1 UL26.5 protein are required for the formation of the capsid shell around the scaffold. J Gen Virol 76:1611-1621.

122. Preston VG, Coates JAV, Rixon FJ. 1983. Identification and Characterization of a Herpes Simplex Virus Gene Product Required for Encapsidation of Virus DNA. J Virol 45:1056-1064.

123. Church GA, Wilson DW. 1997. Study of Herpes Simplex Virus Maturation during a Synchronous Wave of Assembly. J Virol 71:3603-3612.

124. Heymann JB, Cheng N, Newcomb WW, Trus BL, Brown JC, Steven AC. 2003. Dynamics of herpes simplex virus capsid maturation visualized by time-lapse cryo-electron microscopy. Nat Struct Biol 10:334-41.

125. Robertson BJ, McCain III PJ, Matusick-Kumar L, Newcomb WW, Brown JC, Colonno RJ, Gao M. 1996. Separate Functional Domains of the Herpes Simplex Virus Type 1 Protease: Evidence for Cleavage inside Capsids. *J Virol* 70:4317-4328.

126. Sheaffer AK, Newcomb WW, Gao M, Yu D, Weller SK, Brown JC, Tenney DJ. 2001. Herpes simplex virus DNA cleavage and packaging proteins associate with the procapsid prior to its maturation. J Virol 75:687-98.

127. Newcomb WW, Trus BL, Cheng N, Steven AC, Sheaffer AK, Tenney DJ, Weller SK, Brown JC. 2000. Isolation of Herpes Simplex Virus Procapsids from Cells Infected with a Protease-Deficient Mutant Virus. J Virol 74:1663-1673.

128. Rixon FJ, McNab D. 1999. Packaging-Competent Capsids of a Herpes Simplex Virus Temperature-Sensitive Mutant Have Properties Similar to Those of In Vitro-Assembled Procapsids. J Virol 73:5714-5721.

129. Liu F, Roizman B. 1991. The Herpes Simplex Virus 1 Gene Encoding a Protease Also Contains within Its Coding Domain the Gene Encoding the More Abundant Substrate. J Virol 65:5149-5156.

130. DiIanni CL, Drier DA, Deckman IC, McCann III PJ, Liu F, Roizman B, Colonno RJ, Cordingley MG. 1993. Identification of the Herpes Simplex Virus-1 Protease Cleavage Sites by Direct Sequence Analysis of Autoproteolytic Cleavage Products. J Biol Chem 268:2048-2051.

131. Weinheimer SP, McCann III PJ, O'Boyle II DR, Stevens JT, Boyd BA, Drier DA, Yamanaka GA, DiIanni CL, Deckman IC, Cordingley MG. 1993. Autoproteolysis of Herpes Simplex Virus Type 1 Protease Releases an Active Catalytic Domain Found in Intermediate Capsid Particles. J Virol 67:5813-5822.

132. Matusick-Kumar L, Newcomb WW, Brown JC, McCann III P, Hurlburt W, Weinheimer SP, Gao M. 1995. The C-terminal 25 Amino Acids of the Protease and Its Substrate ICP35 of Herpes Simplex Virus Type 1 Are Involved in the Formation of Sealed Capsids. J Virol 69:4347-4356.

133. Desai P, Person S. 1996. Molecular Interactions between the HSV-1 Capsid Proteins as Measured by the Yeast Two-Hybrid System. Virology 220:516-521.

134. Schmidt U, Darke PL. 1997. Dimerization and Activation of the Herpes Simplex Virus Type 1 Protease. J Biol Chem 272:7732-7735.

135. Dasgupta A, Wilson DW. 1999. ATP Depletion Blocks Herpes Simplex Virus DNA Packaging and Capsid Maturation. J Virol 73:2006-2015.

136. Chi JH, Wilson DW. 2000. ATP-Dependent Localization of the Herpes Simplex Virus Capsid Protein VP26 to Sites of Procapsid Maturation. J Virol 74:1468-1476.

137. Klupp BG, Granzow H, Keil GM, Mettenleiter TC. 2006. The capsid-associated UL25 protein of the alphaherpesvirus pseudorabies virus is nonessential for cleavage and encapsidation of genomic DNA but is required for nuclear egress of capsids. J Virol 80:6235-46.

138. McNab AR, Desai P, Person S, Roof LL, Thomsen DR, Newcomb WW, Brown JC, Homa FL. 1998. The Product of the Herpes Simplex Virus Type 1 UL25 Gene is Required for Encapsidation but Not for Cleavage of Replicated Viral DNA. J Virol 72:1060-1070.

139. Thurlow JK, Rixon FJ, Murphy M, Targett-Adams P, Hughes M, Preston VG. 2005. The herpes simplex virus type 1 DNA packaging protein UL17 is a virion protein that is present in both the capsid and the tegument compartments. J Virol 79:150-8.

140. Stevenson AJ, Morrison EE, Chaudhari R, Yang C, Meredith DM. 1997. Processing and intracellular localization of the herpes simplex virus type 1 proteinase. J Gen Virol 78:671-675.

141. Person S, Desai P. 1998. Capsids Are Formed in a Mutant Virus Blocked at the Maturation Site of the UL26 and UL26.5 Open Reading Frames of Herpes Simplex Virus Type 1 but Are Not Formed in a Null Mutant of UL38 (VP19C). Virology 242:193-203.

142. Spear PG, Roizman B. 1972. Proteins Specified by Herpes Simplex Virus. V. Purification and Structural Proteins of the Herpesvirion. J Virol 9:143-159.

143. White CA, Stow ND, Patel AH, Hughes M, Preston VG. 2003. Herpes Simplex Virus Type 1 Portal Protein UL6 Interacts with the Putative Terminase Subunits UL15 and UL28. Journal of Virology 77:6351-6358.

144. Beard PM, Baines JD. 2004. The DNA cleavage and packaging protein encoded by the UL33 gene of herpes simplex virus 1 associates with capsids. Virology 324:475-82.

145. Beard PM, Duffy C, Baines JD. 2004. Quantification of the DNA Cleavage and Packaging Proteins UL15 and UL28 in A and B Capsids of Herpes Simplex Virus Type 1. Journal of Virology 78:1367-1374.

146. Yang K, Homa F, Baines JD. 2007. Putative terminase subunits of herpes simplex virus 1 form a complex in the cytoplasm and interact with portal protein in the nucleus. J Virol 81:6419-33.

147. Yu D, Weller SK. 1998. Herpes Simplex Virus Type 1 Cleavage and Packaging Proteins UL15 and UL28 Are Associated with B but Not C Capsids during Packaging. J Virol 72:7428-7439.

148. Yang K, Wills E, Baines JD. 2009. The putative leucine zipper of the UL6-encoded portal protein of herpes simplex virus 1 is necessary for interaction with pUL15 and pUL28 and their association with capsids. J Virol 83:4557-64.

149. Albright BS, Kosinski A, Szczepaniak R, Cook EA, Stow ND, Conway JF, Weller SK. 2015. The putative herpes simplex virus 1 chaperone protein UL32 modulates disulfide bond formation during infection. J Virol 89:443-53.

150. Fuchs W, Klupp BG, Granzow H, Leege T, Mettenleiter TC. 2009. Characterization of pseudorabies virus (PrV) cleavage-encapsidation proteins and functional complementation of PrV pUL32 by the homologous protein of herpes simplex virus type 1. J Virol 83:3930-43.

151. Newcomb WW, Brown JC. 2009. Time-dependent transformation of the herpesvirus tegument. J Virol 83:8082-9.

152. Remillard-Labrosse G, Guay G, Lippe R. 2006. Reconstitution of herpes simplex virus type 1 nuclear capsid egress in vitro. J Virol 80:9741-53.

153. Roberts AP, Abaitua F, O'Hare P, McNab D, Rixon FJ, Pasdeloup D. 2009. Differing roles of inner tegument proteins pUL36 and pUL37 during entry of herpes simplex virus type 1. J Virol 83:105-16.

154. Stackpole CW. 1969. Herpes-Type Virus of the Frog Renal Adenocarcinoma. J Virol 4:75-93.

155. Vlazny DA, Kwong A, Frenkel N. 1982. Site-specific cleavage/packaging of herpes simplex virus DNA and the selective maturation of nucleocapsids containing full-length viral DNA. PNAS 79:1423-1427.

156. Leelawong M, Lee JI, Smith GA. 2012. Nuclear egress of pseudorabies virus capsids is enhanced by a subspecies of the large tegument protein that is lost upon cytoplasmic maturation. J Virol 86:6303-14.

157. Trus BL, Newcomb WW, Cheng N, Cardone G, Marekov L, Homa FL, Brown JC, Steven AC. 2007. Allosteric signaling and a nuclear exit strategy: binding of UL25/UL17 heterodimers to DNA-Filled HSV-1 capsids. Mol Cell 26:479-89.

158. Bowman BR, Baker ML, Rixon FJ, Chiu W, Quiocho FA. 2003. Structure of the herpesvirus major capsid protein. The EMBO Journal 22:757-765.

159. Wu W, Newcomb WW, Cheng N, Aksyuk A, Winkler DC, Steven AC. 2016. Internal Proteins of the Procapsid and Mature Capsids of Herpes Simplex Virus 1 Mapped by Bubblegram Imaging. J Virol 90:5176-86.

160. Sae-Ueng U, Liu T, Catalano CE, Huffman JB, Homa FL, Evilevitch A. 2014. Major capsid reinforcement by a minor protein in herpesviruses and phage. Nucleic Acids Res 42:9096-107.

161. Snijder J, Radtke K, Anderson F, Scholtes L, Corradini E, Baines J, Heck AJR, Wuite GJL, Sodeik B, Roos WH. 2017. Vertex-Specific Proteins pUL17 and pUL25 Mechanically Reinforce Herpes Simplex Virus Capsids. J Virol 91.

162. Thurlow JK, Murphy M, Stow ND, Preston VG. 2006. Herpes simplex virus type 1 DNA-packaging protein UL17 is required for efficient binding of UL25 to capsids. J Virol 80:2118-26.

163. Homa FL, Huffman JB, Toropova K, Lopez HR, Makhov AM, Conway JF. 2013. Structure of the pseudorabies virus capsid: comparison with herpes simplex virus type 1 and differential binding of essential minor proteins. J Mol Biol 425:3415-28.

164. Roos WH, Radtke K, Kniesmeijer E, Geertsema H, Sodeik B, Wuite GJ. 2009. Scaffold expulsion and genome packaging trigger stabilization of herpes simplex virus capsids. Proc Natl Acad Sci U S A 106:9673-8.

165. Salmon B, Cunningham C, Davison AJ, Harris WJ, Baines JD. 1998. The Herpes Simplex Virus Type 1 UL17 Gene Encodes Virion Tegument Proteins That Are Required for Cleavage and Packaging of Viral DNA. J Virol 72:3779-3788.

166. Cockrell SK, Sanchez ME, Erazo A, Homa FL. 2009. Role of the UL25 protein in herpes simplex virus DNA encapsidation. J Virol 83:47-57.

167. Stow ND. 2001. Packaging of genomic and amplicon DNA by the herpes simplex virus type 1 UL25-null mutant KUL25NS. J Virol 75:10755-65.

168. Newcomb WW, Brown JC. 2002. Inhibition of Herpes Simplex Virus Replication by WAY-150138: Assembly of Capsids Depleted of the Portal and Terminase Proteins Involved in DNA Encapsidation. Journal of Virology 76:10084-10088.

169. Jin F, Li S, Zheng K, Zhuo C, Ma K, Chen M, Wang Q, Zhang P, Fan J, Ren Z, Wang Y. 2014. Silencing herpes simplex virus type 1 capsid protein encoding genes by siRNA: a promising antiviral therapeutic approach. PLoS One 9:e96623.

170. Inoue N, Matsushita M, Fukui Y, Yamada S, Tsuda M, Higashi C, Kaneko K, Hasegawa H, Yamaguchi T. 2012. Identification of a varicella-zoster virus replication inhibitor that blocks capsid assembly by interacting with the floor domain of the major capsid protein. J Virol 86:12198-207.

171. Akanitapichat P, Bastow KF. 2002. The antiviral agent 5-chloro-1,3-dihydroxyacridone interferes with assembly and maturation of herpes simplex virus. Antiviral Res 53:113-126.

172. Piret J, Lamontagne J, Bestman-Smith J, Roy S, Gourde P, Desormeaux A, Omar RF, Juhasz J, Bergeron MG. 2000. In Vitro and In Vivo Evaluations of Sodium Lauryl Sulfate and Dextran Sulfate as Microbicides against Herpes Simplex and Human Immunodeficiency Viruses. J Clin Microbiol 38:110-119.

173. Underwood MR, Harvey RJ, Stanat SC, Hemphill ML, Miller T, Drach JC, Townsend LB, Biron KK. 1998. Inhibition of Human Cytomegalovirus DNA Maturation by a Benzimidazole Ribonucleoside Is Mediated through the UL89 Gene Product. J Virol 72:717-725.

174. Krosky PM, Underwood MR, Turk SR, Feng KWH, Jain RK, Ptak RG, Westerman AC, Biron KK, Townsend LB, Drach JC. 1998. Resistance of Human Cytomegalovirus to Benzimidazole Ribonucleosides Maps to Two Open Reading Frames: UL89 and UL56. J Virol 72:4721-4728.

175. Goldner T, Hewlett G, Ettischer N, Ruebsamen-Schaeff H, Zimmermann H, Lischka P. 2011. The novel anticytomegalovirus compound AIC246 (Letermovir) inhibits human cytomegalovirus replication through a specific antiviral mechanism that involves the viral terminase. J Virol 85:10884-93.

176. Douglas MW, Diefenbach RJ, Homa FL, Miranda-Saksena M, Rixon FJ, Vittone V, Byth K, Cunningham AL. 2004. Herpes simplex virus type 1 capsid protein VP26 interacts with dynein light chains RP3 and Tctex1 and plays a role in retrograde cellular transport. J Biol Chem 279:28522-30.

177. Apcarian A, Cunningham AL, Diefenbach RJ. 2010. Identification of binding domains in the herpes simplex virus type 1 small capsid protein pUL35 (VP26). J Gen Virol 91:2659-63.

178. Ko DH, Cunningham AL, Diefenbach RJ. 2010. The major determinant for addition of tegument protein pUL48 (VP16) to capsids in herpes simplex virus type 1 is the presence of the major tegument protein pUL36 (VP1/2). J Virol 84:1397-405.

179. Antinone SE, Shubeita GT, Coller KE, Lee JI, Haverlock-Moyns S, Gross SP, Smith GA. 2006. The Herpesvirus Capsid Surface Protein, VP26, and the Majority of the Tegument Proteins Are Dispensable for Capsid Transport toward the Nucleus. J Virol 80:5494-8.

180. Dohner K, Radtke K, Schmidt S, Sodeik B. 2006. Eclipse phase of herpes simplex virus type 1 infection: Efficient dynein-mediated capsid transport without the small capsid protein VP26. J Virol 80:8211-24.

181. Coller KE, Lee JI, Ueda A, Smith GA. 2007. The capsid and tegument of the alphaherpesviruses are linked by an interaction between the UL25 and VP1/2 proteins. J Virol 81:11790-7.

182. Coller KE, Smith GA. 2008. Two viral kinases are required for sustained long distance axon transport of a neuroinvasive herpesvirus. Traffic 9:1458-70.

183. Daniel GR, Pegg CE, Smith GA. 2018. Dissecting the herpesvirus architecture by targeted proteolysis. J Virol doi:10.1128/JVI.00738-18.

184. Bigalke JM, Heldwein EE. 2015. Structural basis of membrane budding by the nuclear egress complex of herpesviruses. EMBO J doi:10.15252/embj.201592359.

185. Bigalke JM, Heuser T, Nicastro D, Heldwein EE. 2014. Membrane deformation and scission by the HSV-1 nuclear egress complex. Nat Commun 5:4131.

186. Klupp BG, Granzow H, Fuchs W, Keil GM, Finke S, Mettenleiter TC. 2007. Vesicle formation from the nuclear membrane is induced by coexpression of two conserved herpesvirus proteins. Proc Natl Acad Sci U S A 104:7241-6.

187. Liu Z, Kato A, Shindo K, Noda T, Sagara H, Kawaoka Y, Arii J, Kawaguchi Y. 2014. Herpes Simplex Virus 1 UL47 Interacts with Viral Nuclear Egress factors UL31, UL34 and Us3, and Regulates Viral Nuclear Egress. J Virol doi:10.1128/JVI.00137-14.

188. Maruzuru Y, Shindo K, Liu Z, Oyama M, Kozuka-Hata H, Arii J, Kato A, Kawaguchi Y. 2014. Role of herpes simplex virus 1 immediate early protein ICP22 in viral nuclear egress. J Virol 88:7445-54.

189. Wang Y, Yang Y, Wu S, Pan S, Zhou C, Ma Y, Ru Y, Dong S, He B, Zhang C, Cao Y. 2014. P32 Is a Novel Target for ICP34.5 of Herpes Simplex Virus Type 1, and Facilitates Viral Nuclear Egress. J Biol Chem doi:10.1074/jbc.M114.603845.

190. Bucks MA, O'Regan KJ, Murphy MA, Wills JW, Courtney RJ. 2007. Herpes simplex virus type 1 tegument proteins VP1/2 and UL37 are associated with intranuclear capsids. Virology 361:316-24.

191. Luxton GW, Lee JI, Haverlock-Moyns S, Schober JM, Smith GA. 2006. The pseudorabies virus VP1/2 tegument protein is required for intracellular capsid transport. J Virol 80:201-9.

192. Desai P, Sexton GL, McCaffery JM, Person S. 2001. A null mutation in the gene encoding the herpes simplex virus type 1 UL37 polypeptide abrogates virus maturation. J Virol 75:10259-71.

193. Scholtes LD, Yang K, Li LX, Baines JD. 2010. The capsid protein encoded by U(L)17 of herpes simplex virus 1 interacts with tegument protein VP13/14. J Virol 84:7642-50.

194. Desai PJ. 2000. Mutation in the UL36 Gene of Herpes Simplex Virus Type 1 Results in Accumulation of Unenveloped DNA-Filled Capsids in the Cytoplasm of Infected Cells. J Virol 74:11608-11618.

195. Starkey JL, Han J, Chadha P, Marsh JA, Wills JW. 2014. Elucidation of the block to herpes simplex virus egress in the absence of tegument protein UL16 reveals a novel interaction with VP22. J Virol 88:110-9.

196. Meckes DG, Jr., Marsh JA, Wills JW. 2010. Complex mechanisms for the packaging of the UL16 tegument protein into herpes simplex virus. Virology 398:208-13.

197. Meckes DG, Jr., Wills JW. 2007. Dynamic interactions of the UL16 tegument protein with the capsid of herpes simplex virus. J Virol 81:13028-36.

198. Takakuwa H, Goshima F, Koshizuka T, Murata T, Daikoku T, Nishiyama Y. 2001. Herpes simplex virus encodes a virion-associated protein which promotes long cellular processes in over-expressing cells. Genes to Cells 6.

199. Pettersen EF, Goddard TD, Huang CC, Couch GS, Greenblatt DM, Meng EC, Ferrin TE. 2004. UCSF Chimera--a visualization system for exploratory research and analysis. J Comput Chem 25:1605-12.

200. Gierasch WW, Zimmerman DL, Ward SL, Vanheyningen TK, Romine JD, Leib DA. 2006. Construction and characterization of bacterial artificial chromosomes containing HSV-1 strains 17 and KOS. J Virol Methods 135:197-206.

201. Smith GA, Gross SP, Enquist LW. 2001. Herpesviruses use bidirectional fast-axonal transport to spread in sensory neurons. PNAS 98:3466-3470.

202. Tischer BK, Smith GA, Osterrieder N. 2010. En passant mutagenesis: a two step markerless red recombination system. Methods Mol Biol 634:421-30.

203. Tanaka M, Kagawa H, Yamanashi Y, Sata T, Kawaguchi Y. 2003. Construction of an Excisable Bacterial Artificial Chromosome Containing a Full-Length Infectious Clone of Herpes Simplex Virus Type 1: Viruses Reconstituted from the Clone Exhibit Wild-Type Properties In Vitro and In Vivo. Journal of Virology 77:1382-1391.

204. Tirabassi RS, Enquist LW. 1998. Role of Envelope Protein gE Endocytosis in the Pseudorabies Virus Life Cycle. J Virol 72:4571-4579.

205. Bohannon KP, Sollars PJ, Pickard GE, Smith GA. 2012. Fusion of a fluorescent protein to the pUL25 minor capsid protein of pseudorabies virus allows live-cell capsid imaging with negligible impact on infection. J Gen Virol 93:124-9.

206. Spencer JV, Trus BL, Booy FP, Steven AC, Newcomb WW, Brown JC. 1997. Structure of the Herpes Simplex Virus Capsid: Peptide A862-H880 of the Major Capsid Protein is Displayed on the Rim of the Capsomer Protrusions. Virology 228:229-235.

207. Trus BL, Newcomb WW, Booy FP, Brown JC, Steven AC. 1992. Distinct monoclonal antibodies separately label the hexons or the pentons of herpes simplex virus capsid. PNAS 89:11508-11512.

208. Matusick-Kumar L, Hurlburt W, Weinheimer SP, Newcomb WW, Brown JC, Gao M. 1994. Phenotype of the Herpes Simplex Virus Type 1 Protease Substrate ICP35 Mutant Virus. J Virol 68:5384-5394.

209. Kobayashi R, Kato A, Oda S, Koyanagi N, Oyama M, Kozuka-Hata H, Arii J, Kawaguchi Y. 2015. The Function of the Herpes Simplex Virus 1 Small Capsid Protein VP26 is Regulated by Phosphorylation at a Specific Site. J Virol doi:10.1128/JVI.00547-15.

210. Addison C, Rixon FJ, Preston VG. 1990. Herpes simplex virus type 1 UL28 gene product is important for the formation of mature capsids. J Gen Virol 71:2377-2384.

211. Newcomb WW, Homa FL, Thomsen DR, Trus BL, cheng N, Steven A, Booy F, Brown JC. 1999. Assembly of the Herpes Simplex Virus Procapsid from Purified Components and Identification of Small Complexes Containing the Major Capsid and Scaffolding Proteins. J Virol 73:4239-4250.

212. Gao M, Matusick-Kumar L, Hurlburt W, DiTusa SF, Newcomb WW, Brown JC, McCann III PJ, Deckman IC, Colonno RJ. 1994. The Protease of Herpes Simplex Virus Type 1 is Essential for Functional Capsid Formation and Viral Growth. J Virol 68:3702-3712.

213. Al-Kobaisi MF, Rixon FJ, McDougall I, Preston VG. 1991. The herpes simplex virus UL33 gene product is required for the assembly of full capsids. Virology 180.

214. Nagel CH, Dohner K, Binz A, Bauerfeind R, Sodeik B. 2012. Improper tagging of the non-essential small capsid protein VP26 impairs nuclear capsid egress of herpes simplex virus. PLoS One 7:e44177.

215. Nagel CH, Dohner K, Fathollahy M, Strive T, Borst EM, Messerle M, Sodeik B. 2008. Nuclear egress and envelopment of herpes simplex virus capsids analyzed with dual-color fluorescence HSV1(17+). J Virol 82:3109-24.

216. Shimomura O, Johnson FH, Saiga Y. 1962. Extraction, purification and properties of aequorin, a bioluminescent protein from the luminous hydromedusan, Aequorea. J Cell Comp Physiol 59:223-239.

217. Desai P, Person S. 1998. Incorporation of the Green Fluorescent Protein into the Herpes Simplex Virus Type 1 Capsid. J Virol 72:7563-7568.

218. Bohannon KP, Jun Y, Gross SP, Smith GA. 2013. Differential protein partitioning within the herpesvirus tegument and envelope underlies a complex and variable virion architecture. Proc Natl Acad Sci U S A 110:E1613-20.

219. Hogue IB, Jean J, Esteves AD, Tanneti NS, Scherer J, Enquist LW. 2018. Functional Carboxy-Terminal Fluorescent Protein Fusion to Pseudorabies Virus Small Capsid Protein VP26. J Virol 92:e01193-17.

220. Conway JF, Cockrell SK, Copeland AM, Newcomb WW, Brown JC, Homa FL. 2010. Labeling and localization of the herpes simplex virus capsid protein UL25 and its interaction with the two triplexes closest to the penton. J Mol Biol 397:575-86.

221. Swulius MT, Jensen GJ. 2012. The helical MreB cytoskeleton in Escherichia coli MC1000/pLE7 is an artifact of the N-Terminal yellow fluorescent protein tag. J Bacteriol 194:6382-6.

222. Hanson DA, Ziegler SF. 2004. Fusion of green fluorescent protein to the C-terminus of granulysin alters its intracellular localization in comparison to the native molecule. J Negat Results Biomed 3:2.

223. Spencer JV, Newcomb WW, Thomsen DR, Homa FL, Brown JC. 1998. Assembly of the Herpes Simplex Virus Capsid: Preformed Triplexes Bind to the Nascent Capsid. J Virol 72:3944-3951.

224. Pelletier A, Do F, Brisebois JJ, Lagace L, Cordingley MG. 1997. Self-Association of Herpes Simplex Virus Type 1 ICP35 Is via Coiled-Coil Interactions and Promotes Stable Interaction with the Major Capsid Protein. J Virol 71:5197-5208.

225. Padilla-Meier GP, Gilcrease EB, Weigele PR, Cortines JR, Siegel M, Leavitt JC, Teschke CM, Casjens SR. 2012. Unraveling the role of the C-terminal helix turn helix of the coat-binding domain of bacteriophage P22 scaffolding protein. J Biol Chem 287:33766-80.

226. Fuller MT, King J. 1982. Assembly *in Vitro* of Bacteriophage P22 Procapsids from Purified Coat and Scaffolding Subunits. J Mol Biol 156:633-665.

227. Padilla-Meier GP, Teschke CM. 2011. Conformational changes in bacteriophage P22 scaffolding protein induced by interaction with coat protein. J Mol Biol 410:226-40.

228. Wang WH, Kuo CW, Chang LK, Hung CC, Chang TH, Liu ST. 2015. Assembly of Epstein-Barr Virus Capsid in Promyelocytic Leukemia Nuclear Bodies. J Virol 89:8922-31.

229. Ward PL, O. OW, B. R. 1996. Assemblons: nuclear structures defined by aggregation of immature capsids and some tegument proteins of herpes simplex virus 1. JVirol 70:4623-4631.

230. Lee JI, Luxton GW, Smith GA. 2006. Identification of an Essential Domain in the Herpesvirus VP1/2 Tegument Protein: the Carboxy Terminus Directs Incorporation into Capsid Assemblons. J Virol 80:12086-94.

231. Trus BL, Cheng N, Newcomb WW, Homa FL, Brown JC, Steven AC. 2004. Structure and polymorphism of the UL6 portal protein of herpes simplex virus type 1. J Virol 78:12668-71.